



# รายงานวิจัยฉบับสมบูรณ์

# โครงการ การเตรียมและการหาลักษณะเฉพาะของวัสดุ รีแลกเซอร์เฟร์โรอิเล็กทริกชนิด Pb(*B*<sub>1/3</sub>Nb<sub>2/3</sub>)O<sub>3</sub> ด้วยวิธีการใช้สารตั้งต้นแบบ *B*-site

โดย

รองศาสตราจารย์ ดร. สุพล อนันตา

# รายงานวิจัยฉบับสมบูรณ์

โครงการ การเตรียมและการหาลักษณะเฉพาะของวัสดุ รีแลกเซอร์เฟร์โรอิเล็กทริกชนิด Pb(*B*<sub>1/3</sub>Nb<sub>2/3</sub>)O<sub>3</sub> ด้วยวิธีการใช้สารตั้งต้นแบบ *B*-site

รองศาสตราจารย์ ดร. สุพล อนันตา ภาควิชาฟิสิกส์และวัสดุศาสตร์ คณะวิทยาศาสตร์ มหาวิทยาลัยเชียงใหม่

สนับสนุนโดยสำนักงานคณะกรรมการการอุดมศึกษา และสำนักงานกองทุนสนับสนุนการวิจัย

(ความเห็นในรายงานนี้เป็นของผู้วิจัย สกอ. และ สกว.ไม่จำเป็นต้องเห็นด้วยเสมอไป)

## กิตติกรรมประกาศ

ขอขอบพระคุณสำนักงานคณะกรรมการการอุดมศึกษา (สกอ.) และ สำนักงานกองทุน สนับสนุนการวิจัย (สกว.) ที่ให้โอกาสและการสนับสนุนทุนวิจัยในครั้งนี้ ขอขอบคุณ ภาควิชา ฟิสิกส์และวัสดุศาสตร์ คณะวิทยาศาสตร์ มหาวิทยาลัยเชียงใหม่ ที่อำนวยความสะดวกในการใช้ สถานที่ทำการวิจัย ขอขอบคุณน้ำใจ น้ำอดน้ำทน ความฝันและความมุ่งมั่นอย่างไร้ขีดจำกัดของ ทีมงานผู้ร่วมทำวิจัยทุก ๆท่าน ทั้งที่เป็นเพื่อนคณาจารย์และนักศึกษา ทั้งชาวไทยและ ชาวต่างชาติ ขอขอบคุณ ความรัก ความห่วงใย ความปรารถนาดี คำปรึกษาอันทรงคุณค่า จากผู้ หวังดีทุก ๆท่านที่ได้ช่วยกันสร้างขวัญและกำลังใจให้มาโดยตลอด หากมีสิ่งผิดพลาดบกพร่อง ประการใด ข้าพเจ้าก็ขออภัยมา ณ ที่นี้ สุดท้ายนี้ ข้าพเจ้าหวังใจว่า ผลงานที่ได้จากโครงการวิจัย นี้จักก่อให้เกิดเป็นประโยชน์ในทางสร้างสรรค์และเจริญงอกงามแก่ทุกท่านที่มีความสนใจต่อไป

(รศ.ดร. สุพล อนันตา) หัวหน้าโครงการฯ

# สารบาญ

|                                       | หน้า |
|---------------------------------------|------|
| ปกใน                                  | 1    |
| กิตติกรรมประกาศ                       | 2    |
| Abstract                              | 4    |
| บทคัดย่อ                              | 7    |
| Executive Summary                     | 10   |
| เนื้อหางานวิจัย                       | 11   |
| สรุปผลลัพธ์ (Output) ที่ได้จากโครงการ | 15   |
| ภาคผนวก                               | 25   |

#### **Abstract**

Project Code: RMU4980002

**Project Title:** Preparation and characterization of  $Pb(B_{1/3}Nb_{2/3})O_3$  type relaxor

ferroelectric materials by B-site precursor method

Investigator: Assoc. Prof. Dr. Supon Ananta

E-mail Address: suponananta@yahoo.com

Project Period: 20 July 2006 to 19 July 2009

#### Objectives:

Two major aspects, i.e. powder preparation and ceramic fabrication, have been concentrated in order to investigate the effect of B-site precursor method on the phase formation, microstructure and dielectric property of the  $Pb(B_{1/3}Nb_{2/3})O_3$  type relaxor ferroelectric materials (where B is Mg, Ni or Zn).

#### **Experimental procedures, Results and Discussion:**

(I) Lead-based perovksite ferroelectric powders in the  $Pb(B_{1/3}Nb_{2/3})O_3$  system (where B is Mg, Ni or Zn) have been prepared via a solid-state reaction method that involves niobate compounds with the columbite- and the corundum-type structures as B-site precursors. Phase formation and morphology of the calcined powders have been investigated as a function of calcination conditions. It has been found that the starting B-site precursor and firing condition have a pronounced effect on the phase formation and morphology of the calcined powders. The use of either columbite or corundum B-site precursor routes to prepare pure PMN and PNN powders with the pervoskite structure has been successful, but not for the PZN powders where a stable pyrochlore phase is formed preferentially. However, by employing higher perovskite phase stabilizers such as BaTiO<sub>3</sub> and PZT additives, the perovksite stability of the PZN phase can be successfully improved. In addition, it is seen that lower optimized calcination temperatures for the production of pure perovskite PMN and PNN powders can be obtained by using the columbite-route, whereas the smallest particle size was found in the corundum route powders.

(II) The ceramics in the  $Pb(B_{1/3}Nb_{2/3})O_3$  system (where B is Mg, Ni or Zn) have been fabricated by using a traditional sintering method. Selected compositions were also fabricated by employing a modified two-stage sintering method. Attention has been focused on relationships between chemical composition, sintering condition, phase formation, densification, microstructure and dielectric properties of the sintered products. It has been found that by using either the columbite or the corundum B-site precursor routes, conformable perovskite PMN and PNN ceramics with high density were successfully fabricated, except for PZN. Pure perovskite phase PMN ceramics with slightly higher dielectric constant can be produced at lower sintering temperature by using a corundum route. Whilst the fabrication of pure perovskite PNN ceramics with larger grain size, higher density and better dielectric properties can be obtained via a columbite route. Perhaps for PZN, in addition to the pyrochlore formation, the tolerance factor, bonding and structural parameters e.g. cation valence stability, ordering parameters, etc. should also be considered. The presence of pyrochlore-type phases downgrades the dielectric properties of the final products.

#### **Conclusions:**

Lead-based perovksite relaxor ferroelectric materials  $Pb(B_{1/3}Nb_{2/3})O_3$  (where B is Mg, Ni or Zn) have been prepared via a solid-state reaction method that involves niobate compounds as B-site precursors. The B-site precursor method has been employed in two different routes, namely the columbite and the corundum methods. Optimisation of processing parameters especially the starting B-site precursor and the calcination condition can lead to single-phase PMN and PNN powders of the desired compositions. This study clearly shows the influences of the B-site precursor processing on the variation of the phase formation characteristic, the microstructural evolution and the dielectric properties of  $Pb(B_{1/3}Nb_{2/3})O_3$  ceramics. Under suitable two-stage sintering schemes, dense and pure perovskite ceramics can be successfully achieved with better dielectric properties than those of ceramics from a conventional sintering technique. It has been found that this two-stage sintering technique can effectively suppress the grain growth in both perovskite PMN and PNN ceramics.

Suggestion for further work:

(I) Further investigation on the effect of A-site precursor route on phase formation,

microstructure and dielectric properties of the  $Pb(B_{1/3}Nb_{2/3})O_3$  system would be useful for

developing a potentially alternative processing route.

(II) Some improvement may be achieved by increasing the perovskite stability of the

samples in this study by using higher perovskite phase stabilizer e.g. BaTiO<sub>3</sub>, PbTiO<sub>3</sub> or

PZT additives. However, their size effects and appropriated adding amounts would need

to be considered.

(III) Further work on surface analysis, microstructural characterization especially at the

grain boundaries and their ferroelectric properties measurements would facilitate a

deeper understanding of these lead-based perovskite relaxor ferroelectrics in general.

Keywords: Relaxor ferroelectrics, Perovskites, B-site precursor, Dielectric properties

6

#### บทคัดย่อ

รหัสโครงการ: RMU4980002

**ชื่อโครงการ:** การเตรียมและการหาลักษณะเฉพาะของวัสดุรีแลกเซอร์เฟร์โรอิเล็กทริกชนิด

 $Pb(B_{1/3}Nb_{2/3})O_3$  ด้วยวิธีการใช้สารตั้งต้นแบบ B-site

**ชื่อนักวิจัย:** รองศาสตราจารย์ ดร. สุพล อนันตา

ที่อยู่อีเมล: suponananta@yahoo.com

ระยะเวลาโครงการ: 20 กรกฎาคม 2549 ถึง 19 กรกฎาคม 2552

# วัตถุประสงค์:

เน้นทำการวิจัยในสองประเด็นหลัก คือ กระบวนการเตรียมผงและการประดิษฐ์เซรามิก เพื่อ ศึกษาถึงอิทธิพลของวิธีการใช้สารตั้งต้นแบบ *B*-site ที่มีต่อการเกิดเฟส โครงสร้างจุลภาคและ สมบัติไดอิเล็กทริกของวัสดุในกลุ่มรีแลกเซอร์เฟร์โรอิเล็กทริกชนิด Pb(*B*<sub>1/3</sub>Nb<sub>2/3</sub>)O<sub>3</sub> โดยที่ *B* คือ Mg, Ni หรือ Zn

#### วิธีทดลอง ผลการทดลองและวิจารณ์ผลการทดลอง

(I) ได้ทำการสังเคราะห์ผงของวัสดุเพอร์รอฟสไกด์รีแลกเซอร์เฟร์โรอิเล็กทริกในระบบ Pb(B<sub>1/3</sub>Nb<sub>2/3</sub>)O<sub>3</sub> โดยที่ B คือ Mg, Ni หรือ Zn ด้วยเทคนิค solid-state reaction ที่ใช้ สารประกอบกลุ่มในโอเบตชนิดที่มีโครงสร้างโคลัมใบต์และคอรันดัมมาเป็นสารตั้งตันแบบ B-site แล้วนำสารที่เตรียมได้มาตรวจสอบการเกิดเฟสและสัณฐานของผงที่ผ่านการเผาแคลไซน์ด้วย เงื่อนไขต่างๆ ซึ่งจากผลการทดลองพบว่า ชนิดของสารตั้งตันแบบ B-site และเงื่อนไขในการเผาแคล ไซน์ด้วย และสัณฐานของผงที่ผ่านการเผาแคล ไซน์ โดยในงานวิจัยนี้สามารถทำการสังเคราะห์ผงบริสุทธิ์ของสาร PMN และ PNN ที่มี โครงสร้างแบบเพอร์รอฟสไกด์ได้สำเร็จทั้งในกรณีที่ใช้สารตั้งตันตันแบบ B-site ประเภทโคลัม ไบต์และประเภทคอรันดัม แต่ไม่สามารถทำการสังเคราะห์ผงบริสุทธิ์ของสาร PZN ได้ โดยจะพบ เฟสของสารที่มีเสถียรภาพของโครงสร้างแบบไพโรคลอร์ปรากฏอยู่เสมอ อย่างไรก็ตาม เมื่อ ทดลองใช้วิธีเติมสารเฟร์โรอิเล็กทริกชนิดที่มีเสถียรภาพของเฟสเพอร์รอฟสไกด์สูงๆ อย่างเช่น BaTiO<sub>3</sub> และ PZT ลงไปพบว่าวิธีนี้สามารถช่วยปรับปรุงเสถียรภาพของเฟสเพอร์รอฟสไกด์ใน สาร PZN ได้สำเร็จ นอกจากนี้ ยังพบอีกว่าการผลิตผง PMN และ PNN เฟสบริสุทธิ์ด้วยการใช้ สารตั้งต้นประเภทโคลัมไบต์จะใช้อุณหภูมิที่เหมาะสมสำหรับการแคลไซน์ต่ำกว่าในขณะที่ วิธีการใช้สารตั้งต้นประเภทโคลัมไบต์จะใช้อุณหภูมิที่เหมาะสมสำหรับการแคลไซน์ต่ำกว่าในขณะที่ วิธีการใช้สารตั้งต้นประเภทคอรันดัมจะให้ผงที่มีขนาดอนุภาคเล็กที่สุดได้เล็กกว่า

(II) ได้ทำการประดิษฐ์สารเซรามิกในระบบ  $\mathsf{Pb}(B_{1/3}\mathsf{Nb}_{2/3})\mathsf{O}_3$  ที่ B คือ  $\mathsf{Mg}$ ,  $\mathsf{Ni}$  หรือ  $\mathsf{Zn}$  ด้วย เทคนิคการเผาซินเทอร์แบบที่ไม่มีการเพิ่มความดัน และทำการประดิษฐ์สารเซรามิกบางสูตรโดย ใช้เทคนิคการเผาซินเทอร์แบบสองขั้นตอน แล้วศึกษาความสัมพันธ์ระหว่างองค์ประกอบทางเคมี เงื่อนไขในการเผาซินเทอร์ การเกิดเฟส การแน่นตัว โครงสร้างจุลภาค และสมบัติไดอิเล็กทริก ของผลิตภัณฑ์ที่ได้จากการเผาด้วยเงื่อนไขต่าง ๆ ซึ่งจากผลการทดลองพบว่า สามารถประดิษฐ์ สารเซรามิก PMN และ PNN ความหนาแน่นสูงที่มีโครงสร้างแบบเพอร์รอฟสไกด์ใด้สำเร็จทั้งใน กรณีที่ใช้สารตั้งต้นต้นแบบ B-site ประเภทโคลัมไบต์และประเภทคอรันดัม โดยเซรามิก PMN เฟสบริสุทธิ์ที่เตรียมด้วยวิธีการใช้สารตั้งต้นต้นแบบ B-site ประเภทคอรันดัมจะใช้อุณหภูมิใน การเผาซินเทอร์ที่ต่ำกว่าและสามารถแสดงสมบัติไดอิเล็กทริกที่ดีกว่าวิธีการใช้สารตั้งต้นแบบ *B*site ประเภทโคลัมใบต์ ในขณะที่ เซรามิก PNN เฟสบริสุทธิ์ที่เตรียมด้วยวิธีการใช้สารตั้งต้น ์ ต้นแบบ B-site ประเภทโคลัมใบต์กลับมีขนาดเกรนที่โตกว่า มีความหนาแน่นสูงกว่าและสามารถ แสดงสมบัติใดอิเล็กทริกที่ดีกว่าวิธีการใช้สารตั้งต้นต้นแบบ B-site ประเภทคอรันดัม สำหรับ ปัญหาที่ตรวจพบในกรณีของการประดิษฐ์สารเซรามิก PZN นั้น คาดว่าน่าจะเกิดจากอิทธิพล ของปัจจัยหลักๆ คือ เรื่องของค่าตัวประกอบ tolerance ลักษณะทางพันธะเคมีและปัจจัยทาง โครงสร้างต่างๆ อาทิเช่น ความเสถียรทางเวเลนต์ของแคตไอออน และความเป็นระเบียบของ แคตไอออน โดยพบว่าเฟสของสารที่มีโครงสร้างแบบไพโรคลอร์เหล่านี้ล้วนแต่ส่งผลเสียต่อ สมบัติใดอิเล็กทริกของผลิตภัณฑ์ที่ได้

### สรุปผล

โครงการวิจัยนี้ได้พัฒนากระบวนการเตรียมวัสดุเพอร์รอฟสไกด์รีแลกเซอร์เฟร์โรอิเล็กทริกใน ระบบ Pb(B<sub>1/3</sub>Nb<sub>2/3</sub>)O<sub>3</sub> ที่ B คือ Mg, Ni หรือ Zn ด้วยเทคนิค solid-state reaction ที่ใช้ สารประกอบกลุ่มในโอเบตเป็นสารตั้งต้นแบบ B-site และพบว่าการเตรียมผงบริสุทธิ์ของสารที่มี องค์ประกอบตามต้องการนั้นสามารถกระทำได้โดยอาศัยวิธีการควบคุมปัจจัยในกระบวนการ เตรียมให้มีความเหมาะสม โดยเฉพาะอย่างยิ่ง ชนิดของสารตั้งต้นแบบ B-site และเงื่อนไขใน การเผาแคลไซน์ ซึ่งโครงการนี้ได้แสดงให้เห็นถึงอิทธิพลของวิธีการใช้สารตั้งต้นแบบ B-site ที่มี ต่อการเกิดเฟส พัฒนาการของโครงสร้างจุลภาคและสมบัติใดอิเล็กทริกของสารเซรามิกในระบบ Pb(B<sub>1/3</sub>Nb<sub>2/3</sub>)O<sub>3</sub> อย่างซัดเจน นอกจากนี้ยังได้ค้นพบวิธีการประดิษฐ์สารเซรามิกกลุ่มเพอรอพส ใกด์ที่มีเฟสบริสุทธิ์ มีความหนาแน่นสูงและมีสมบัติใดอิเล็กตริกดีกว่าเทคนิคการเผาแบบดั้งเดิม โดยอาศัยเทคนิคการเผาซินเทอร์แบบสองขั้นตอนภายใต้เงื่อนไขที่เหมาะสม โดยพบว่าเทคนิค การเผาซินเทอร์แบบสองขั้นตอนนั้นมีผลสำคัญต่อการช่วยยับยั้งการเติบโตของเกรนในเซรามิก เพอร์รอฟสไกด์ PMN และ PNN

#### ข้อเสนอแนะสำหรับงานวิจัยในอนาคต

- (I) การศึกษาวิจัยต่อไปโดยเน้นไปที่การศึกษาถึงอิทธิพลของวิธีการใช้สารตั้งต้นแบบ A-site ที่มี ต่อการเกิดเฟส โครงสร้างจุลภาคและสมบัติไดอิเล็กทริกของวัสดุรีแลกเซอร์เฟร์โรอิเล็กทริกชนิด Pb(B<sub>1/3</sub>Nb<sub>2/3</sub>)O<sub>3</sub> เหล่านี้ อาจนำไปสู่การพัฒนากระบวนการสังเคราะห์สารที่มีศักยภาพใน รูปแบบใหม่ๆได้
- (II) การศึกษาวิจัยเพื่อปรับปรุงเสถียรภาพของเฟสเพอร์รอฟสไกด์ในสารกลุ่ม  $Pb(B_{1/3}Nb_{2/3})O_3$  เหล่านี้ด้วยการใช้วิธีเติมสารเฟร์โรอิเล็กทริกชนิดที่มีเสถียรภาพของเฟสเพอร์รอฟสไกด์สูง ๆ อย่างเช่น  $BaTiO_3$ ,  $PbTiO_3$  หรือ PZT ก็เป็นประเด็นที่น่าสนใจ แต่ก็ควรจะต้องพิจารณาถึง ผลกระทบข้างเคียงและความเหมาะสมของปริมาณสารที่จะใช้เติมลงไป
- (III) งานวิจัยในอนาคตที่มุ่งเน้นเรื่องการตรวจวิเคราะห์พื้นผิว การตรวจสอบโครงสร้างจุลภาค โดยเฉพาะที่บริเวณขอบเกรนและการตรวจสอบสมบัติเฟร์โรอิเล็กทริกของวัสดุเหล่านี้ น่าจะช่วย เสริมสร้างความรู้ความเข้าใจในเรื่องของสารรีแลกเซอร์เฟร์โรอิเล็กทริกกลุ่มเพอรอพสไกด์ให้มี ความลึกซึ้งมากยิ่งขึ้น

**คำหลัก:** รีแลกเซอร์เฟร์โรอิเล็กทริก, เพอร์รอฟสไกด์, สารตั้งต้นแบบ *B*-site, สมบัติไดอิเล็กทริก

#### **Executive Summary**

โครงการวิจัยนี้ได้มุ่งเน้นการศึกษาถึงอิทธิพลของเทคนิควิธีการใช้สารตั้งต้นแบบ *B*-site ที่มีต่อการเกิดเฟส โครงสร้างจุลภาคและสมบัติไดอิเล็กทริกของวัสดุรีแลกเซอร์เฟร์โรอิเล็กทริกชนิด Pb( $B_{1/3}$ Nb<sub>2/3</sub>)O<sub>3</sub> โดยสามารถสรุปเนื้อหาสาระสำคัญของงานวิจัยออกได้เป็นสองส่วนหลักคือ 1) ส่วนของกระบวนการเตรียมผง และ 2) ส่วนของกระบวนการประดิษฐ์เซรามิก ดังนี้

ในส่วนแรก ทางผู้วิจัยได้ทำการศึกษาและพัฒนากระบวนการสังเคราะห์ผงเพอรอฟสไกด์ สูตรต่าง ๆในระบบ  $Pb(B_{1/3}Nb_{2/3})O_3$  ได้แก่  $Pb(Mg_{1/3}Nb_{2/3})O_3$  (PMN),  $Pb(Ni_{1/3}Nb_{2/3})O_3$  (PNN), และ  $Pb(Zn_{1/3}Nb_{2/3})O_3$  (PZN) ด้วยการใช้เทคนิค solid-state reaction ร่วมกับการใช้สารตั้งต้น กลุ่มในโอเบตแบบ B-site ได้แก่  $MgNb_2O_6$ ,  $Mg_4Nb_2O_9$ ,  $NiNb_2O_6$ ,  $Ni_4Nb_2O_9$ ,  $ZnNb_2O_6$ , และ  $Zn_3Nb_2O_8$  เป็นหลัก พร้อมทั้งทำการศึกษาความสัมพันธ์ระหว่างปัจจัยในกระบวนการเตรียม ได้แก่ สารตั้งต้น วิธีการบดย่อย อุณหภูมิที่ใช้ในการเผา ระยะเวลาเผาแช่ อัตราการขึ้นและลง ของอุณหภูมิ กับพฤติกรรมการเกิดเฟส สัณฐาน การแจกแจงของขนาดอนุภาคผงที่ได้ ซึ่งจาก ผลการวิจัยพบว่า สามารถทำการพัฒนากระบวนการสังเคราะห์ผง PMN และ PNN ให้มีความ บริสุทธิ์สูงได้เป็นผลสำเร็จด้วยการเลือกใช้สารตั้งต้นแบบ B-site และเงื่อนไขในการเผาแคลไซน์ ที่เหมาะสม และยังสามารถทำการพัฒนาเทคนิคการสังเคราะห์สารประกอบกลุ่มในโอเบตสูตร  $Ni_4Nb_2O_9$ ,  $Zn_3Nb_2O_8$  รวมถึงสารเพอรอฟสไกด์ PMN และ PNN โดยใช้สารตั้งต้นกลุ่ม corundum ได้เป็นผลสำเร็จเป็นครั้งแรกอีกด้วย

ในส่วนที่สอง ทางผู้วิจัยได้ทำการศึกษาและพัฒนากระบวนการประดิษฐ์เชรามิกจากการ ใช้ผงสูตรต่างๆที่เตรียมได้จากการวิจัยในส่วนแรก ด้วยการใช้เทคนิคการเผาซินเทอร์แบบดั้งเดิม และแบบดัดแปลง พร้อมทั้งทำการศึกษาความสัมพันธ์ระหว่างปัจจัยในกระบวนการเตรียม ได้แก่ อุณหภูมิที่ใช้ในการเผา ระยะเวลาเผาแช่ อัตราการขึ้นและลงของอุณหภูมิ กับพฤติกรรมการเกิด เฟส การแน่นตัว โครงสร้างจุลภาค และสมบัติไดอิเล็กทริกของสารเซรามิกที่ได้ ซึ่งจาก ผลการวิจัยพบว่า สามารถทำการประดิษฐ์สารเซรามิกสูตรต่างๆเหล่านี้ให้มีความหนาแน่นและมี ความบริสุทธิ์สูงได้เป็นผลสำเร็จด้วยการเลือกใช้เงื่อนไขในการเผาซินเทอร์ที่เหมาะสม และยัง สามารถทำซ้ำใหม่ได้ดีอย่างแม่นยำ ยกเว้นกรณีของสาร PZN เท่านั้นที่จำเป็นต้องมีการเติมสาร เฟร์โรอิเล็กทริกชนิดที่มีความเสถียรของเฟสเพอร์รอฟสไกด์สูงอย่าง BT และ PZT เข้ามาช่วยใน การก่อเกิดเฟสเพอร์รอฟสไกด์ด้วย โดยพบว่าสารเซรามิกเหล่านี้สามารถแสดงพฤติกรรมของ ความเป็นเฟร์โรอิเล็กทริก ที่มีการแน่นตัวและสมบัติไดอิเล็กทริกเปลี่ยนแปลงไปตามชนิดของ สารตั้งตันแบบ B-site เทคนิคในการเผาและเงื่อนไขในการเผาที่เลือกใช้เป็นปัจจัยสำคัญ

# เนื้อหางานวิจัย

# 1. ความสำคัญและที่มาของปัญหา

วัสดุในกลุ่มเพอรอพสไกด์รีแลกเซอร์เฟร์โรอิเล็กทริกชนิดในโอเบตที่มีตะกั่วเป็น องค์ประกอบหลัก สูตร Pb(B<sub>1/3</sub>Nb<sub>2/3</sub>)O<sub>3</sub> โดย B เป็นแคตไอออนประจุ 2+ เช่น Pb(Mg<sub>1/3</sub>Nb<sub>2/3</sub>)O<sub>3</sub> หรือ PMN, Pb(Ni<sub>1/3</sub>Nb<sub>2/3</sub>)O<sub>3</sub> หรือ PNN, และ Pb(Zn<sub>1/3</sub>Nb<sub>2/3</sub>)O<sub>3</sub> หรือ PZN นั้น จัดว่าเป็นวัสดุที่ ได้รับความสนใจในการศึกษาคันคว้าอย่างกว้างขวางมาเป็นเวลานานทั้งในเชิงวิชาการและเชิง พาณิชย์ สำหรับตัวอย่างของการนำวัสดุเหล่านี้มาใช้เป็นชิ้นส่วนและอุปกรณ์อิเล็กทรอนิกส์ ประเภทต่าง ๆ ได้แก่ capacitors, sensors, transducers, non-destructive testing detectors และอุปกรณ์ทางการแพทย์ชนิดต่าง ๆ เป็นต้น [1-4] วัสดุที่มีความเหมาะสมสำหรับการนำมาใช้ ในงานเหล่านี้ต้องมีค่าคงที่ไดอิเล็กทริกสูงอยู่ในช่วงอุณหภูมิและความถี่ที่ครอบคลุมการทำงาน ของอุปกรณ์ มีการสูญเสียพลังงานในระหว่างการใช้งานที่ต่ำ และต้องทำการเตรียมได้ง่าย มี ความเสถียรของเฟสที่ต้องการสูงและสามารถหาวัตถุดิบได้ง่าย เป็นต้น [4-6] การผลิตวัสดุใน กลุ่มนี้มักจะมีปัญหาเรื่องการควบคุมปริมาณสารสัมพันธ์ของสารเป้าหมาย โดยมีปัจจัยหลาย ประการที่เข้ามาเกี่ยวข้อง นับตั้งแต่การคัดเลือกชนิดและคุณภาพของสารตั้งต้นที่ใช้ วิธีการ สังเคราะห์ผงที่ใช้ ประสิทธิภาพของแต่ละวิธีในการทำให้สารองค์ประกอบสามารถเข้ากันได้ดีจน ก่อเกิดเป็นเฟสที่มีสูตรตรงตามที่ออกแบบไว้ และเทคนิคการเผาซินเทอร์เพื่อประดิษฐ์สารเหล่านี้ ให้กลายเป็นเซรามิก ที่มีทั้งความหนาแน่นและความบริสุทธิ์ของเฟสที่ต้องการสูงๆ

สำหรับการพัฒนาแบบก้าวกระโดดของการใช้เทคนิค solid-state reaction ผลิตสารใน กลุ่มเพอรอพสไกด์รีแลกเซอร์เฟร์โรอิเล็กทริกชนิดที่มีตะกั่วเป็นองค์ประกอบหลัก จะอาศัย วิธีการแบบ B-site precursor [7-12] โดยในขั้นแรกจะนำสารองค์ประกอบชนิด B กับ  ${
m Nb_2O_5}$  มา ทำปฏิกิริยากันก่อน แล้วจึงนำสารผลิตภัณฑ์มาทำปฏิกิริยากับ PbO ในขั้นที่สอง เพื่อให้เกิดเป็น สารเป้าหมาย อย่างไรก็ตาม การวิจัยที่มุ่งสังเคราะห์สารตั้งต้นแบบ B-site ชนิดที่มีโครงสร้าง แบบ columbite โดยตรงนั้นยังมีอยู่น้อย ส่วนการสังเคราะห์สารตั้งต้นแบบ B-site โครงสร้างแบบอื่นๆยิ่งมีน้อยลงไปอีก นอกจากนี้การวิจัยเรื่องเทคนิคการเผาและอิทธิพลของ ้ ปัจจัยในการเผาซินเทอร์ที่มีต่อการเกิดเฟส โครงสร้างจุลภาคและสมบัติไดอิเล็กทริกที่สารเหล่านี้ แสดงออกมาก็มีความน่าสนใจอย่างยิ่ง ด้วยเหตุผลดังกล่าว ทางผู้วิจัยจึงสนใจที่จะทำการวิจัย และพัฒนากระบวนการสังเคราะห์สารรีแลกเซอร์เฟร์โรอิเล็กทริกชนิด  $Pb(B_{1/3}Nb_{2/3})O_3$  ที่ B เป็น ไอออน  ${\rm Mg}^{2^+}$ ,  ${\rm Ni}^{2^+}$  และ  ${\rm Zn}^{2^+}$  ได้แก่  ${\rm Pb}({\rm Mg}_{1/3}{\rm Nb}_{2/3}){\rm O}_3$ ,  ${\rm Pb}({\rm Ni}_{1/3}{\rm Nb}_{2/3}){\rm O}_3$  และ  ${\rm Pb}({\rm Zn}_{1/3}{\rm Nb}_{2/3}){\rm O}_3$ ์ด้วยวิธีการแบบ *B*-site precursors โดยอาศัยเทคนิค solid-state reaction เปรียบเทียบกัน รวมถึงการศึกษาความสัมพันธ์ระหว่างปัจจัยในกระบวนการเตรียม การเกิดเฟส โครงสร้าง จุลภาคและสมบัติไดอิเล็กทริกของเซรามิกเหล่านี้อย่างเป็นระบบ ควบคู่กันไปกับการศึกษาและ พัฒนากระบวนการสังเคราะห์สารประกอบกลุ่มในโอเบตชนิดต่างๆ ด้วยเทคนิค solid-state reaction เพื่อจะได้นำมาใช้เป็นสารตั้งต้นแบบ B-site precursors ต่อไป

## 2. วัตถุประสงค์

- 2.1 เพื่อศึกษาและพัฒนากระบวนการสังเคราะห์สารในกลุ่มรีแลกเซอร์เฟร์โรอิเล็กทริก  $Pb(B_{1/3}Nb_{2/3})O_3$  ชนิดที่ B เป็นไอออน  $Mg^{2^+}$ ,  $Ni^{2^+}$  และ  $Zn^{2^+}$  ด้วยวิธีการแบบ B-site precursors โดยอาศัยเทคนิค solid-state reaction
- 2.2 เพื่อศึกษาและพัฒนากระบวนการสังเคราะห์สารประกอบกลุ่มในโอเบตชนิดต่างๆ ด้วย เทคนิค solid-state reaction เพื่อนำมาใช้เป็นสารตั้งต้นแบบ *B*-site precursors ต่อไป
- 2.3 เพื่อศึกษาอิทธิพลของปัจจัยหลักในกระบวนการสังเคราะห์สารด้วยเทคนิค solid-state reaction ที่มีต่อพฤติกรรมการก่อเกิดเฟส สัณฐานวิทยาและองค์ประกอบทางเคมีระดับจุลภาค ของผงสารรีแลกเซอร์เฟร์โรอิเล็กทริก
- 2.4 เพื่อศึกษาอิทธิพลของปัจจัยหลักในกระบวนการเผาซินเทอร์ที่มีต่อพฤติกรรมการก่อ เกิดเฟส โครงสร้างจุลภาคและสมบัติไดอิเล็กทริกของเซรามิกรีแลกเซอร์เฟร์โรอิเล็กทริก
- 2.5 เพื่อศึกษาความสัมพันธ์ระหว่างปัจจัยในกระบวนการเตรียม การก่อเกิดเฟส โครงสร้าง และสมบัติใดอิเล็กทริกของเซรามิกในกลุ่มเพอรอพสไกด์รีแลกเซอร์เฟร์โรอิเล็กทริก Pb(B<sub>1/3</sub>Nb<sub>2/3</sub>)O<sub>3</sub>

#### 3. ระเบียบวิธีวิจัย

โครงการวิจัยนี้มุ่งเน้นเรื่อง การเตรียมและการหาลักษณะเฉพาะของผงและเซรามิกของสาร ในกลุ่มเพอรอพสไกด์รีแลกเซอร์เฟร์โรอิเล็กทริกชนิด  $Pb(B_{1/3}Nb_{2/3})O_3$  ด้วยวิธีการผสมออกไซด์ แบบดั้งเดิม เปรียบเทียบกับวิธีการใช้สารประกอบกลุ่มในโอเบตชนิด columbite และชนิดอื่นๆ เช่น corundum เป็นสารตั้งต้น แบบ B-site precursor โดยมีรายละเอียดดังนี้

- 3.1 สังเคราะห์สาร PMN, PNN และ PZN ด้วยวิธีการผสมออกไซด์แบบดั้งเดิมโดยใช้เทคนิค solid-state reaction เพื่อใช้เป็นสารชุดควบคุม
- 3.2 สังเคราะห์สารประกอบกลุ่มในโอเบตชนิดที่มีโครงสร้างแบบ columbite ได้แก่ MgNb<sub>2</sub>O<sub>6</sub>, NiNb<sub>2</sub>O<sub>6</sub>, และ ZnNb<sub>2</sub>O<sub>6</sub> และชนิดอื่น ๆ ได้แก่ Mg<sub>4</sub>Nb<sub>2</sub>O<sub>9</sub>, Ni<sub>4</sub>Nb<sub>2</sub>O<sub>9</sub>, และ Zn<sub>3</sub>Nb<sub>2</sub>O<sub>8</sub> ด้วยการ ใช้เทคนิค solid-state reaction
- 3.3 สังเคราะห์สาร PMN, PNN และ PZN ด้วยการใช้สารที่เตรียมได้จากข้อ 3.2 พร้อมกับ ศึกษาอิทธิพลของปัจจัยในกระบวนการสังเคราะห์สารเหล่านี้ ที่มีต่อการเกิดเฟส สัณฐานวิทยา และองค์ประกอบทางเคมีระดับจุลภาคของสารแต่ละสูตร

- 3.4 นำผง PMN, PNN และ PZN ที่ได้มาขึ้นรูปแล้วประดิษฐ์เป็นเซรามิกด้วยการเผาซินเทอร์ พร้อมกับศึกษาอิทธิพลของปัจจัยในกระบวนการเผาที่มีต่อการเกิดเฟส โครงสร้างจุลภาคและ สมบัติไดอิเล็กทริกของเซรามิกที่ได้
- 3.5 ศึกษาความสัมพันธ์ระหว่างปัจจัยในกระบวนการเตรียม การเกิดเฟส โครงสร้างจุลภาค และสมบัติใดอิเล็กทริกของเซรามิกเหล่านี้

## 4. ประโยชน์ที่ได้รับจากโครงการวิจัยนี้

- 4.1 องค์ความรู้ใหม่ในการสังเคราะห์สารในกลุ่มเพอรอพสไกด์วีแลกเซอร์เฟร์โรอิเล็กทริก Pb( $B_{1/3}$ Nb $_{2/3}$ )O $_3$  ชนิด Pb(Mg $_{1/3}$ Nb $_{2/3}$ )O $_3$ , Pb(Ni $_{1/3}$ Nb $_{2/3}$ )O $_3$  และPb(Zn $_{1/3}$ Nb $_{2/3}$ )O $_3$  ด้วยการใช้ เทคนิค solid-state reaction ที่มีการนำสารประกอบชนิดใหม่ ๆมาทำเป็นสารตั้งต้นแบบ B-site
- 4.2 องค์ความรู้ใหม่ในการสังเคราะห์สารประกอบกลุ่มในโอเบต ชนิด  $MgNb_2O_6$ ,  $NiNb_2O_6$ ,  $ZnNb_2O_6$ ,  $Mg_4Nb_2O_9$ ,  $Ni_4Nb_2O_9$ , และ  $Zn_3Nb_2O_8$  ด้วยเทคนิค solid-state reaction
- 4.3 องค์ความรู้ใหม่ในการศึกษาอิทธิพลของเทคนิคและเวลาในการบดย่อย รวมถึงเงื่อนไขใน การแคลไซน์ที่มีต่อการเกิดเฟสและสัณฐานของสารรีแลกเซอร์เฟร์โรอิเล็กทริก Pb(B<sub>1/3</sub>Nb<sub>2/3</sub>)O<sub>3</sub> และสารประกอบกลุ่มในโอเบตชนิดต่างๆ
- 4.4 องค์ความรู้ใหม่ในการศึกษาอิทธิพลของเทคนิคและเงื่อนไขในการเผาซินเทอร์ที่มีต่อการ เกิดเฟส โครงสร้างจุลภาคและสมบัติไดอิเล็กทริกของเซรามิกเฟร์โรอิเล็กทริก Pb(B<sub>1/3</sub>Nb<sub>2/3</sub>)O<sub>3</sub>
- 4.5 องค์ความรู้ใหม่ในเรื่องของความสัมพันธ์ระหว่างปัจจัยในกระบวนการเตรียม การเกิดเฟส โครงสร้างจุลภาคและสมบัติไดอิเล็กทริกของเซรามิกเฟร์โรอิเล็กทริก Pb(B<sub>1/3</sub>Nb<sub>2/3</sub>)O<sub>3</sub>
- 4.6 องค์ความรู้ที่สามารถนำไปใช้เป็นกรณีศึกษาพัฒนาการเรียนการสอนในหลักสูตรวัสดุ ศาสตร์ที่ทีมผู้วิจัยรับผิดชอบอยู่ รวมถึงการนำไปใช้ออกแบบต่อยอดการทำงานวิจัย
- 4.7 ผลงานวิจัยในรูปของสิ่งตีพิมพ์ ได้แก่ สิ่งตีพิมพ์ในวารสารทางวิชาการต่าง ๆและการ นำเสนอผลงานในการประชุมวิชาการ
- 4.8 บุคลากรที่มีทักษะและความรู้ทางด้านสารเฟร์โรอิเล็กทริกกลุ่มเพอรอพสไกด์และแนวทาง ในการกำหนดหัวข้อวิทยานิพนธ์สำหรับการพัฒนาบุคลากรอย่างต่อเนื่อง
- 4.9 แนวทางการพัฒนาชุดโครงการวิจัยและการสร้างความร่วมมือของกลุ่มนักวิจัยภายใน สถาบันต้นสังกัดและระหว่างกลุ่มวิจัยต่าง ๆที่สนใจในเรื่องที่เกี่ยวข้องกัน

#### รายการเอกสารอ้างอิง

- 1) Moulson A.J., Herbert J.M. *Electroceramics: Materials, Properties and Applications*. 2<sup>nd</sup> ed. Wiley, Chichester, 2003.
- 2) Buchanan R.C. *Ceramic Materials for Electronics*. 3<sup>rd</sup> ed. Marcel Dekker, New York, 2004.
- 3) Uchino K. Ferroelectric Devices. Marcel Dekker, New York, 2000.
- 4) Haertling G.H. Ferroelectric ceramics: history and technology. *J Am Ceram Soc* 1999; **82**: 797-818.
- 5) Uchino K. Electrostrictive actuators: materials and applications. *Am Ceram Soc Bull.* 1986; **65**: 647-652.
- 6) Xu Y. Ferroelectric Materials and Their Applications. North-Holland, New York, 1991.
- 7) Swartz S.L., Shrout T.R. Fabrication of perovskite lead magnesium niobate. *Mater Res Bull.* 1982; **17**: 1245-1250.
- 8) Sekar, M.M.A., Halliyal A., Patil K.C. Synthesis, characterization and properties of lead-based relaxor ferroelectrics. *J Mater Res.* 1996; **11**: 1210-1218.
- 9) Halliyal A., Kumar U., Newnham R.E., Cross L.E. Stabilization of the perovskite phase and dielectric properties of ceramics in the Pb(Zn<sub>1/3</sub>Nb<sub>2/3</sub>)O<sub>3</sub>-BaTiO<sub>3</sub> system. Am Ceram Soc Bull. 1987; 66: 671-676.
- Shrout T.R., Halliyal A. Preparation of lead-based ferroelectric relaxors for capacitors. Am Ceram Soc Bull. 1987; 66: 704-711.
- 11) Ananta S., Thomas N.W. A modified two-stage mixed oxide synthetic route to lead magnesium niobate and lead iron niobate. J Eur Ceram Soc 1999; 19: 155-163.
- 12) Alberta E.F., Bhalla A.S. Low-temperature properties of lead nickel niobate ceramics. *Mater Lett* 2002; **54**: 47-54.

# สรุปผลลัพธ์ (Output) ที่ได้จากโครงการ

#### 1. ผลงานตีพิมพ์ในวารสารวิชาการนานาชาติ จำนวน 51 เรื่อง ได้แก่

- Wongmaneerung R., Sarakonsri T., Yimnirun R., Ananta S. Effects of milling method and calcination condition on phase and morphology characteristics of Mg<sub>4</sub>Nb<sub>2</sub>O<sub>9</sub> powders. *Mat Sci Eng B-Solid* 2006; 130: 246-253.
- Wongmaneerung R., Sarakonsri T., Yimnirun R., Ananta S. Effects of magnesium niobate precursor and calcination condition on phase and morphology of lead magnesium niobate powders. *Mat Sci Eng B-Solid* 2006; 132: 292-299.
- 3) Ngamjarurojana A., Khamman O., Yimnirun R., **Ananta S.** Effect of calcinations on phase formation and particle size of zinc niobate powders synthesized by solid-state reaction. *Mater Lett* 2006; **60**: 2867-2872.
- 4) Wongmaneerung R., Yimnirun R., **Ananta S.**, Guo R., Bhalla A.S. Polarization behavior in the two-stage sintered lead titanate ceramics. *Ferroelectrics Lets* 2006; **33**: 137-146.
- 5) Khamman O., Yimnirun R., **Ananta S.** Effect of calcination conditions on phase formation and particle size of nickel niobate powders synthesized by solid-state reaction. *Mater Lett* 2006; **61**: 639-643.
- 6) Khamman O., Yimnirun R., **Ananta S.** Phase and morphology evolution of corundum-type Ni<sub>4</sub>Nb<sub>2</sub>O<sub>9</sub> powders synthesized by solid-state reaction. *Mater Lett* 2007; **61**: 2565-2570.
- Yimnirun R., Wongmaneerung R., Wongsaenmai S., Ngamjarurojana A., Ananta S., Laosiritaworn Y. Temperature scaling of dynamic hysteresis in soft lead zirconate titanate bulk ceramic. Appl Phys Lett 2007; 90: 112906-1-3.
- Yimnirun R., Wongmaneerung R., Wongsaenmai S., Ngamjarurojana A., Ananta S., Laosiritaworn Y. Dynamic hysteresis and scaling behavior of hard lead zirconate titanate bulk ceramics. Appl Phys Lett 2007; 90: 112908-1-3.
- 9) Prasatkhetragarn A., Yimnirun R., **Ananta S.** Effect of calcination conditions on phase formation and particle size of Zn<sub>3</sub>Nb<sub>2</sub>O<sub>8</sub> powders synthesized by solid-state reaction. *Mater Lett* 2007; **61**: 3873-3877.
- 10)Khamman O., Yimnirun R., **Ananta S.** Effect of calcination conditions on phase formation and particle size of lead nickel niobate powders synthesized by using Ni<sub>4</sub>Nb<sub>2</sub>O<sub>9</sub> precursor. *Mater Lett* 2007; **61**: 4466-4470.

- 11) Chaisan W., Yimnirun R., **Ananta S.**, Cann D.P. Dielectric and ferroelectric properties of lead zirconate titanate-barium titanate ceramics prepared by a modified mixed-oxide method. *Mater Chem Phys* 2007; **104**: 113-118.
- 12) Rujiwatra A., Wongtawan C., Pinyo W., **Ananta S.** Sonocatalyzed hydrothermal preparation of lead titanate nanopowders. *Mater Lett* 2007; **61**: 4522-4524.
- 13)Khamman O., Sarakonsri T., Rujiwatra A., Laosiritaworn Y., Yimnirun R., Ananta S. Effect of milling time and calcination condition on phase formation and particle size of lead zirconate nanopowders prepared by vibro-milling. *J Mater Sci* 2007; 42: 8438-8446.
- 14)Yimnirun R., Ngamjarurojana A., Wongmaneerung R., Wongseanmai S., Ananta S., Laosiritaworn Y. Temperature scaling of ferroelectric hysteresis in hard lead zirconate titanate bulk ceramics. *Appl Phys A-Mater* 2007; 89: 737-741.
- 15) Wongsaenmai S., Yimnirun R., **Ananta S.**, Guo R., Bhalla, A.S. Effect of addition of BT on relaxor behavior of PIN-PT ceramics. *Integr Ferroelectr* 2007; **91**: 142-152.
- 16)Yimnirun R., Triamnak N., Ngamjarurojana A., Laosiritaworn Y., **Ananta S.** Dielectric properties of Pb(Zr<sub>1/2</sub>Ti<sub>1/2</sub>)O<sub>3</sub>-Pb(Zn<sub>1/3</sub>Nb<sub>2/3</sub>)O<sub>3</sub> ceramics under compressive stress. *Ferroelectrics* 2007; **355**: 257-263.
- 17) Prasatkhetragarn A., Yimnirun R., **Ananta S.** Effect of calcination condition on phase formation of zirconium titanate powders synthesized by the solid-state reaction. *Ferroelectrics* 2007; **356**: 203-208.
- 18) Chaisan W., Khamman O., Yimnirun R., **Ananta S.** A two-stage solid-state reaction to lead zirconate titanate powders. *Ferroelectrics* 2007; **356**: 242-246.
- 19) Yimnirun R., **Ananta S.**, Laosiritaworn Y., Ngamjarurojana A., Wongsaenmai S. Scaling behavior of dynamic ferroelectric hysteresis in soft PZT ceramics: stress dependence. *Ferroelectrics* 2007; **358**: 3-11.
- 20)Chaisan W., Yimnirun R., **Ananta S.** Changes in ferroelectric properties of barium titanate ceramic with compressive stress. *Phys Scr* 2007; **T129**: 205-208.
- 21)Yimnirun R., Wongsaenmai S., Wongmaneerung R., Wongdamnern N., Ngamjarurojana A., Ananta S., Laosiritaworn Y. Stress- and temperature-dependent scaling behavior of dynamic hysteresis in soft PZT bulk ceramics. *Phys Scr* 2007; T129: 184-189.

- 22)Wongseanmai S., Qu W., **Ananta S.**, Yimnirun R., Tan X. Effect of Ba-substitution on the structure and properties of Pb<sub>0.8</sub>Ba<sub>0.2</sub>[(In<sub>1/2</sub>Nb<sub>1/2</sub>)<sub>1-x</sub>Ti<sub>x</sub>]O<sub>3</sub> ceramics. *Appl Phys A-Mater* 2007; **88**: 757-761.
- 23) Wongmaneerung R., Tan X., McCallum R.W., Ananta S., Yimnirun R. Cation, dipole, and spin order in Pb(Fe<sub>2/3</sub>W<sub>1/3</sub>)O<sub>3</sub>-based magnetoelectric multiferroic compounds. *Appl Phys Lett* 2007; **90**: 242905.
- 24) Wongsaenmai S., **Ananta S.**, Yimnirun R., Guo R., Bhalla, A.S. Dielectric properties and relaxor behavior of PIN based system. *Ferroelectrics Lets* 2007; **34**: 36-45.
- 25)Khamman O., Yimnirun R., **Ananta S.** Effect of vibro-milling on phase formation and particle size of nickel niobate nanopowders. *Mat Sci Eng B-Solid* 2008; **150**: 12-17.
- 26)Ngamjarurojana A., Ural S., Park S.H., **Ananta S.**, Yimnirun R., Uchino K. Piezoelectric properties of low temperature sintering in Pb(Zr,Ti)O<sub>3</sub>-Pb(Zn,Ni)<sub>1/3</sub>Nb<sub>2/3</sub>O<sub>3</sub> ceramics for piezoelectric transformer applications. *Ceram Int* 2008; **34**: 705-708.
- 27)Laosiritaworn W., Khamman O., **Ananta S.**, Yimnirun R., Laosiritaworn Y. Artificial neural network modeling of ceramics powder preparation: application to NiNb<sub>2</sub>O<sub>6</sub>. *Ceram Int* 2008; **34**: 809-812.
- 28)Yimnirun R., Wongdamnern N., Triamnak N., Unruan M., Ngamjarurojana A., **Ananta S.**, Laosiritaworn Y. Stress-dependent scaling behavior of subcoercive field dynamic ferroelectric hysteresis in Pb(Zn<sub>1/3</sub>Nb<sub>2/3</sub>)O<sub>3</sub>-modified Pb(Zr<sub>1/2</sub>Ti<sub>1/2</sub>)O<sub>3</sub> ceramic. *J Appl Phys* 2008; **103**: 086105-1-3.
- 29) Wongmaneerung R., Guo R., Bhalla A.S., Yimnirun R., **Ananta S.** Thermal expansion properties of PMN-PT ceramics. *J Alloys Compds* 2008; **461**: 565-569.
- 30)Unruan M., Ngamjarurojana A., Laosiritaworn Y., **Ananta S.**, Yimnirun R. Influences of perpendicular compressive stress on the dielectric and ferroelectric properties of electrostrictive and piezoelectric Pb(Mg<sub>1/3</sub>Nb<sub>2/3</sub>)O<sub>3</sub>-PbTiO<sub>3</sub> ceramics. *J Appl Phys* 2008; **104**: 034101.
- 31)Khamman O., Yimnirun R., **Ananta S.** Effect of niobate B-site precursor on phase formation of lead nickel niobate powders *J Alloy Compd* 2008; **465**: 522-526.
- 32)Unruan M., Wongmaneerung R., Ngamjarurojana A., Laosiritaworn Y., **Ananta S.**, Yimnirun R. Changes in ferroelectric properties of ceramics in lead magnesium niobate-lead titanate system with compressive stress. *J Appl Phys* 2008; **104**: 064107.

- 33)Yimnirun R., Wongdamnern N., Triamnak N., Unruan M., Ngamjarurojana A., **Ananta S.**, Laosiritaworn Y. Scaling and stress dependence of sub-coercive field dynamic ferroelectric hysteresis in 0.6Pb(Zr<sub>1/2</sub>Ti<sub>1/2</sub>)O<sub>3</sub>-0.4Pb(Zn<sub>1/3</sub>Nb<sub>2/3</sub>)O<sub>3</sub> ceramic. *J Phys: Conden Mater.* 2008; **20**: 415202.
- 34)Yimnirun R., Wongdamnern N., Triamnak N., Sareein T., Unruan M., Ngamjarurojana A., **Ananta S.**, Laosiritaworn Y. Power-law scaling of sub-coercive field dynamic hysteresis response in 0.7Pb(Zr<sub>1/2</sub>Ti<sub>1/2</sub>)O<sub>3</sub>-0.3Pb(Zn<sub>1/3</sub>Nb<sub>2/3</sub>)O<sub>3</sub> ceramic. *J Phys D: Appl Phys* 2008; **41**: 205415.
- 35) **Ananta S.**, Yimnirun R., Khamman O. Effect of nickel niobate B-site precursors on phase formation, microstructure and dielectric properties of perovskite PNN ceramics. *Functional Materials Letters*, 2008; **1(3)**: 229-233.
- 36)Yimnirun R., Wongdamnern N., Triamnak N., Unruan M., Ngamjarurojana A., **Ananta S.**, Laosiritaworn S. Stress dependence and scaling of subcoercive field dynamic hysteresis in 0.5Pb(Zr<sub>1/2</sub>Ti<sub>1/2</sub>)O<sub>3</sub>-0.5Pb(Zn<sub>1/3</sub>Nb<sub>2/3</sub>)O<sub>3</sub> ceramic. *J Appl Phys* 2008; **104**: 104103-1-4.
- 37)Unruan M., Prasatkhetragarn A., Laosiritaworn Y., **Ananta S.**, Yimnirun R. Changes in dielectric properties of Pb(Zr<sub>1/2</sub>Ti<sub>1/2</sub>)O<sub>3</sub>-Pb(Co<sub>1/3</sub>Nb<sub>2/3</sub>)O<sub>3</sub> ceramics under compressive stress applied perpendicularly to the electric field. *J Phys D: Appl Phys* 2008; **41**: 245405-1-4.
- 38)Unruan M., Prasatkhetragarn A., Laosiritaworn Y., **Ananta S.**, Yimnirun R. Dielectric properties of PZT-PCN ceramics under compressive stress. *Phys Scr* 2008; **77**: 045702-1-4.
- 39)Unruan M., Wongsaenmai S., Laosiritaworn Y., **Ananta S.**, Yimnirun R. Changes in dielectric properties of Pb(In<sub>1/2</sub>Nb<sub>1/2</sub>)O<sub>3</sub>-PbTiO<sub>3</sub> ceramics under compressive stress applied perpendicularly to an electric field. *J Phys D: Appl Phys* 2008; **41**: 085406-1-5.
- 40)Prasatkhetragarn A., Vittayakorn N., **Ananta S.**, Yimnirun R., Cann D.P. Synthesis and dielectric and ferroelectric properties of ceramics in (1-x)Pb(Zr<sub>1/2</sub>Ti<sub>1/2</sub>)O<sub>3</sub>-xPb(Co<sub>1/3</sub>Nb<sub>2/3</sub>)O<sub>3</sub> system. *Jpn J Appl Phys* 2008; **47**: 998-1002.
- 41)Wongsaenmai S., Yimnirun R., **Ananta S.**, Guo R., Bhalla, A.S. Thermal expansion measurements in the relaxor ferroelectric PIN-PT system. *Mater Lett* 2008; **62**: 352-356.

- 42)Wongmaneerung R., Yimnirun R., **Ananta S.** Effect of two-stage sintering on phase formation, microstructure and dielectric properties of perovskite PMN ceramics derived from a corundum Mg<sub>4</sub>Nb<sub>2</sub>O<sub>9</sub> precursor. *Mater Chem Phys* 2009; 114: 569-575.
- 43) Wongdamnern N., Ngamjarurojana A., Laosiritaworn Y., **Ananta S.**, Yimnirun R. Dynamic ferroelectric hysteresis scaling of BaTiO<sub>3</sub> single crystals. *J Appl Phys* 2009; **105**: 044109.
- 44)Khamman O., Tan X., **Ananta S.**, Yimnirun R. The morphotropic phase boundary and electrical properties of (1-x)Pb(Zn<sub>1/2</sub>W<sub>1/2</sub>)O<sub>3</sub>-xPb(Zr<sub>0.5</sub>Ti<sub>0.5</sub>)O<sub>3</sub> ceramics. *J Mater Sci* 2009; **44**: 1868-1872.
- 45)Unruan M., Prasatkhetragarn A., Ngamjarurojana A., Laosiritaworn Y., **Ananta S.**, Yimnirun R. Dielectric and ferroelectric properties of lead zirconate titanate-lead nickel niobate ceramics under compressive stress. *J Appl Phys* 2009; **105**: 084111.
- 46) Wongmaneerung W., Yimnirun R., **Ananta S.** Effect of magnesium niobate precursors on phase formation, microstructure and dielectric properties of perovskite lead magnesium niobate ceramics. *J Alloy Compd* 2009; **477**: 805-810.
- 47) Chaisan W., Yimnirun R., **Ananta S.** Effect of vibro-milling time on phase formation and particle size of barium titanate nanopowders. *Ceram Int* 2009; **35**: 173-176.
- 48) Chaisan W., Yimnirun R., **Ananta S.** Preparation and characterization of ceramic nanocomposites in the PZT-BT system. *Ceram Int* 2009; **35**: 121-124.
- 49) Wongmaneerung W., Rujiwatra A., Yimnirun R., **Ananta S.** Fabrication and dielectric properties of lead titanate nanocomposites. *J Alloy Compd* 2009; **475**: 473-478.
- 50) Wongmaneerung W., Singjai P., Yimnirun R., **Ananta S.** Effects of SiC nanofibers addition on microstructure and dielectric properties of lead titanate ceramics. *J Alloy Compd* 2009; **475**: 456-462.
- 51)Wongmaneerung R., Yimnirun R, **Ananta S.** Fabrication and characterization of perovskite ferroelectric PMN/PT ceramic nanocomposites. *J Mater Sci* 2009; DOI 10.1007/s 10853-009-3621-6 (*Invited paper*).

#### 2. การนำผลงานวิจัยไปใช้ประโยชน์

#### 2.1 เชิงพาณิชย์

โครงการวิจัยนี้ได้สร้างองค์ความรู้ใหม่ในการสังเคราะห์สารกลุ่มเพอร์รอฟสไกด์รีแลก เซอร์เฟร์โรอิเล็กทริกชนิด Pb(B<sub>1/3</sub>Nb<sub>2/3</sub>)O<sub>3</sub> ด้วยการใช้สารตั้งต้นแบบ B-site ประเภทต่างๆ และ ยังได้พัฒนาเทคนิคการผลิตสารประกอบกลุ่มในโอเบตที่มีความบริสุทธิ์สูงด้วยต้นทุนต่ำ ซึ่ง ทั้งตัวสารเคมีสูตรต่างๆและเทคนิคที่ผลิตได้จากโครงการวิจัยนี้สามารถนำไปใช้ต่อยอดงานวิจัย ในสาขาอื่นๆที่เกี่ยวข้องรวมถึงการผลิตในเชิงอุตสาหกรรม นอกจากนี้ ยังเป็นการพัฒนาวิธีการ ผลิตวัสดุกลุ่มเพอร์รอฟสไกด์เฟร์โรอิเล็กทริกที่มีราคาแพงหลายๆสูตรขึ้นมาใช้เองภายในกลุ่ม วิจัยทำให้ช่วยลดการนำเข้าจากต่างประเทศได้อีกทางหนึ่ง

#### 2.2 เชิงนโยบาย

ผลการวิจัยที่ได้จากโครงการนี้ได้ถูกนำไปใช้ประกอบการวางแผนในการกำหนดทิศ ทางการทำงานวิจัยของทีมผู้ร่วมวิจัยทั้งสำหรับการต่อยอดและการแตกแขนงแนวทางในการทำ วิจัย รวมถึงการนำไปใช้เป็นฐานข้อมูลในการร่างข้อเสนอโครงการวิจัยสำหรับขอรับการ สนับสนุนทุนวิจัยจากแหล่งต่าง ๆของผู้ร่วมทีมวิจัยและนอกจากนี้ยังใช้ในการกำหนดหัวข้อวิจัย ของนักศึกษา ซึ่งเป็นส่วนหนึ่งของการส่งเสริมให้เกิดกลุ่มวิจัยแบบมีทิศทางมากขึ้นด้วย

#### 2.3 เชิงสาธารณะ

โครงการวิจัยนี้ได้สร้างเครือข่ายความร่วมมือระหว่างนักวิจัยรุ่นต่างๆทั้งที่เป็นชาวไทย และชาวต่างชาติ ได้แก่ ผศ.ดร. รัตติกร ยิ้มนิรัญ ภาควิชาฟิสิกส์และวัสดุศาสตร์ คณะ วิทยาศาสตร์ มหาวิทยาลัยเชียงใหม่ ในการศึกษาสมบัติทางไฟฟ้าของเซรามิกเหล่านี้ภายใต้ สภาวะที่มีแรงเค้น ความร่วมมือกับ ดร. อธิพงศ์ งามจารุโรจน์ ภาควิชาฟิสิกส์และวัสดุศาสตร์ คณะวิทยาศาสตร์ มหาวิทยาลัยเชียงใหม่ ในการขยายขอบเขตการวิจัยไปยังสารเซรามิกกลุ่ม อื่นๆที่มีสาร PZN เป็นองค์ประกอบหลัก ความร่วมมือกับ รศ. ดร. อภินภัส รุจิวัตร์ และ ผศ.ดร. ฐปนีย์ สาครศรี ภาควิชาเคมี คณะวิทยาศาสตร์ มหาวิทยาลัยเชียงใหม่ ในการพัฒนาวิธีการ ้สังเคราะห์สารเหล่านี้โดยใช้เทคนิคทางเคมี รวมถึงการตรวจวิเคราะห์ด้วยเทคนิคจุลทรรศน์ อิเล็กตรอนแบบทะลุผ่าน นอกจากนี้ก็ยังมีความร่วมมือกับ ดร. วรรณวิลัย ไชยสาร ดร.อรวรรณ คำมั่น และ ผศ.ดร. ยงยุทธ เหล่าศิริถาวร ภาควิชาฟิสิกส์และวัสดุศาสตร์ คณะวิทยาศาสตร์ มหาวิทยาลัยเชียงใหม่ ดร. เรวดี วงศ์มณีรุ่ง และ ดร. สุพัตรา วงศ์แสนใหม่ ภาควิชาฟิสิกส์ คณะ วิทยาศาสตร์ มหาวิทยาลัยแม่โจ้ ดร. อนุรักษ์ ประสาทเขตร์การ และ ดร. ปิยชนน์ เกษสุวรรณ ภาควิชาฟิสิกส์ มหาวิทยาลัยนเรศวรวิทยาเขตสารสนเทศพะเยา Prof. D.P. Cann (Oregon State University) Prof. X. Tan (Iowa State University) Prof. K. Uchino, Prof. A.S. Bhalla และ Prof. R. Guo (Penn State University) ประเทศสหรัฐอเมริกา และ Prof. R. Steven (Bath University) ประเทศสหราชอาณาจักร เป็นต้น

### 2.4 เชิงวิชาการ (พัฒนาการเรียนการสอน/สร้างนักวิจัยใหม่)

ผลการวิจัยที่ได้จากโครงการนี้ได้ถูกนำไปใช้พัฒนาการเรียนการสอนโดยการทำเป็น ตัวอย่างหรือเป็นกรณีศึกษาสำหรับประกอบการเรียนการสอนในกระบวนวิชาต่าง ๆในสาขาวิชา วัสดุศาสตร์ที่ทางทีมผู้วิจัยรับผิดชอบอยู่ เช่น ในกระบวนวิชา MATS 210723 Ferroelectric Materials, MATS 210743 Electroceramics, MATS 210741 Physics of Advanced Ceramics, MATS 210701 Characterization and Properties of Materials และ MATS 210703 Fabrication Processes of Materials นอกจากนี้ยังเป็นการช่วยสร้างนักวิจัยใหม่ โดย การฝึกฝนทักษะและประสบการณ์ในการทำงานวิจัยร่วมกันระหว่างนักศึกษาและคณาจารย์ที่ เป็นนักวิจัยใหม่ในทีม มีทั้งกิจกรรมการฝึกทักษะในการเขียน คิดวิเคราะห์และทบทวนบทความ ทางวิชาการเพื่อการเผยแพร่ การไปร่วมเสนอผลงานในการประชุมวิชาการต่าง ๆทั้งภายในและ ภายนอกประเทศ โดยที่โครงการวิจัยนี้ได้มีส่วนในการผลิตบุคลากรรุ่นใหม่ที่มีความเชี่ยวชาญใน สาขาวิชาออกมา ได้แก่ มหาบัณฑิตจำนวน 5 ท่าน ดุษฎีบัณฑิตจำนวน 6 ท่าน และคณาจารย์ นักวิจัยรุ่นใหม่ที่ได้รับทุนสนับสนุนจากทางสกว.และสกอ. ในเวลาต่อมาอีกจำนวน 9 ท่าน

- 3. ผลงานอื่น ๆ (เช่น ผลงานที่นำเสนอในการประชุมวิชาการระดับนานาชาติ) จำนวน 30 เรื่อง ได้แก่
- 1) Khamman O., Yimnirun R., Laosiritaworn Y., **Ananta S.** Effects of vibro-milling time and calcination on phase formation and particle size of lead zirconate nanopowders. In *Proceeding of the 5<sup>th</sup> Asian Meeting on Ferroelectrics (AFM-5)*, 3-7 Sept. 2006, Noda, Japan.
- 2) Ketsuwan P., Laosiritaworn Y., **Ananta S.**, Yimnirun R. Effect of Nb-doped on electrical properties of Pb(Zr<sub>0.52</sub>Ti<sub>0.48</sub>)O<sub>3</sub> ceramics. In *Proceeding of the 5<sup>th</sup> Asian Meeting on Electroceramics (AMEC-5)*, 10-14 Dec. 2006, Bangkok, Thailand.
- 3) Ngamjarurojana A., Ural S., Park S.H., **Ananta S.**, Yimnirun S., Uchino K. Piezoelectric property of low temperature sintering in Pb(Zr,Ti)O<sub>3</sub>-Pb(Zn,Ni)<sub>1/3</sub>Nb<sub>2/3</sub>O<sub>3</sub> ceramics for piezoelectric transformer applications. In *Proceeding of the 5<sup>th</sup> Asian Meeting on Electroceramics (AMEC-5)*, 10-14 Dec. 2006, Bangkok, Thailand.
- 4) Sukthomya W., Khamman O., **Ananta S.**, Yimnirun R., Laosiritaworn Y. Artificial neural network modeling of ceramics powder preparation: application to NiNb<sub>2</sub>O<sub>6</sub>. In *Proceeding of the 5<sup>th</sup> Asian Meeting on Electroceramics (AMEC-5)*, 10-14 Dec. 2006, Bangkok, Thailand.
- 5) Yimnirun R., Ngamjarorojana A., **Ananta** S., Triamnak N. Stress-dependent ferroelectric properties of ceramics in Pb(Zr<sub>1/2</sub>Ti<sub>1/2</sub>)O<sub>3</sub>-Pb(Zn<sub>1/3</sub>Nb<sub>2/3</sub>)O<sub>3</sub> system. In

- Proceeding of the 5<sup>th</sup> Asian Meeting on Electroceramics (AMEC-5), 10-14 Dec. 2006, Bangkok, Thailand.
- 6) Prasatkhetragarn A., Vittayakorn N., **Ananta S.**, Yimnirun R. Processing and electrical properties of ceramics in Pb(Zr<sub>1/2</sub>Ti<sub>1/2</sub>)O<sub>3</sub>-Pb(Zn<sub>1/3</sub>Nb<sub>2/3</sub>)O<sub>3</sub> system. In *Proceeding of the 5<sup>th</sup> Asian Meeting on Electroceramics (AMEC-5)*, 10-14 Dec. 2006, Bangkok, Thailand.
- 7) Ngamjarurojana A., Ural S., Park S.H., Ananta S., Yimnirun R., Uchino K. Piezoelectric and dielectric properties of MnO<sub>2</sub>-doped 0.2Pb(Zn<sub>1/3</sub>Nb<sub>2/3</sub>)O<sub>3</sub>-0.8Pb(Zr<sub>1/2</sub>Ti<sub>1/2</sub>)O<sub>3</sub> ceramic materials. In *Proceeding of the 5<sup>th</sup> Asian Meeting on Electroceramics (AMEC-5)*, 10-14 Dec. 2006, Bangkok, Thailand.
- 8) Wongmaneerung R., Udomporn A., Yimnirun R., **Ananta S.** Processing and properties of Pb(Mg<sub>1/3</sub>Nb<sub>2/3</sub>)O<sub>3</sub>-PbTiO<sub>3</sub> based ceramics. In *Proceeding of the 5<sup>th</sup> Asian Meeting on Electroceramics (AMEC-5)*, 10-14 Dec. 2006, Bangkok, Thailand.
- 9) Wongmaneerung R., Chaisan W., Khamman O., Yimnirun R., **Ananta S.** Potential of vibro-milling technique for preparation of electroceramic nanopowders. In *Proceeding* of the 5<sup>th</sup> Asian Meeting on Electroceramics (AMEC-5), 10-14 Dec. 2006, Bangkok, Thailand.
- 10) Khamman O., Yimnirun R., **Ananta S.** A modified two-stage mixed oxide synthetic route to lead nickel niobate powders. In *Proceeding of the 5<sup>th</sup> Asian Meeting on Electroceramics (AMEC-5)*, 10-14 Dec. 2006, Bangkok, Thailand.
- 11) Chaisan W., Yimnirun R., **Ananta S.** Effect of vibro-milling time on phase formation and particle size of barium titanate nanopowders. In *Proceeding of the 5<sup>th</sup> Asian Meeting on Electroceramics (AMEC-5)*, 10-14 Dec. 2006, Bangkok, Thailand.
- 12) Khamman O., Yimnirun R., **Ananta S.** Effect of vibro-milling time and calcination condition on phase formation and particle size of nickel niobate nanopowders. In *Proceeding of the 5<sup>th</sup> Asian Meeting on Electroceramics (AMEC-5)*, 10-14 Dec. 2006, Bangkok, Thailand.
- 13) Wongdamnern N., Triamnak N., Laosiritaworn Y., **Ananta S.**, Yimnirun R. Comparative studies of dynamic hysteresis responses in hard and soft PZT ceramics. In *Proceeding of the 5<sup>th</sup> Asian Meeting on Electroceramics (AMEC-5)*, 10-14 Dec. 2006, Bangkok, Thailand.
- 14) **Ananta S.** Potential of physical solid-state reaction approach for preparation of smart-material nanopowders. In *Proceeding of Siam Physics Congress 2007: Physics and Technologies for Self-Reliance*, 22-24 March 2007, Nakorn Pathom, Thailand. (*Invited speaker*)

- 15) Yimnirun R., Wongsaenmai S., Wongmaneerung R., Wongdamnern N., Ngamjarurojana A., **Ananta S.**, Laosiritaworn Y. Stress- and temperature-dependent scaling behavior of dynamic hysteresis in soft PZT bulk ceramics. In *Proceeding of the International Symposium on Functional Materials* (ISFM-2007) 16-19 May 2007, Hangzhou, China.
- 16) Chaisan W., Yimnirun R., Ananta S. Effects of compressive stress of ferroelectric properties of BT ceramics. In *Proceeding of the International Symposium on Functional Materials* (ISFM-2007) 16-19 May 2007, Hangzhou, China.
- 17) Wongdamnern N., **Ananta S.**, Laosiritaworn Y., Yimnirun R. Stress-dependent scaling behavior of dynamic hysteresis in hard lead zirconate titanate ceramic. In *Proceeding of the International Conference on Materials for Advanced Technologies* (ICMAT-2007) 1-6 July 2007, Singapore.
- 18) Wongmaneerung R., Yimnirun R., **Ananta S.**, Bhalla A.S., Guo R. Thermal expansion measurement in the 0.9PMN-0.1PT ceramics. In *Proceeding of the International Conference on Materials for Advanced Technologies* (ICMAT-2007) 1-6 July 2007, Singapore.
- 19) Wongmaneerung R., Yimnirun R., **Ananta S.** Dielectric properties of PMN-PT ceramics. In *Proceeding of the First Thailand National Nanotechnology Conference*, 14-16 Aug. 2007, Chiang Mai, Thailand.
- 20) Khamman O., Yimnirun R., **Ananta S.** A two-stage solid state reaction of lead nickel niobate powders. In *Proceeding of* the Materials Science and Technology (MS&T'07), 16-20 Sept. 2007, Detroit, USA.
- 21) **Ananta S.** Potential of mechanical milling for preparation of smart-material nanopowders. In *Proceeding of the 2<sup>nd</sup> Progress in Advanced Materials: Micro/Nano Materials and Applications*, 16-18 Jan. 2008, Khon Kaen, Thailand. *(Invited lecture)*
- 22) Ngamjarurojana A., **Ananta S.**, Yimnirun R. Effect of Al<sub>2</sub>O<sub>3</sub> addition on dielectric, piezoelectric and ferroelectric properties of 0.2Pb(Zn<sub>1/3</sub>Nb<sub>2/3</sub>)O<sub>3</sub>-0.8Pb(Zr<sub>1/2</sub>Ti<sub>1/2</sub>)O<sub>3</sub> ceramics. In *Proceeding of the International Conference on Smart Materials:* Smart/Intelligent Materials and Nanotechnology-2008 (SmartMat'08 and IWOFM-2), 22-25 Apr. 2008, Chiang Mai, Thailand.
- 23) Unruan M., Wongmaneerung R., Laosiritaworn Y., **Ananta S.**, Yimnirun R. Changes in ferroelectric properties of 0.7PMN-0.3PT ceramics with compressive stress. In *Proceeding of the International Conference on Smart Materials: Smart/Intelligent*

- Materials and Nanotechnology-2008 (SmartMat'08 and IWOFM-2), 22-25 Apr. 2008, Chiang Mai, Thailand.
- 24) Unruan M., Ngamjarurojana A., Laosiritaworn Y., **Ananta S.**, Yimnirun R. Dielectric properties of Pb(Zr<sub>1/2</sub>Ti<sub>1/2</sub>)O<sub>3</sub>-Pb(Zn<sub>1/3</sub>Nb<sub>2/3</sub>)O<sub>3</sub> ceramics under compressive stress applied perpendicular to electric field. In *Proceeding of the 6<sup>th</sup> Asian Meeting of Ferroelectrics (AMF-6)*, 2-6 Aug. 2008, Taipei, Taiwan.
- 25) Unruan M., Prasatkhetragarn A., Ngamjarurojana A., Laosiritaworn Y., **Ananta S.**, Yimnirun R. Ferroelectric properties of Pb(Zr<sub>1/2</sub>Ti<sub>1/2</sub>)O<sub>3</sub>-Pb(Zn<sub>1/3</sub>Nb<sub>2/3</sub>)O<sub>3</sub> ceramics under compressive stress applied perpendicular to electric field. In *Proceeding of the 6<sup>th</sup> Asian Meeting of Ferroelectrics (AMF-6)*, 2-6 Aug. 2008, Taipei, Taiwan.
- 26) Wongdamnern N., Laosiritaworn Y., Ngamjarurojana A., **Ananta S.**, Yimnirun R. Stress-dependent scaling behavior of PZT-PZN ceramics under sub-coercive field condition. In *Proceeding of the 6<sup>th</sup> Asian Meeting of Ferroelectrics (AMF-6)*, 2-6 Aug. 2008, Taipei, Taiwan.
- 27) Srisombat L., Khamman O., Yimnirun R., **Ananta S.** XPS characterization of relaxor perovskite PNN ceramics prepared by corundum precursor method. In *Proceeding of the 6<sup>th</sup> Asian Meeting on Electroceramics (AMEC-6)*, 22-24 Oct. 2008, Tsukuba, Japan.
- 28) Ngamjarurojana A., Yimnirun R., **Ananta S.** Effect of vibro milling time on phase formation and particle size of ZnNb<sub>2</sub>O<sub>6</sub> nano-powders. In *Proceeding of the 6<sup>th</sup> Asian Meeting on Electroceramics (AMEC-6)*, 22-24 Oct. 2008, Tsukuba, Japan.
- 29) Unruan M., Prasatkhetragarn A., Ngamjarurojana A., Laosiritaworn Y., **Ananta S.**, Yimnirun R. Ferroelectric properties of Pb(Zr<sub>1/2</sub>Ti<sub>1/2</sub>)O<sub>3</sub>-Pb(Zn<sub>1/3</sub>Nb<sub>2/3</sub>)O<sub>3</sub> ceramics under compressive stress applied perpendicular to electric field. In *Proceeding of the 6<sup>th</sup> Asian Meeting on Electroceramics (AMEC-6)*, 22-24 Oct. 2008, Tsukuba, Japan.
- 30) Ananta S. Potential of nanocomposite technique for fabrication of smart ceramics. In Proceeding of the Inaugural CMU-UNSW Science Symposium 2009, 12-13 March 2009, Chiang Mai, Thailand. (Invited speaker)

# ภาคผนวก

# Reprint

ผลงานที่ได้ตีพิมพ์เผยแพร่ในวารสารวิชาการนานาชาติ (จำนวน 51 เรื่อง)





www.elsevier.com/locate/mseb

# Effects of milling method and calcination condition on phase and morphology characteristics of Mg<sub>4</sub>Nb<sub>2</sub>O<sub>9</sub> powders

R. Wongmaneerung <sup>a</sup>, T. Sarakonsri <sup>b</sup>, R. Yimnirun <sup>a</sup>, S. Ananta <sup>a,\*</sup>

<sup>a</sup> Department of Physics, Faculty of Science, Chiang Mai University, Chiang Mai, 50200, Thailand <sup>b</sup> Department of Chemistry, Faculty of Science, Chiang Mai University, Chiang Mai, 50200, Thailand

Received 9 November 2005; received in revised form 23 February 2006; accepted 19 March 2006

#### Abstract

Magnesium niobate,  $Mg_4Nb_2O_9$ , powders has been synthesized by a solid-state reaction. Both conventional ball- and rapid vibro-milling have been investigated as milling methods, with the formation of the  $Mg_4Nb_2O_9$  phase investigated as a function of calcination conditions by DTA and XRD. The particle size distribution of the calcined powders was determined by laser diffraction technique, while morphology, crystal structure and phase composition were determined via a combination of SEM, TEM and EDX techniques. The type of milling method together with the designed calcination condition was found to show a considerable effect on the phase and morphology evolution of the calcined  $Mg_4Nb_2O_9$  powders. It is seen that optimization of calcination conditions can lead to a single-phase  $Mg_4Nb_2O_9$  in both milling methods. However, the formation temperature and dwell time for single-phase  $Mg_4Nb_2O_9$  powders were lower with the rapid vibro-milling technique.

© 2006 Elsevier B.V. All rights reserved.

Keywords: Magnesium niobate; Milling; Calcination; Phase formation; X-ray diffraction

#### 1. Introduction

To date, magnesium niobate, Mg<sub>4</sub>Nb<sub>2</sub>O<sub>9</sub>, is one of the four possible magnesium-niobium oxides which have been recognized [1]. It has an ordered corundum-type hexagonal structure and has been investigated as a potential candidate for the synthesis of low loss microwave dielectric materials [2] and as buffer layer materials for manufacturing ferroelectric memory devices [3]. It is also an important material which shows self activated photoluminescence at room temperature [4]. You et al. [5] reported that cerium-doped Mg<sub>4</sub>Nb<sub>2</sub>O<sub>9</sub> exhibited improved luminescence properties. Recent work on the preparation of relaxor ferroelectric Pb(Mg<sub>1/3</sub>Nb<sub>2/3</sub>)O<sub>3</sub> [6,7], has also shown that Mg<sub>4</sub>Nb<sub>2</sub>O<sub>9</sub> is a better precursor than the columbite MgNb<sub>2</sub>O<sub>6</sub> [8,9] for the successful preparation of single-phase perovskite PMN which is becoming increasingly important for electroceramic components such as multilayer ceramic capacitors and electrostrictive actuators [10–12].

The evolution of a method to produce particular powders of precise stoichiometry and desired properties is complex, depending on a number of variables such as raw materials, their purities, processing history, temperature, time, etc. For example, the synthesis of stoichiometric lead magnesium niobate (PMN) using Mg<sub>4</sub>Nb<sub>2</sub>O<sub>9</sub> as a key precursor by a conventional solid-state reaction [7] requires an additional amount of PbO to convert the pyrochlore phase to PMN. However, the effect of excess PbO on PMN preparation is still a matter of debate, and appears to depend critically on the amount of PbO added [13-15]. Determination of the appropriate excess of PbO is currently a matter of trial and error. Furthermore, it has been reported that residual MgO present in the sample after the reaction has to be removed by treating with dilute nitric acid. Interestingly, a two-stage mixed oxide route has also been employed with minor modifications in the synthesis of Mg<sub>4</sub>Nb<sub>2</sub>O<sub>9</sub> itself [16,17]. In general, production of single-phase Mg<sub>4</sub>Nb<sub>2</sub>O<sub>9</sub> is not straightforward, as minor concentrations of the MgNb<sub>2</sub>O<sub>6</sub> phases and/or MgO inclusion are sometimes formed alongside the major phase of Mg<sub>4</sub>Nb<sub>2</sub>O<sub>9</sub> [15,17,18].

The development of  $Mg_4Nb_2O_9$  powders, to date, has not been as extensive as that of  $MgNb_2O_6$ . Much of the work concerning the compound  $Mg_4Nb_2O_9$  has been directed towards determining luminescent [4,5] or microwave dielectric [2] properties, and fabrication of  $Mg_4Nb_2O_9$  single crystal [19] or PMN powders [6,7]. Only limited attempts have been made to improve

<sup>\*</sup> Corresponding author. Tel.: +66 53 943367; fax: +66 53 943445. E-mail address: suponananta@yahoo.com (S. Ananta).

the yield of  $Mg_4Nb_2O_9$  powders derived from the solid-state reaction by optimizing milling method or calcination condition [13,20,21]. Moreover, the optimization of a combination between the milling method and the calcination condition in the mixed oxide process has not been studied. The purpose of this work was to explore a simple mixed oxide synthetic route for the production of  $Mg_4Nb_2O_9$  powders and compare the characteristics of the resulting powders. Two milling techniques were employed as the mixing method. A conventional ball milling was compared against a rapid vibro-milling in terms of their phase formation, particle size, morphology and microchemical compositions of the powders calcined at various conditions.

#### 2. Experimental procedure

The starting materials used in the present study were commercially available magnesium oxide, MgO and niobium oxide, Nb<sub>2</sub>O<sub>5</sub> (Fluka, 98% purity). These two oxide powders exhibited an average particle size in the range of 5.0–10.0 µm. Mg<sub>4</sub>Nb<sub>2</sub>O<sub>9</sub> powders were synthesized by the solid-state reaction of appropriate amounts of MgO and Nb2O5 powders that were mixed using two wet-milling methods (Fig. 1). The ball-milling operation was carried out for 48 h [7,13,20,22] with zirconia balls [22] in isopropanal. For comparison, a McCrone vibro-milling technique [9] was carried out on another set of powders with corundum cylindrical media in isopropanal for 1 h [21]. After drying at 120 °C for 2 h, various calcination conditions, i.e. temperatures ranging from 550 to 1100 °C and dwell times ranging from 2 to 5h with heating/cooling rates ranging from 10 to 30 °C/min. [22] were applied in order to investigate the formation of Mg<sub>4</sub>Nb<sub>2</sub>O<sub>9</sub> phase in powders from both milling methods. The reactions of the uncalcined powders taking place during heat treatment were investigated by thermal gravimetric and differ-

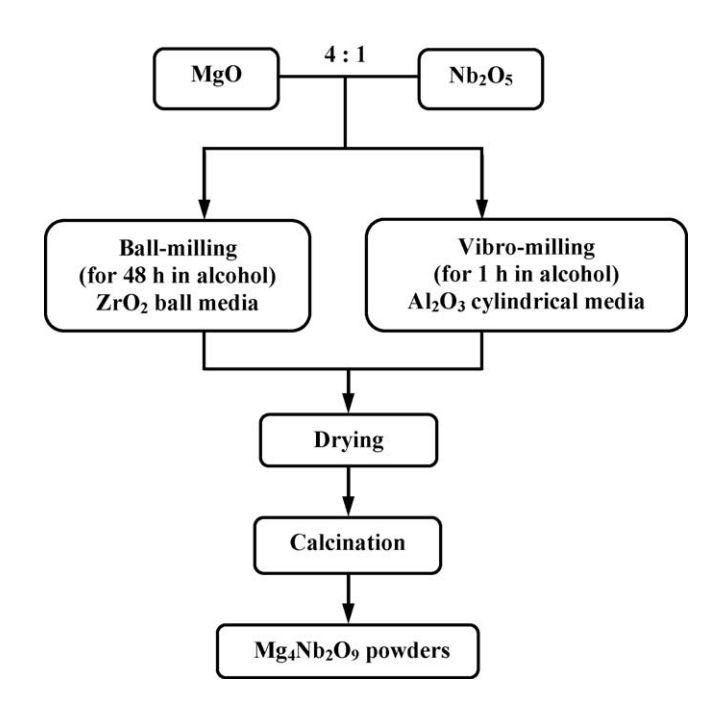


Fig. 1. Flow chart for preparing  $Mg_4Nb_2O_9$  powders by ball- and vibro-milling methods.

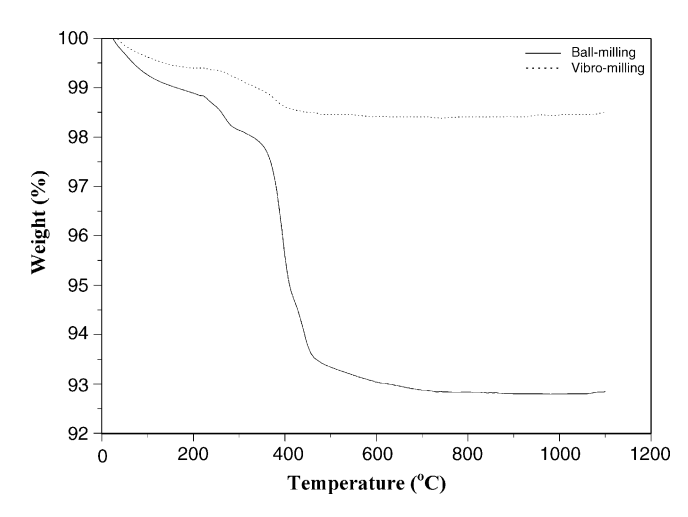


Fig. 2. TGA curves of the two  $MgO-Nb_2O_5$  mixtures derived from (a) ball-milling and (b) vibro-milling methods.

ential thermal analysis (TG-DTA, Shimadzu) using a heating rate of 10 °C/min. in air from room temperature up to 1100 °C. Calcined powders were subsequently examined by room temperature X-ray diffraction (XRD; Philips PW 1729 diffractometer) using Ni filtered Cu Kα radiation, to identify the phases formed and optimum calcination conditions for the manufacture of Mg<sub>4</sub>Nb<sub>2</sub>O<sub>9</sub> powder. The mean crystallite size was determined using the diffraction peak (104) of the corundum pattern by using Scherrer equation [23]. Particle size distributions of the powders were determined by laser diffraction technique (DIAS 1640 laser diffraction spectrometer), with the grain size and morphologies of the powders observed by scanning electron microscopy (SEM; JEOL JSM-840A). The chemical composition and structure of the phases formed were elucidated by transmission electron microscopy (CM 20 TEM/STEM) operated at 200 keV and fitted with an energy-dispersive X-ray (EDX) analyzer with an ultra-thin window. EDX spectra were quantified with the virtual standard peaks supplied with the Oxford Instruments eXL software. Powder samples were dispersed in solvent and deposited by pipette on to 3 mm holey copper grids for TEM observation. In addition, attempt was made to evaluate the crystal structures of the observed compositions/phases by correcting the XRD and TEM diffraction data.

#### 3. Results and discussion

TGA and DTA results for the mixture of MgO and Nb<sub>2</sub>O<sub>5</sub> milled by both methods are shown in Figs. 2 and 3, respectively. In general, similar trend of thermal characteristics is observed in both precursors. As shown in Fig. 2, the precursors prepared with both milling methods exhibit two distinct weight losses below 600 °C. The first weight loss occurs below 200 °C and the second one above 250 °C. In the temperature range from room temperature to  $\sim 150$  °C, both samples show small exothermic peaks in the DTA curves at  $\sim 120$  °C (Fig. 3), which are related to the first weight loss. These DTA peaks can be attributed to the decomposition of the organic species such as rubber lining from the milling process similar to those reported earlier [20]. In comparison between the two milling methods,

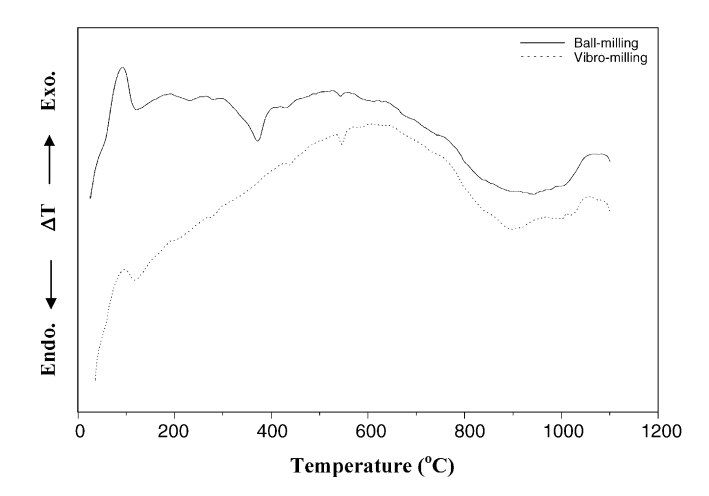


Fig. 3. DTA curves of the two MgO–Nb $_2$ O $_5$  mixtures derived from (a) ball-milling and (b) vibro-milling methods.

after the first weight loss, the ball-milling precursor (solid line) shows a slightly less weight loss over the temperature range of  $\sim\!150\!-\!250\,^{\circ}\text{C}$ , followed by a much more sharp fall in specimen weight with increasing temperature from  $\sim\!250\!-\!500\,^{\circ}\text{C}$ . This precursor also exhibits a significantly larger overall weight loss ( $\sim\!7.25\%$ ) than that of the vibro milling ( $\sim\!1.50\%$ ). This may be accounted for by the fact that the vibro-milling method provides faster size reduction rate and is able to enhance mixing capability with lower contamination possibility due to shorter milling time applied as suggested by several authors [9,24,25].

Corresponding to the second fall in specimen weight, by increasing the temperature up to  $\sim$ 700 °C, the solid-state reaction occurs between magnesium oxide and niobium oxide. The broad exothermic characteristic in both DTA curves represents that reaction, which has a maximum at ~550 and 620 °C for balland vibro-milling precursors, respectively. No significant weight loss was observed for the temperatures above 800 °C in the TG curves (Fig. 2), indicating that the minimum firing temperature to obtain MgO-Nb<sub>2</sub>O<sub>5</sub> compounds is in good agreement with XRD results (Figs. 4 and 5) and other workers [6,9,16]. However, the DTA curves show that there are other small peaks with maximum at ~1080 °C (for ball-milling) and 1050 °C (for vibromilling). It is to be noted that there is no obvious interpretation of these peaks, although it is likely to correspond to a phase transition reported by a number of workers [14,17,22]. The different temperature, intensities, and shapes of the thermal peaks for the two precursors are probably related to the different milling conditions between the two methods, and consequently caused by the removal of organic species (such as rubber lining) and reactivity of species differently milled (difference in size and size distribution) and mixed in the powders. These data were used to define the range of temperatures for XRD investigation to between 550 and 1100 °C.

To further study the phase development with increasing calcination temperature in each of the two precursors, they were calcined for 2h in air with a constant heating/cooling rates of  $10\,^{\circ}\text{C/min}$  at various temperatures, up to  $1100\,^{\circ}\text{C}$ , followed by phase analysis using XRD. As shown in Figs. 4 and 5, for the powders calcined at  $550\,^{\circ}\text{C}$ , only X-ray peaks of MgO and

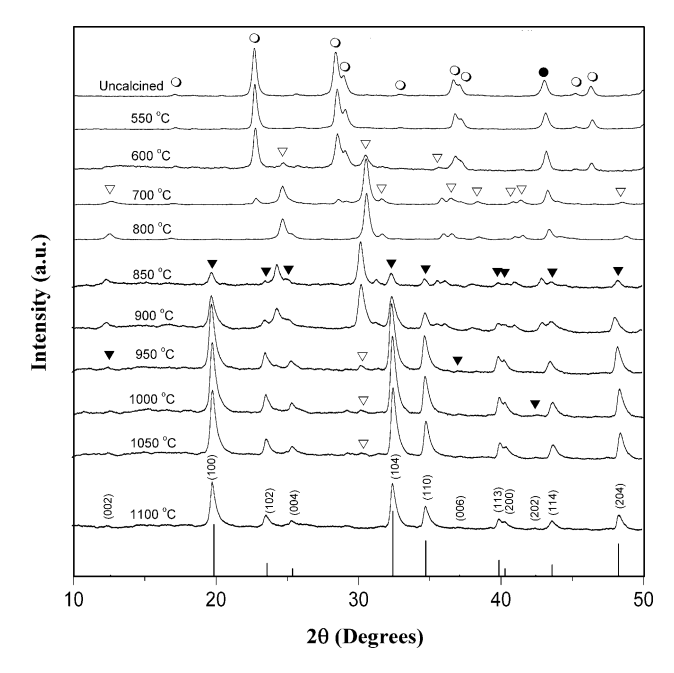


Fig. 4. Powder XRD patterns of the ball-milling powders calcined at various conditions for 2 h with constant heating/cooling rates of 10 °C/min (●, MgO; ○, Nb<sub>2</sub>O<sub>5</sub>; ∇, MgNb<sub>2</sub>O<sub>6</sub>; ▼, Mg<sub>4</sub>Nb<sub>2</sub>O<sub>9</sub>; ICDD file No. 38–1459: Mg<sub>4</sub>Nb<sub>2</sub>O<sub>9</sub>).

Nb<sub>2</sub>O<sub>5</sub> are present, indicating that the elimination of organic species occurs below 500 °C, which agrees with the TG-DTA results determined previously. The strongest reflections of the mixed phases of MgO ( $\bullet$ ) and Nb<sub>2</sub>O<sub>5</sub> ( $\bigcirc$ ) can be correlated with ICDD file Nos. 71–1176 [26] and 28–317 [27], respectively.

From Figs. 4 and 5, it is seen that little crystalline phase of  $MgNb_2O_6$  ( $\nabla$ ), earlier reported by many researchers [6,17,28] was found at 600 °C as separated phases in both calcined powders. This  $MgNb_2O_6$  phase (ICDD file No. 33–0875 [29])

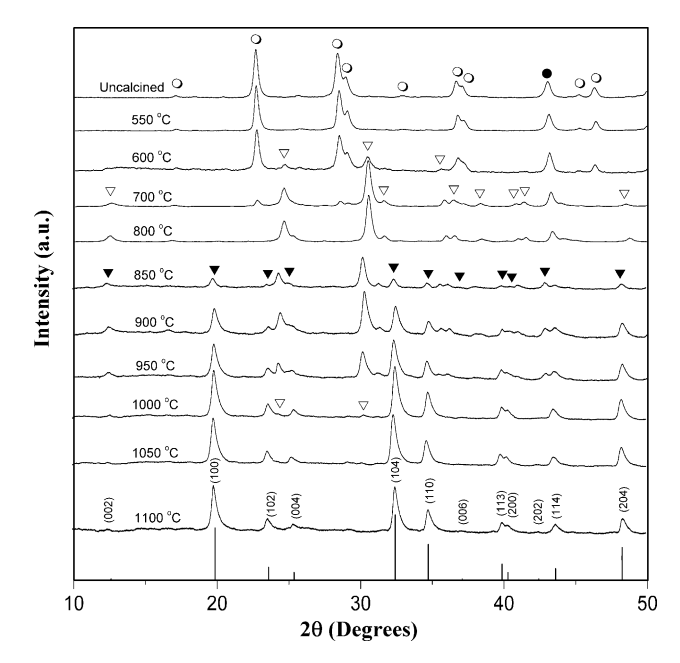


Fig. 5. Powder XRD patterns of the vibro-milling powders calcined at various conditions for 2 h with constant heating/cooling rates of  $10^{\circ}$ C/min ( $\bigcirc$ , MgO;  $\bigcirc$ , Nb<sub>2</sub>O<sub>5</sub>;  $\nabla$ , MgNb<sub>2</sub>O<sub>6</sub>;  $\nabla$ , Mg<sub>4</sub>Nb<sub>2</sub>O<sub>9</sub>; ICDD file No. 38–1459: Mg<sub>4</sub>Nb<sub>2</sub>O<sub>9</sub>).

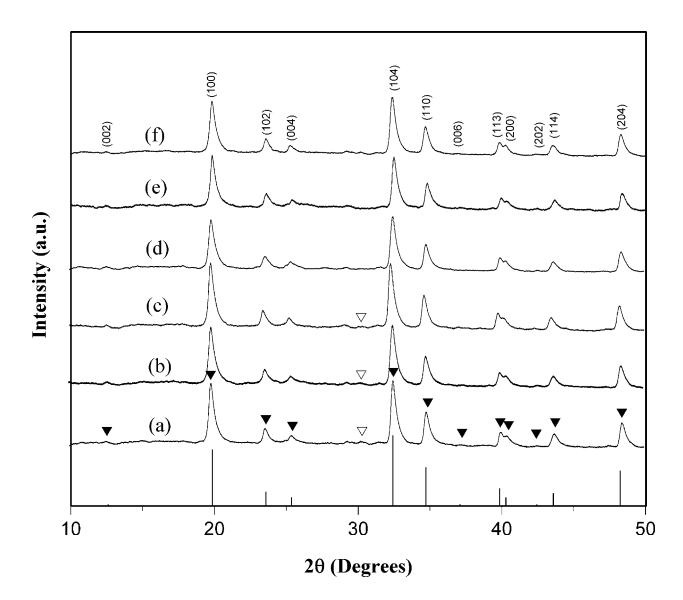


Fig. 6. Powder XRD patterns of the ball-milling powders calcined at  $1050\,^{\circ}$ C with heating/cooling rates of  $10\,^{\circ}$ C/min. for (a) 2 h, (b) 3 h, (c) 4 h and (d) 5 h, and at  $1050\,^{\circ}$ C for 5 h with heating/cooling rates of (e)  $20\,^{\circ}$ C/min and (f)  $30\,^{\circ}$ C/min ( $\nabla$ , MgNb<sub>2</sub>O<sub>6</sub>;  $\nabla$ , Mg<sub>4</sub>Nb<sub>2</sub>O<sub>9</sub>; ICDD file No. 38–1459: Mg<sub>4</sub>Nb<sub>2</sub>O<sub>9</sub>).

has a columbite-type structure with an orthorhombic unit cell (a = 5.70 Å, b = 14.19 Å and c = 5.032 Å) with space group  $I4_1/amd$  (No. 141), in agreement with literature [14,17,28]. As the temperature increased to 700 °C, the intensity of the MgNb<sub>2</sub>O<sub>6</sub> peaks in both calcined powders was further enhanced and became the predominant phase, in consistent with the TG-DTA results. From Figs. 4 and 5, it is seen that the peaks corresponding to MgO and Nb2O5 phases were completely eliminated after calcination at 800 °C in both powders. These observations are associated to the DTA peaks found at the same temperature range within the broad exothermic effects (Fig. 3). After calcination at 850 °C, some new peaks (▼) of the desired Mg<sub>4</sub>Nb<sub>2</sub>O<sub>9</sub> started to appear, mixing with MgNb<sub>2</sub>O<sub>6</sub> and MgO phases in both powders, in consistent with Ananta [20]. To a first approximation, this Mg<sub>4</sub>Nb<sub>2</sub>O<sub>9</sub> phase (ICDD file No. 38–1459 [30]) has a corundum-type structure with a hexagonal unit cell (a = 5.162 Å and c = 14.024 Å) with space group (no. 165), in consistent with other researchers [5,19,20].

Upon calcination at 1100 °C, the major phase of Mg<sub>4</sub>Nb<sub>2</sub>O<sub>9</sub> has been clearly identified in the ball-milling powders and most of second phases were eliminated. In particular, the peaks corresponding to MgNb<sub>2</sub>O<sub>6</sub> disappeared. However, in comparison, a single phase of Mg<sub>4</sub>Nb<sub>2</sub>O<sub>9</sub> is already formed when the vibromilling precursor was calcined at 1050 °C. Apart from calcination temperature, the effect of dwell time was also found to be significant (Figs. 6 and 7). It is seen that an essentially monophasic Mg<sub>4</sub>Nb<sub>2</sub>O<sub>9</sub> of corundum structure is obtainable in the ball-milling powders when the dwell time was extended to 5 h at 1050 °C (Fig. 6), which is 3 h longer than that of the vibromilling precursor (Fig. 7). In this work, an attempt was also made to calcine these powders under various heating/cooling rates (Figs. 6(d-f) and 7(e-g)). In this connection, it is shown that the yield of Mg<sub>4</sub>Nb<sub>2</sub>O<sub>9</sub> phase did not vary significantly with different heating/cooling rates ranging from 10 to 30 °C/min, in

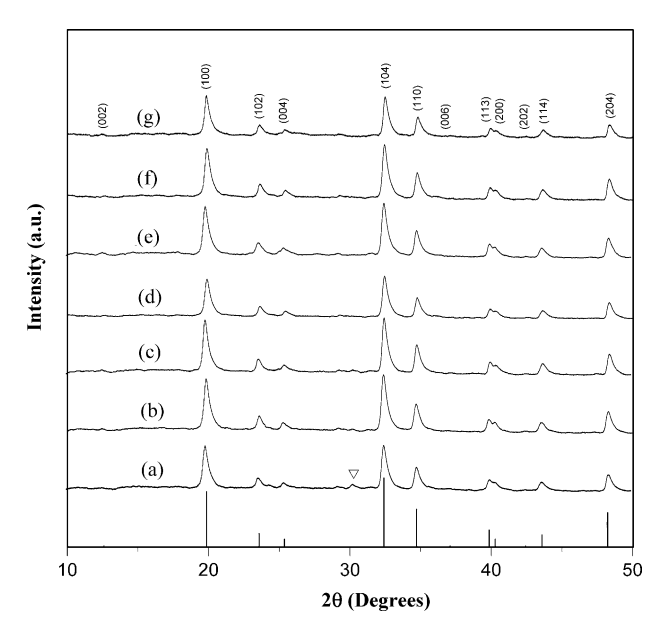


Fig. 7. Powder XRD patterns of the vibro-milling powders calcined at  $1050\,^{\circ}$ C with heating/cooling rates of  $10\,^{\circ}$ C/min. for (a) 1 h, (b) 2 h, (c) 3 h, (d) 4 h and (e) 5 h, and at  $1050\,^{\circ}$ C for 5 h with heating/cooling rates of (f)  $20\,^{\circ}$ C/min and (g)  $30\,^{\circ}$ C/min ( $\nabla$ , MgNb<sub>2</sub>O<sub>6</sub>; ICDD file No. 38–1459: Mg<sub>4</sub>Nb<sub>2</sub>O<sub>9</sub>).

good agreement with earlier results reported by Ananta et al. [20,31] for the mixture of the two kinds of refractory oxides.

The amount of corundum phase present in each of the powders was estimated using the following equation:

corundum phase (wt.%) = 
$$\left[\frac{I_{\text{Cor}}}{(I_{\text{Cor}} + I_{\text{Col}})}\right] \times 100$$
 (1)

This equation is analogous to well-known equation [6,8] widely employed in connection with the fabrication of complex perovskite materials. It should be seen as a first approximation since its applicability requires comparable maximum intensities of the peaks of corundum and columbite phases. Here  $I_{\text{Cor}}$  refers to the intensity of the corundum (1 0 4) peak and  $I_{\text{Col}}$  the intensity of the columbite (1 3 1) peak [32]. For the purpose of estimating the concentration of the phase present, Eq. (1) has been applied to the powder XRD patterns obtained as given in Table 1.

It is well established that the columbite-type  $MgNb_2O_6$  tends to form together with the corundum-type  $Mg_4Nb_2O_9$ , depending on calcination conditions [18,20,32]. In the work reported here, evidence for the formation of  $MgNb_2O_6$  phase, which coexists with the  $Mg_4Nb_2O_9$  phase, is found after calcination at temperature  $\sim\!850\text{--}950\,^{\circ}\text{C}$ , similar to those reported by Ananta [20] and Yu et al. [22]. The formation temperature and dwell times for high purity  $Mg_4Nb_2O_9$  observed in the powders derived from a combination of a mixed oxide synthetic route and a careful calcination condition (especially with a rapid vibro-milling technique) are slightly lower than those reported for the powders prepared via many other conventional mixed oxide methods [3–5,13].

Based on the DTA and XRD data, it may be concluded that, over a wide range of calcination conditions, single-phase Mg<sub>4</sub>Nb<sub>2</sub>O<sub>9</sub> cannot be straightforwardly formed via a solid-state mixed oxide synthetic route, as verified by a number of

 $\label{eq:calculated} Table~1~$  Calculated amount of  $Mg_4Nb_2O_9$  phase as a function of calcination conditions and milling methods

| Calcination conditions |                | Qualitative concentrations of phases <sup>a</sup>     |   |   |   |
|------------------------|----------------|---|---|---|---|
| Temperature (°C)       | Dwell time (h) | Ball-milling  |   | Ball-milling  |   |
|                        |                | Mg <sub>4</sub> Nb <sub>2</sub> O <sub>9</sub> (wt.%) | MgNb <sub>2</sub> O <sub>6</sub> (wt.%) | Mg <sub>4</sub> Nb <sub>2</sub> O <sub>9</sub> (wt.%) | MgNb <sub>2</sub> O <sub>6</sub> (wt.%) |
| 850                    | 2              | 20.88   | 79.12                                   | 5.00  | 95.00                                   |
| 900                    | 2              | 42.44   | 57.56                                   | 21.33   | 78.67                                   |
| 950                    | 2              | 91.22   | 8.78                                    | 58.81   | 41.19                                   |
| 1000                   | 2              | 93.69   | 6.31                                    | 93.44   | 6.56                                    |
| 1050                   | 1              | <del>-</del> -  | _                                       | 98.29   | 1.71                                    |
| 1050                   | 2              | 93.96   | 6.04                                    | 100.00  | 0.00                                    |
| 1050                   | 3              | 99.02   | 0.98                                    | 100.00  | 0.00                                    |
| 1050                   | 4              | 99.13   | 0.87                                    | 100.00  | 0.00                                    |
| 1050                   | 5              | 100.00  | 0.00                                    | 100.00  | 0.00                                    |
| 1100                   | 2              | 100.00  | 0.00                                    | 100.00  | 0.00                                    |

<sup>&</sup>lt;sup>a</sup> The estimated precision of the concentrations for the two phases is  $\pm 1\%$ .

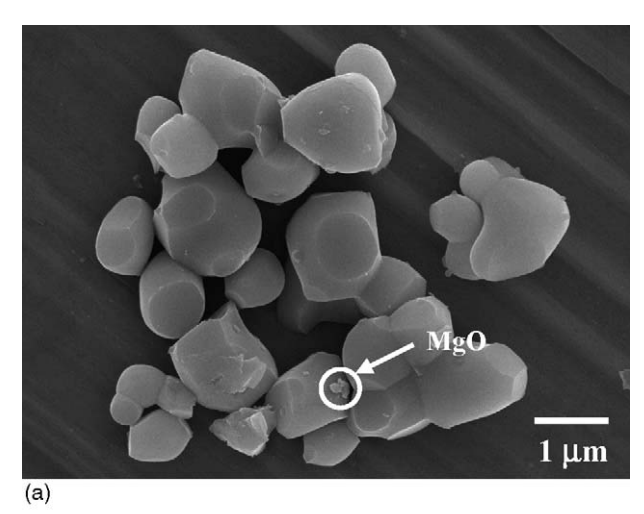
researchers [16,17,20]. The experimental work carried out here suggests that the optimal calcination conditions for single-phase Mg<sub>4</sub>Nb<sub>2</sub>O<sub>9</sub> are 1050 °C for 5 h or 1100 °C for 2 h (ball-milling) and 1050 °C for 2 h (vibro-milling), with heating/cooling rates as fast as 30 °C/min. The optimized formation temperature of single-phase Mg<sub>4</sub>Nb<sub>2</sub>O<sub>9</sub> was lower for the vibro-milling method probably due to the higher degree of mixing with more effective size reduction. Therefore, in general, the methodology presented in this work provides a simple method for preparing corundum Mg<sub>4</sub>Nb<sub>2</sub>O<sub>9</sub> powders via a solid-state mixed oxide synthetic route. It is interesting to note that, by using either ball-milling or vibro-milling methods with its respective optimized calcination condition, the reproducible, lower cost and flexible process involving simple synthetic route can produce high purity corundum Mg<sub>4</sub>Nb<sub>2</sub>O<sub>9</sub> (with impurities undetected by XRD technique) from relatively impure and inexpensive commercially available raw materials.

SEM micrographs of the calcined  $Mg_4Nb_2O_9$  powders derived from ball- and vibro-milling methods are shown in Fig. 8(a) and (b), respectively. In general, the particles are agglomerated and basically irregular in shape, with a substantial variation in particle size. Observed diameters range from 0.5 to 1.6 and 0.1 to 1.8  $\mu$ m for ball- and vibro-milling methods, respectively (Table 2). However, it is seen that higher degree of agglomeration with more rounded particle morphology is observed in the powders produced by vibro-milling. The strong inter-particle bond within each aggregate is evidenced by the formation of a well-established necking between neighbouring particles. This observation could be attributed to the mechanism of surface energy reduction of the ultrafine powders, i.e. the

 $\label{eq:continuous} Table~2~$  Particle size range of  $Mg_4Nb_2O_9$  particles measured by different techniques

|   | · · · · · · · · · · · · · · · · · · · | -             |
|---|---------------------------------------|---------------|
| Measurement techniques                    | Particle size range                   | ;             |
|   | Ball-milling                          | Vibro-milling |
| XRD (nm, ±2.0)                            | 23.9                                  | 23.4          |
| Laser diffraction ( $\mu m$ , $\pm 0.2$ ) | 2.0-5.0                               | 0.3-6.5       |
| SEM ( $\mu$ m, $\pm 0.1$ )                | 0.5-1.6                               | 0.1-1.8       |
| TEM ( $\mu$ m, $\pm 0.01$ )               | 0.01-1.0                              | 0.01-0.03     |
|   |                                       |               |

smaller the powder the higher the specific surface area [24,25]. In general, it is seen that higher and longer heat treatment of ball-milling powders leads to larger particle sizes with hard agglomeration. The averaged particle size of vibro-milling Mg<sub>4</sub>Nb<sub>2</sub>O<sub>9</sub> powders with finer particle size is regarded as



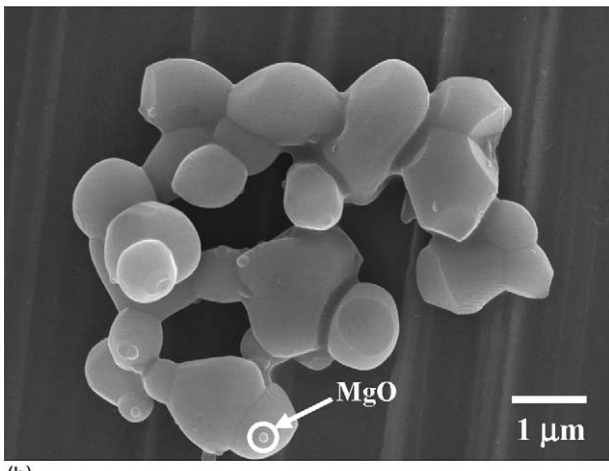


Fig. 8. SEM micrographs of the (a) ball-milling and (b) vibro-milling Mg<sub>4</sub>Nb<sub>2</sub>O<sub>9</sub> powders after calcined at their optimal conditions.

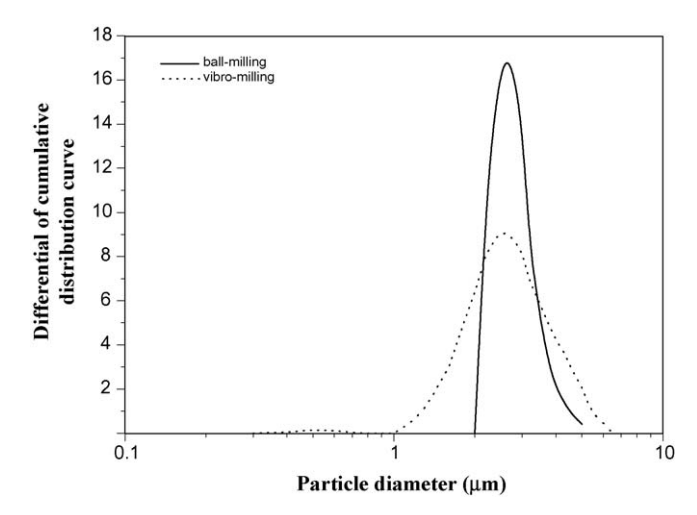


Fig. 9. The particle size curves of the ball- and vibro-milling  $Mg_4Nb_2O_9$  powders after calcined at their optimal conditions.

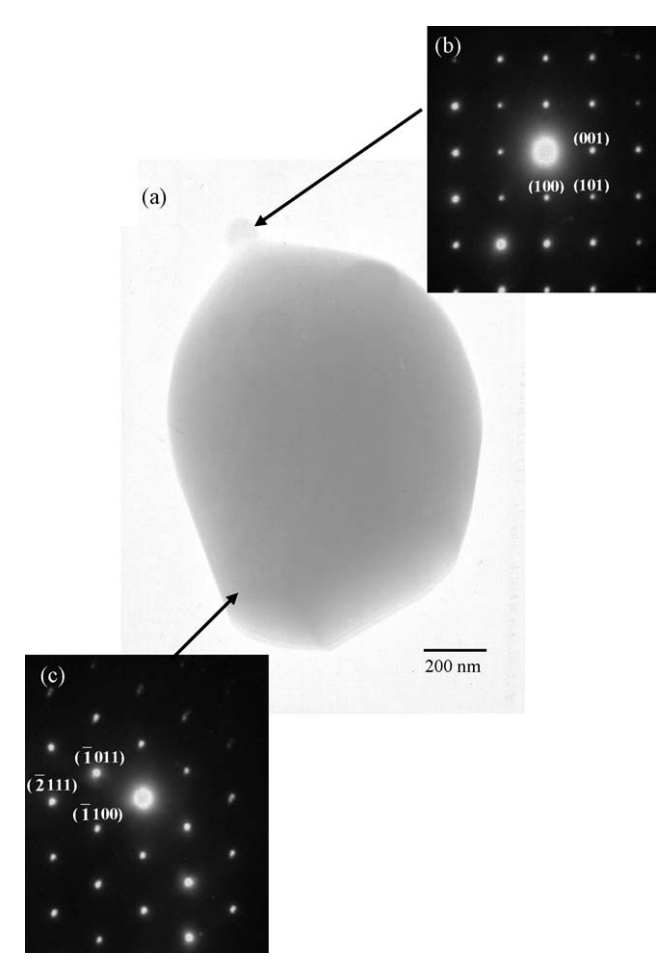


Fig. 10. (a) TEM micrograph of ball-milling  $Mg_4Nb_2O_9$  particles and SAED patterns of (b) the major phase of hexagonal  $Mg_4Nb_2O_9$  (zone axes [1 1 1]) and (c) the minor phase of orthorhombic  $MgNb_2O_6$  (zone axes [0 1 0]).

advantage for better reactivity. A combination of SEM and EDX techniques has demonstrated that an MgO-rich phase (spherical particle with diameter of  $\sim 50-100\,\mathrm{nm}$ ) exists neighbouring the Mg4Nb2O9 parent phase, as circled in Figs. 8(a) and 9b). The existence of discrete nano-sized MgO phase points to the poor

reactivity of MgO, although the concentration is too low for detection by XRD in consistent with earlier work by Ananta [20]. Fig. 9 shows the particle size distribution curves of calcined Mg<sub>4</sub>Nb<sub>2</sub>O<sub>9</sub> powders derived from both milling methods. As listed in Table 2, the particle size falls within the range of 2.0–5.0 and 0.3–6.5 µm for powders from ball- and vibro-milling methods, respectively. Even taking into account that the analysis does not reveal the real dimension of single particles (due to agglomeration effects as expected from the SEM results in Fig. 8), a uniform frequency distribution curve was observed for the ball-milling powders whilst broad distribution curve with tiny tail at front covering the range of 0.3–0.8 µm in sizes was found for the vibro-milling powders (dashed line), reflecting more of the size of agglomerates than the real size of particles, in good agreement with the SEM results previously determined.

Bright field TEM images of discrete particles of the calcined  $Mg_4Nb_2O_9$  powders are shown in Fig. (ball-milling) and Fig. 11 (vibro-milling), indicating the particle sizes and shapes at higher magnifications. The observed morphology reveals the considerable difference in both size and shapes between the two particles. Primary particle in vibro-milling powders is clearly smaller in size than the ball-milling powders. As seen in Fig. 10(a), the ball-milling powders consist mainly of irregular round shape primary particles with a diameter of  $\sim 1~\mu m$  or less. In addition to the primary particles, the powders have another kind of very fine particle (brighter area)

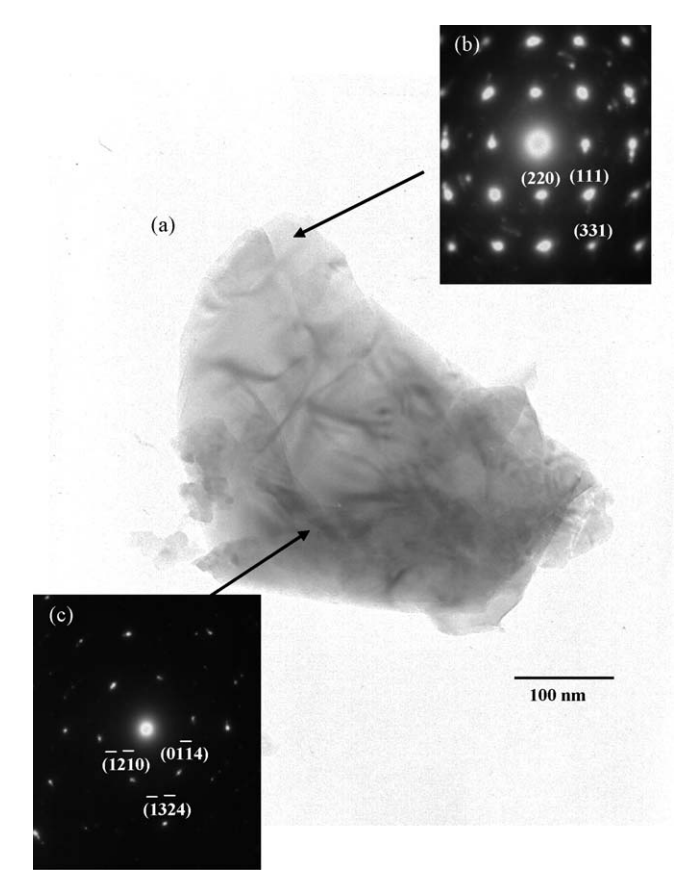


Fig. 11. (a) TEM micrograph of vibro-milling  $Mg_4Nb_2O_9$  particles and SAED patterns of (b) the major phase of hexagonal  $Mg_4Nb_2O_9$  (zone axes  $[\bar{8}\ \bar{4}\ 1]$ ) and (c) the minor phase of orthorhombic  $MgNb_2O_6$  (zone axes  $[0\ 0\ 1]$ ).

with diameter of about 93 nm (it is referred to as nanoparticle). Only single nanoparticle can be observed in this TEM micrograph. In contrast, the vibro-milling powders consist mainly of submicrometer-sized primary particles accompanying with several dark and bright areas (Fig. 11(a)). The particle diameters in these TEM micrographs are also given in Table 2. It is possible to observe in Table 2 that the particle sizes determined by XRD technique have almost the same value in nanometer range for different milling methods. It should be noted that the calculated values from the XRD technique were determined from the XRD peak-broadening and actually present the crystallite sizes [33], whereas the values from other methods as listed in Table 2 represent the particle sizes, which include polycrystalline, agglomerates, defects, etc. [23,33]. In addition, these other methods also provide information on particle morphology and powder quality, which is not available from the XRD technique alone. Thus the combination of the data listed in Table 2 provides better assessment of the powders produced from different milling techniques.

By employing a combination of both selected area electron diffraction (SAED) and crystallographic analysis, the major phase of hexagonal Mg<sub>4</sub>Nb<sub>2</sub>O<sub>9</sub> (Figs. 10(b) and 11(b)) and minor phase of MgNb<sub>2</sub>O<sub>6</sub> nanoparticles in orthorhombic form were identified (Figs. 10(c) and 11(c)), in good agreement with the XRD results. In general, EDX analysis using a 20 nm probe from a large number of particles of the two calcined powders

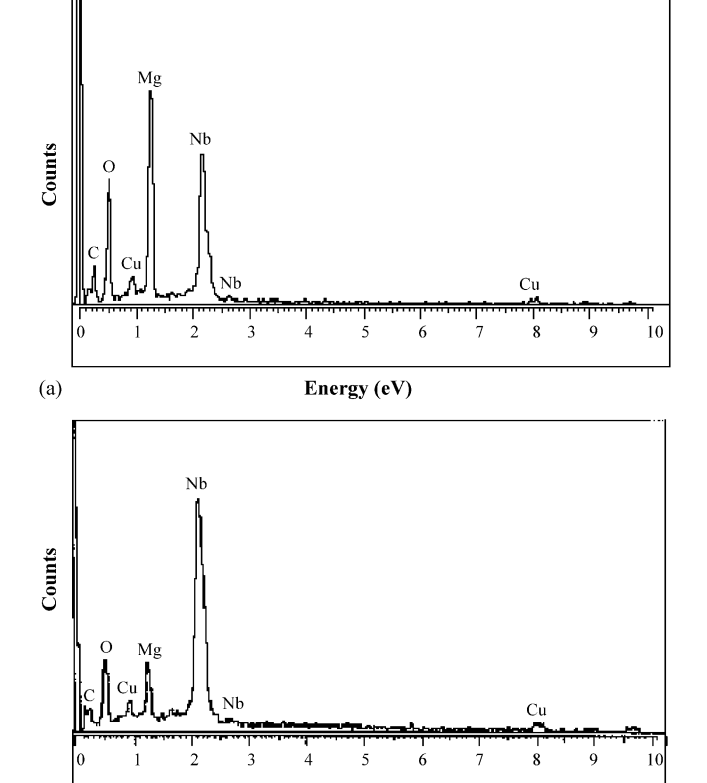
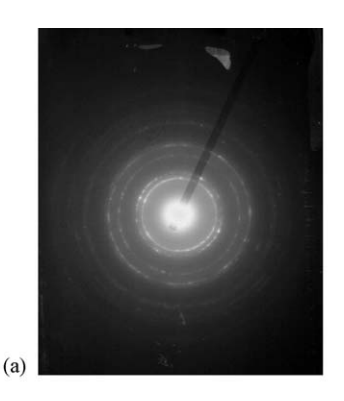


Fig. 12. EDX analysis of (a) the major phase Mg<sub>4</sub>Nb<sub>2</sub>O<sub>9</sub> and (b) the minor phase MgNb<sub>2</sub>O<sub>6</sub> (some signals of C and Cu come from coated electrodes and sample stubs, respectively).

Energy (eV)



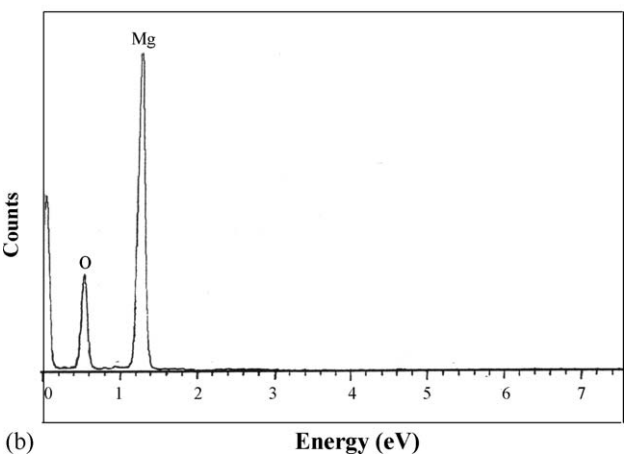


Fig. 13. (a) SAED pattern of the unreacted MgO phase and (b) EDX analysis of the MgO-rich phase.

confirmed the parent composition to be  $Mg_4Nb_2O_9$  (Fig. 12(a)). Minor phase of  $MgNb_2O_6$  was also confirmed by this technique, as illustrated in Fig. 12(b). It is interesting to noted that limited evidence for the presence of the unreacted starting precursor MgO (Fig. 13(a) the ring patterns indicating the polycrystalline nature and hence fine scale of this phase Fig. 13(b)) in good agreement with the SEM results, and nano-scale particle of  $MgNb_2O_6$  was also found in the TEM–EDX investigation, even though this could not be detected by XRD. It is, therefore, intriguing to note the advantage of a combination between TEM and EDX techniques, which lies in its ability to reveal microstructural features often missed by the XRD diffraction method which requires at least 5 wt.% of the component [23].

#### 4. Conclusions

It has been shown that pure corundum  $Mg_4Nb_2O_9$  powders can be formed by the reaction of niobium oxide with magnesium oxide via either ball-milling or vibro-milling methods at about  $1050-1100\,^{\circ}C$ . Evidence for the formation of a columbite  $MgNb_2O_6$  minor phase, which coexists with the corundum  $Mg_4Nb_2O_9$  parent phase, is found at calcination temperatures ranging from 800 to  $1050\,^{\circ}C$ . Between the two methods, it is seen that lower optimized calcination temperature and dwell time for the production of pure  $Mg_4Nb_2O_9$  powders can be obtained by using vibro-milling method. This technique was superior to ball-milling as measured by the required minimum firing temperature

and dwell time for the yield of single-phase Mg<sub>4</sub>Nb<sub>2</sub>O<sub>9</sub> in the powders together with the smallest particle size achieved.

#### Acknowledgments

The authors gratefully acknowledge the Thailand Research Fund (TRF), the Department of Physics, the Faculty of Science and the Graduate School, Chiang Mai University for all supports.

#### References

- S. Pagola, R.E. Carbonio, J.A. Alonso, M.T. Fernández-Díaz, J. Solid State Chem. 134 (1997) 76.
- [2] A. Yokoi, H. Ogawa, A. Kan, H. Ohsato, Y. Higashida, J. Eur. Ceram. Soc. 25 (2005) 2871.
- [3] C.W. Hwang, S.K. Lee, Japanese Patent No. JP97-293619 (1998).
- [4] A. Wachtel, J. Electrochem. Soc. 111 (1964) 534.
- [5] Y.C. You, N. Park, K.H. Jung, H.L. Park, K.C. Kim, S.I. Mho, T.W. Kim, J. Mater. Sci. Lett. 13 (1994) 1682.
- [6] P.A. Joy, K. Sreedhar, J. Am. Ceram. Soc. 80 (1997) 770.
- [7] C.H. Lu, H.S. Yang, Mater. Sci. Eng. B 84 (2001) 159.
- [8] S.L. Swartz, T.R. Shrout, Mater. Res. Bull. 17 (1982) 1245.
- [9] S. Ananta, N.W. Thomas, J. Eur. Ceram. Soc. 19 (1999) 155.
- [10] G. Haertling, J. Am. Ceram. Soc. 82 (1999) 797.
- [11] A.J. Moulson, J.M. Herbert, Electroceramics, 2nd ed., Wiley, Chichester, 2003
- [12] K. Uchino, Piezoelectrics and Ultrasonic Applications, Kluwer, 1998.
- [13] E. Goo, T. Yamamoto, K. Okazaki, J. Am. Ceram. Soc. 69 (1986) C-188.
- [14] D.H. Kang, K.H. Yoon, Ferroelectrics 87 (1988) 255.

- [15] P.A. Joy, Mater. Lett. 32 (1997) 347.
- [16] Y.C. You, H.L. Park, Y.G. Song, H.S. Moon, G.C. Kim, J. Mater. Sci. Lett. 13 (1994) 1487.
- [17] K. Sreedhar, N.R. Pavaskar, Mater. Lett. 53 (2002) 452.
- [18] N.K. Kim, Mater. Lett. 32 (1997) 127.
- [19] N. Kumada, K. Taki, N. Kinomura, Mater. Res. Bull. 35 (2000) 1017.
- [20] S. Ananta, Mater. Lett. 58 (2004) 2530.
- [21] S. Ananta, Mater. Lett. 58 (2004) 2834.
- [22] Y.H. Yu, C.D. Feng, W.L. Yao, Y. Yang, C.E. Li, H.X. Yan, J. Mater. Sci. Lett. 20 (2001) 2189.
- [23] H.P. Klug, L.E. Alexander, X-ray Diffraction Procedures, 2nd ed., Wiley, New York, 1974.
- [24] J.S. Reeds, Principles of Ceramics Processing, 2nd ed., Wiley, New York, 1995.
- [25] D. Richerson, Modern Ceramic Engineering, 3rd ed., CRC Press, New York, 2005.
- [26] Powder Diffraction File No. 71–1176, International Centre for Diffraction Data, Newton Square, PA, 2000.
- [27] Powder Diffraction File No. 28–317, International Centre for Diffraction Data, Newton Square, PA, 2000.
- [28] S. Ananta, Mater. Lett. 58 (2004) 2781.
- [29] Powder Diffraction File No. 33–875, International Centre for Diffraction Data, Newton Square, PA, 2000.
- [30] Powder Diffraction File No. 38–1459, International Centre for Diffraction Data, Newton Square, PA, 2000.
- [31] S. Ananta, R. Tipakontitikul, T. Tunkasiri, Mater. Lett. 57 (2003) 2637
- [32] S. Ananta, R. Brydson, N.W. Thomas, J. Eur. Ceram. Soc. 19 (1999) 355
- [33] B.D. Cullity, Elements of X-Ray Diffraction, 2nd ed., Addison-Wesley Publishing Company Inc., Reading, 1978.



Materials Science and Engineering B 132 (2006) 292-299



www.elsevier.com/locate/mseb

# Effects of magnesium niobate precursor and calcination condition on phase formation and morphology of lead magnesium niobate powders

R. Wongmaneerung <sup>a</sup>, T. Sarakonsri <sup>b</sup>, R. Yimnirun <sup>a</sup>, S. Ananta <sup>a,\*</sup>

<sup>a</sup> Department of Physics, Faculty of Science, Chiang Mai University, Chiang Mai 50200, Thailand <sup>b</sup> Department of Chemistry, Faculty of Science, Chiang Mai University, Chiang Mai 50200, Thailand

Received 1 March 2006; received in revised form 26 April 2006; accepted 28 April 2006

#### Abstract

A perovskite phase of lead magnesium niobate,  $Pb(Mg_{1/3}Nb_{2/3})O_3$  or PMN, powders has been synthesized by a rapid vibro-milling technique. Both columbite  $MgNb_2O_6$  and corundum  $Mg_4Nb_2O_9$  have been employed as magnesium niobate precursors, with the formation of the PMN phase investigated as a function of calcination conditions by thermal gravimetric and differential thermal analysis (TG–DTA) and X-ray diffraction (XRD). The particle size distribution of the calcined powders was determined by laser diffraction technique. Morphology, crystal structure and phase composition have been determined via a combination of scanning electron microscopy (SEM), transmission electron microscopy (TEM) and energy-dispersive X-ray (EDX) techniques. The magnesium niobate precursor and calcination condition have been found to have a pronounced effect on the phase and morphology evolution of the calcined PMN powders. It is seen that optimisation of calcination conditions can lead to a single-phase PMN in both methods. However, the formation temperature and dwell time for single-phase PMN powders were lower for the synthetic method employing a columbite  $MgNb_2O_6$  precursor. © 2006 Elsevier B.V. All rights reserved.

Keywords: Lead magnesium niobate; Magnesium niobate; Perovskite; Powder synthesis; Calcination

#### 1. Introduction

Lead magnesium niobate, Pb(Mg<sub>1/3</sub>Nb<sub>2/3</sub>)O<sub>3</sub> or PMN, is one of the most widely investigated relaxor ferroelectric materials with a perovskite structure. The excellent dielectric broadening and electrostrictive properties make it a promising electroceramic material for capacitor, electrostrictive actuator, electromechanical transducer and electro-optic applications [1-3]. There has been a great deal of interest in the preparation of single-phase PMN powders as well as in the sintering and dielectric properties of PMN-based ceramics [4-6]. However, it is well documented that the formation of PMN perovskite via the solid-state reaction is often accompanied by the occurrence of unwanted pyrochloretype phases because of the volatilisation of PbO, the low dispersion of MgO and the differences of the reactive temperature between Pb-Nb and Pb-Mg [7-9]. Hence, several innovation techniques [10–12] have been utilized to minimize the amount of pyrochlore phase formed.

The initial work of Lejeune and Boilot [10] considered the many parameters which influence the synthesis of PMN from PbO, MgO and Nb<sub>2</sub>O<sub>5</sub> precursors, concluding that the formation of a pyrochlore phase could not be completely eliminated. Moreover, it was proposed that the reactivity of magnesium oxide with lead and niobium oxides was the definitive factor governing products of the reaction. These authors later proposed the use of MgCO3 in place of MgO to increase the yield of perovskite PMN. Swartz and Shrout [7] developed an effective way of producing PMN powder in high yield by the introduction of a two-step process (the B-site precursor approach). In the method, an intermediate step to give columbite-type MgNb<sub>2</sub>O<sub>6</sub> precursor is used to bypass the formation of the pyrochlore phases. Alternatively, Joy and Sreedhar [11] proposed the use of Mg<sub>4</sub>Nb<sub>2</sub>O<sub>9</sub> precursor in place of MgNb<sub>2</sub>O<sub>6</sub> for the fabrication of pyrochlore-free PMN. More recently, Lu and Yang [12] adopted a two-stage synthesis method by precalcining the mixture of MgO and Nb<sub>2</sub>O<sub>5</sub> at 1000 °C to form Mg<sub>4</sub>Nb<sub>2</sub>O<sub>9</sub>. This compound was then quenched at 850-900 °C with PbO to form PMN without further soaking. This approach yielded perovskite PMN as the dominant phase, with pyrochlore impurities of less than 5% and some residual MgO. It was also claimed that the pyrochlore

<sup>\*</sup> Corresponding author. Tel.: +66 53 943367; fax: +66 53 943445. E-mail address: suponananta@yahoo.com (S. Ananta).

phases and the residual MgO could be eliminated completely with the introduction of excess PbO and nitric acid, respectively. However, the preparation of PMN using  $Mg_4Nb_2O_9$  precursor, to date, has not been extensive as that of PMN using  $MgNb_2O_6$  precursor. Moreover, its effect on the formation of perovskite PMN phase under various calcination conditions (especially the effects of applied dwell time and heating/cooling rates) has not been adequately characterized.

The purpose of this study was to compare the two B-site precursor synthetic routes of PMN formation and the characteristics of the resulting powders. The phase formation and morphology of the powders calcined at various conditions will be studied and discussed.

#### 2. Experimental procedure

Pb( $Mg_{1/3}Nb_{2/3}$ )O<sub>3</sub> was synthesised by a similar methodology of B-site precursor mixed oxide synthetic route, as reported earlier [4]. Starting precursors were as follows: PbO (JCPDS file number 77-1971), MgO (periclase: JCPDS file number 71-1176) and  $Nb_2O_5$  (JCPDS file number 80-2493) (Aldrich, 99% purity). These three oxide powders exhibited an average particle size in the range of  $3.0–5.0~\mu m$ . First, two intermediate phases of magnesium niobate:  $MgNb_2O_6$  and  $Mg_4Nb_2O_9$  were separately prepared by the solid-state reaction method previously reported [13,14], employing an optimised calcination conditions of 1000~C for 4 h with heating/cooling rates of 30~C/min and 950~C for 2 h with heating/cooling rates of 25~C/min, respectively. The following reaction sequences were then proposed for the formation of PMN:

#### 1. The columbite route:

$$3PbO(s) + MgNb_2O_6(s) \rightarrow 3Pb(Mg_{1/3}Nb_{2/3})O_3(s)$$
 (1)

#### 2. The corundum route:

$$12PbO(s) + Mg_4Nb_2O_9(s) + 3Nb_2O_5(s)$$

$$\rightarrow 12Pb(Mg_{1/3}Nb_{2/3})O_3(s)$$
 (2)

Instead of employing a ball-milling procedure (ZrO $_2$  media under acetone for 24 h [7]), a McCrone vibro-milling was used. In order to improve the reactivity of the constituents, the milling process was carried for 2 h (instead of 30 min [4]) with corundum media in isoproponal. After drying at 120 °C for 2 h, various calcination conditions were applied in order to investigate the formation of PMN phase in each calcined powders.

The reactions of the uncalcined powders taking place during heat treatment were investigated by thermal gravimetric and differential thermal analysis (TG–DTA, Shimadzu) using a heating rate of 10 °C/min in air from room temperature up to 900 °C. Calcined powders were subsequently examined by room temperature X-ray diffraction (XRD; Philips PW 1729 diffractometer) using Ni-filtered Cu K $\alpha$  radiation, to identify the phases formed and optimum calcination conditions for the manufacture of PMN powders. The mean crystallite size was determined using the

diffraction peak (110) of the perovskite pattern by using Scherrer equation [15]. Particle size distributions of powders were determined by laser diffraction technique (DIAS 1640 laser diffraction spectrometer), with the grain size and morphologies of powders observed by scanning electron microscopy (SEM; JEOL JSM-840A). The chemical composition and structure of the phases formed were elucidated by transmission electron microscopy (CM 20 TEM/STEM) operated at 200 keV and fitted with an energy-dispersive X-ray (EDX) analyser with an ultra-thin window. EDX spectra were quantified with the virtual standard peaks supplied with the Oxford Instruments eXL software. Powder samples were dispersed in solvent and deposited by pipette on to 3 mm holey copper grids for observation by TEM. In addition, attempt was made to evaluate the crystal structures of the observed compositions/phases by correcting the XRD and TEM diffraction data.

#### 3. Results and discussion

TGA and DTA results for the mixtures synthesized by both Bsite precursor methods are shown in Figs. 1 and 2, respectively. In general, similar trend of thermal characteristics is observed in both precursors. As shown in Fig. 1, the powders prepared via both B-site precursor mixed oxide methods demonstrate three distinct weight losses. The first weight loss occurs below 200 °C, the second one between 200–300 °C and the final one after 750 °C. In the temperature range from room temperature to  $\sim$ 150 °C, both samples show small thermal peaks in the DTA curves, Fig. 2, which are related to the first weight loss. These DTA peaks can be attributed to the decomposition of the organic species such as rubber lining from the milling process similar to our earlier reports [13,16]. In comparison between the two B-site precursor routes, after the first weight loss, the columbite route shows a slightly higher weight loss over the temperature range of ~50-220 °C, followed by a much sharper fall in specimen weight with increasing temperature from  $\sim$ 250 to 350 °C. This columbite-precursor method also exhibits larger overall weight loss ( $\sim$ 1.25%) than that of the corundum route ( $\sim$ 1.00%).

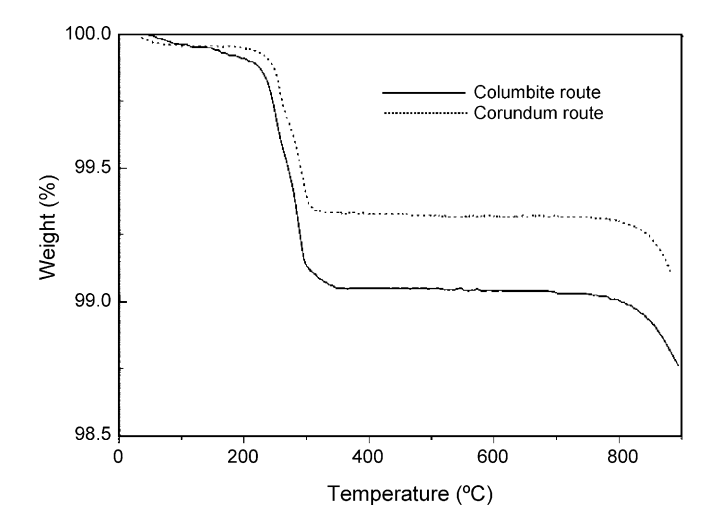


Fig. 1. TGA curves of the mixtures derived from columbite- and corundum-route.

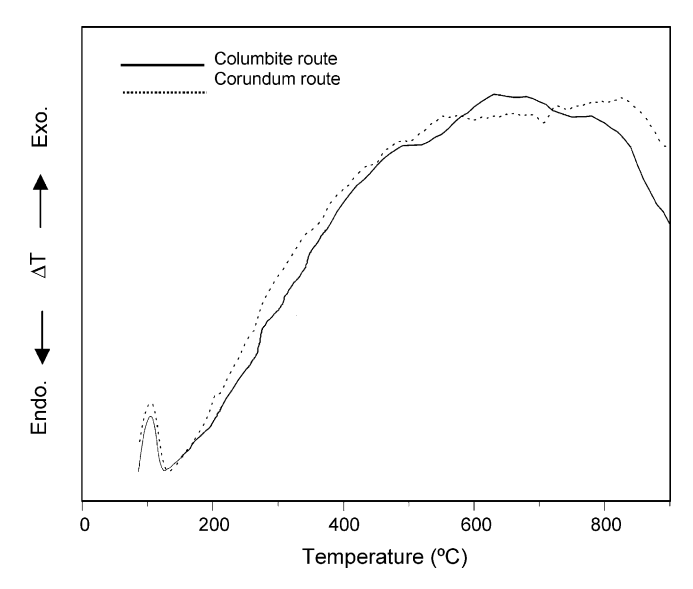


Fig. 2. DTA curves of the mixtures derived from columbite- and corundum-route.

Corresponding to the second fall in specimen weight, by increasing the temperature up to ~700 °C, the solid-state reaction occurs between oxide precursors. The broad exothermic characteristic in both DTA curves represents that reaction, which has a maximum at ~600 and 800 °C for columbite- and corundum-routes, respectively. However, it is to be noted that there is no obvious interpretation of these peaks, although it is likely to correspond to a phase transition reported by a number of workers [4–8]. The different temperature, intensities and shapes of the thermal peaks for the two precursors here probably are related to the different starting materials especially magnesium niobate and consequently, caused by the removal of species differently bonded in the network, reactivity of different species (difference in type and dispersion of MgO) in the powders. These data were used to define the range of temperatures for XRD investigation between 550 and 1000 °C. It is to be noted that a significant weight loss in TG curves associated with large thermal change in DTA curves observed at temperatures above 750 °C (Figs. 1 and 2) may be attributed to the PbO volatilisation typically found in lead-based ferroelectrics, consistent with other investigators [17–19].

To study the phase development with increasing calcination temperature in each synthetic route, they were calcined at various temperatures for 1 h in air with constant heating/cooling rates of 10 °C/min, followed by phase analysis using XRD technique. As shown in Fig. 3, for the uncalcined powder and the powder calcined at 550 °C (columbite route), only X-ray peaks of PbO and MgNb<sub>2</sub>O<sub>6</sub> precursors are present. Similarly, it is seen that unreacted precursors of PbO and Mg<sub>4</sub>Nb<sub>2</sub>O<sub>9</sub> are detected from the original mixture up to 650 °C for the corundum route (Fig. 4). These observations indicate that no reaction was yet triggered during the vibro-milling or low firing processes, in agreement with literature [4,13,16]. It is seen that PMN crystallites were developed in the powder at a calcination temperature as low as 600 and 650 °C for columbite- and corundum-routes, respectively. The results of X-ray diffraction measurement sup-

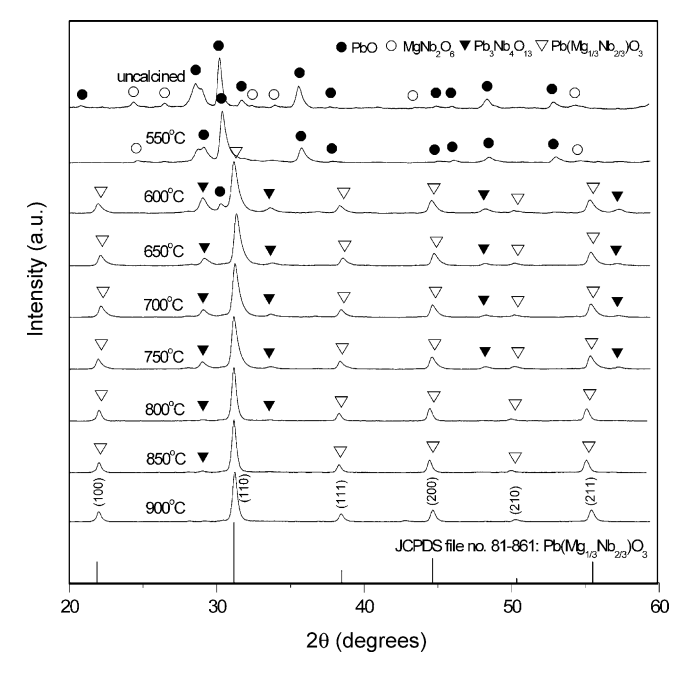


Fig. 3. XRD patterns of the columbite-route powders calcined at various conditions for 1 h with constant heating/cooling rates of 10  $^{\circ}$ C/min.

ported the DTA observation (Fig. 2) that PMN phase is formed at approximately 600–800 °C. In general, the strongest reflections apparent in the majority of these XRD patterns indicate the formation of the lead magnesium niobate, PMN ( $\nabla$ ). These can be matched with JCPDS file number 81-0861 for the cubic phase, in space group  $Pm\bar{3}m$  (no. 221) with cell parameters a=404 pm [20] consistent with other workers [4,5]. According to Fig. 3, the formation of Pb<sub>3</sub>Nb<sub>4</sub>O<sub>13</sub> ( $\blacktriangledown$ ) earlier reported by many researchers [4,21–23] has been found at 600 °C, which

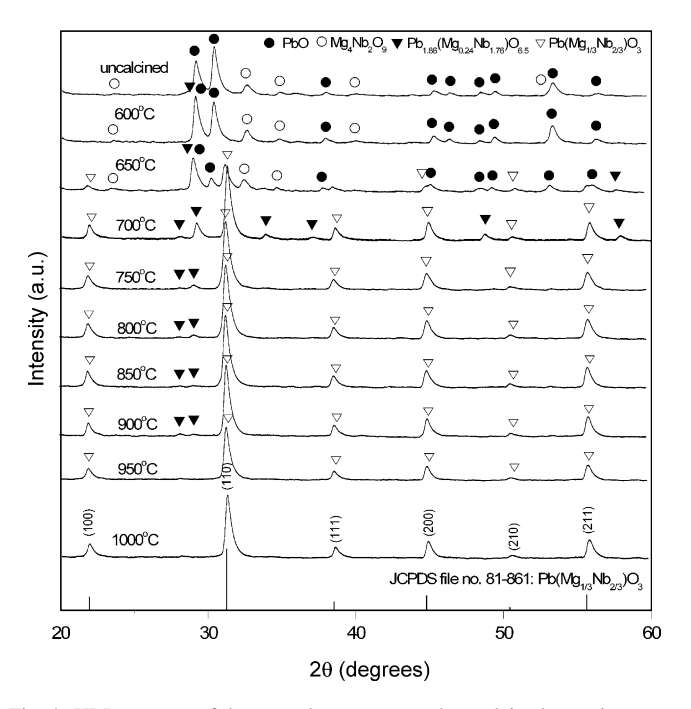


Fig. 4. XRD patterns of the corundum-route powders calcined at various conditions for 1 h with constant heating/cooling rates of 10  $^{\circ}$ C/min.

is associated to the second TG–DTA response in Figs. 1 and 2. This pyrochlore phase has a cubic structure with cell parameter a = 1.056 nm in space group Fd3m (no. 227) (JCPDS file number 25-0443) [24]. Upon calcination at 650 °C, the peak corresponding to PbO disappeared (not detectable by XRD). By increasing the calcination temperature from 650 to 850 °C, the yield of the cubic PMN phase increases significantly until at 900 °C, a single-phase of perovskite PMN is formed for the columbite route.

From Fig. 4, it is seen that calcination at  $600\,^{\circ}\text{C}$  resulted in some new peak ( $\nabla$ ) of the Pb<sub>1.86</sub>(Mg<sub>0.24</sub>Nb<sub>1.76</sub>)O<sub>6.5</sub> phase (JCPDS file number 82-0338) [25] mixing with the unreacted PbO and Mg<sub>4</sub>Nb<sub>2</sub>O<sub>9</sub> phases. To a first approximation, this Pb<sub>1.86</sub>(Mg<sub>0.24</sub>Nb<sub>1.76</sub>)O<sub>6.5</sub> phase earlier reported by many researchers [23,26,27] has a pyrochlore-type structure with a cubic unit cell a = 1.060 nm, space group Fd3m (no. 227). This pyrochlore phase was found at  $600\,^{\circ}\text{C}$  and totally disappeared at 950 °C. As the temperature increased to 900 °C, the intensity of the PMN peaks was further enhanced and PMN becomes the predominant phase, in good agreement with the earlier TG–DTA results. This study also shows that PMN is the only detectable phase in the corundum-route powders after calcination in the range 950–1000 °C.

In the present study, an attempt was also made to calcine both precursors under various dwell times and heating/cooling rates (Figs. 5 and 6). In this connection, it is seen that the single-phase of PMN (yield of 100% within the limitation of the XRD technique) was also found to be possible in columbite-precursor powders calcined at 850 °C for 3 h with heating/cooling rates as fast as 30 °C/min (Fig. 5). The appearance of Nb<sub>2</sub>O<sub>5</sub> and Pb<sub>3</sub>Nb<sub>4</sub>O<sub>13</sub> phases indicated that chemical decomposition probably caused by PbO volatilisation has occurred at relatively high firing temperatures (>850 °C) with long dwell times, consistent with other workers [4–8]. It is also interesting to note that in this

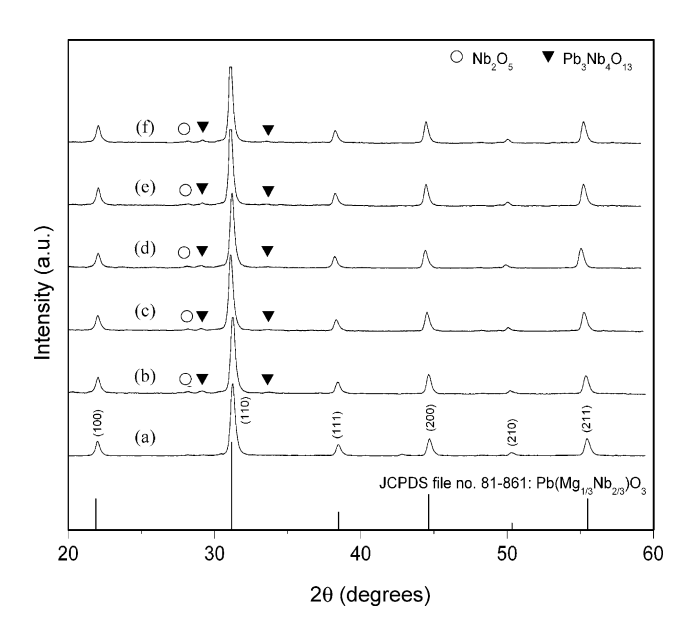


Fig. 5. XRD patterns of the columbite-route powders calcined at  $850\,^{\circ}$ C, for 3 h with heating/cooling rates of (a)  $30\,^{\circ}$ C/min, (b)  $20\,^{\circ}$ C/min and (c)  $10\,^{\circ}$ C/min, (d) for 2 h with heating/cooling rates of  $10\,^{\circ}$ C/min and for 1 h with heating/cooling rates of (e)  $30\,^{\circ}$ C/min and (f)  $20\,^{\circ}$ C/min.

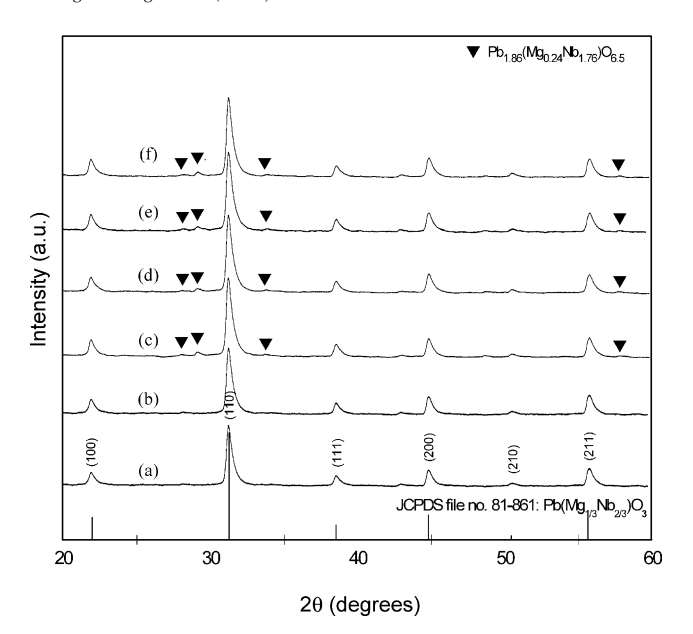


Fig. 6. XRD patterns of the corumdum-route powders calcined at 950 °C for 1 h with heating/cooling rates of (a) 30 °C/min and (b) 20 °C/min, at 900 °C for (c) 2 h (d) 3 h and (e) 4 h, with heating/cooling rates of 10 °C/min, and (f) at 950 °C, for 4 h with heating/cooling rates of 30 °C/min.

work the effects of both dwell time and heating/cooling rates were also found to be significant for the formation of perovskite PMN by using a corundum route (Fig. 6). It is seen that singlephase of PMN powders was also successfully obtained for a calcination temperature of 950 °C for 1 h with heating/cooling rates of 20 or 30 °C/min applied. The observation that the dwell time or heating/cooling rates may also play an important role in obtaining a single-phase of lead-based perovskite ferroelectrics is also consistent with other investigators [4,19,28]. However, some additional peaks at  $2\theta \sim 43^{\circ}$  are found in the Figs. 5(a) and 6(a). It is to be noted that there is no obvious interpretation of these peaks, although it is likely to correspond to a trace of MgO precursor. Nonetheless, with the limitation of X-ray technique and the inherent only single peak with very low intensity comparable to noise originated from the diffractometer, an accurate evaluation of the phase is not possible [15].

It is well established that the perovskite-type PMN tend to form together with the pyrochlore-type PbO–Nb<sub>2</sub>O<sub>5</sub> compounds, depending on calcination conditions [7,8,23]. In the work reported here, evidence for the formation of PMN phase, which coexists with the cubic pyrochlore phase, is found after calcination at temperature  $\sim$ 650–900 °C, in agreement with literature [4,7,12,22]. No evidence of Pb<sub>1.83</sub>Mg<sub>0.29</sub>Nb<sub>1.71</sub>O<sub>6.39</sub> was found, nor was there any indication of the pyrochlore phase of Pb<sub>3</sub>Nb<sub>2</sub>O<sub>8</sub> and Pb<sub>5</sub>Nb<sub>4</sub>O<sub>15</sub> [21–23] being present. In general, the formation temperature and dwell times for high purity PMN observed in the powders derived from a combination of a mixed oxide synthetic route and a carefully determined calcination condition (especially with a rapid vibro-milling technique) are slightly lower than those reported for the powders prepared via many other conventional mixed oxide methods [7–11].

Based on the TG-DTA and XRD data, it may be concluded that, over a wide range of calcination conditions, single-

phase perovskite PMN cannot be straightforwardly formed via a two-step B-site precursor method, as verified by a number of researchers [4,7,8]. The experimental work carried out here suggests that the optimal calcination conditions for single-phase PMN are 900 °C for 1 h or 850 °C for 3 h (columbite route) and 950 °C for 1 h (corundum route), with heating/cooling rates as fast as 30 °C/min. The optimised formation temperature of single-phase PMN was lower for the columbite route probably due to the higher degree of reactivity with less reacting species involved [7,8]. As suggested by several workers [8,17], the degree of cation mixing in precursors significantly affects the phase formation behavior in the B-site synthesis of PMN. This observation may be accounted for by the fact that the columbite route possibly provides faster chemical reaction rate (only the reaction between PbO and MgNb<sub>2</sub>O<sub>6</sub>) and is able to enhance the formation of perovskite PMN phase by increasing the reactivity of MgO [8]. However, the minimum firing temperature required for the manufacturing of single-phase corundum  $Mg_4Nb_2O_9~(\sim\!950\,^{\circ}C~[14])$  is lower than that of columbite  $MgNb_2O_6$  (~1000 °C [13]).

Therefore, in general, the methodology presented in this work provides a simple method for preparing perovskite PMN powders via a solid-state mixed oxide synthetic route. It is interesting to note that, by using either columbite- or corundum-routes, with an optimal calcination condition, the reproducible, low cost and flexible process involving simple solid-state reaction synthetic route can produce high purity perovskite PMN (with impurities undetected by XRD technique) from relatively impure and inexpensive commercially available raw materials.

To further study the influence of precursor on the characteristics of the resulting PMN powders, a combination of particle size analysis, SEM, TEM and EDX is used to examine the powders obtained, as shown in Figs. 7–10 and Table 1. Fig. 7 compares the particle size distribution curves of calcined PMN powders derived from both B-site precursor methods, which indicate an appreciable size fractions at approximately 0.75–1.08 µm diam-

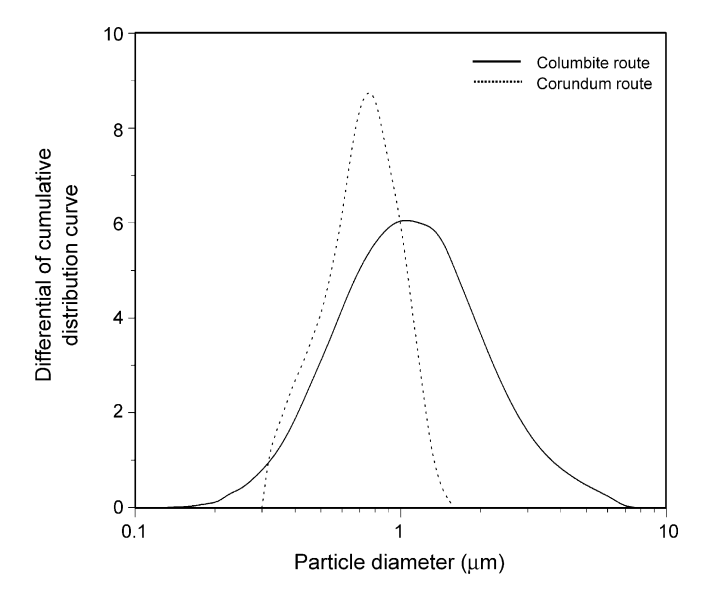
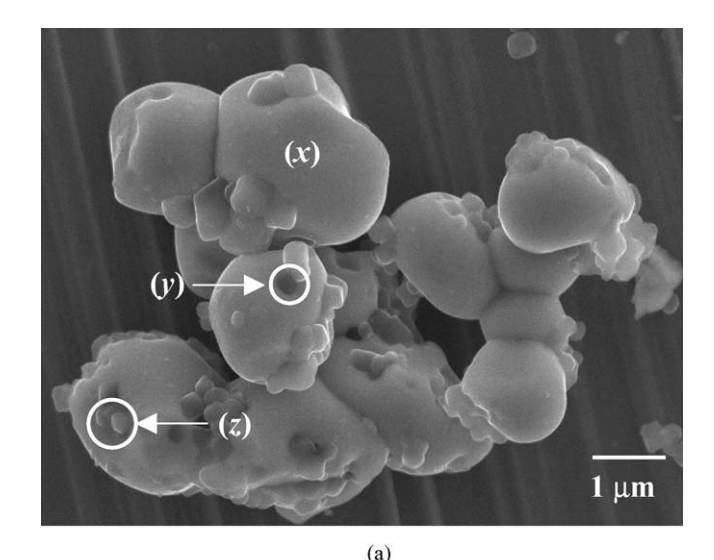


Fig. 7. The particle size curves of the columbite- and corundum-route PMN powders after calcined at their optimised conditions.



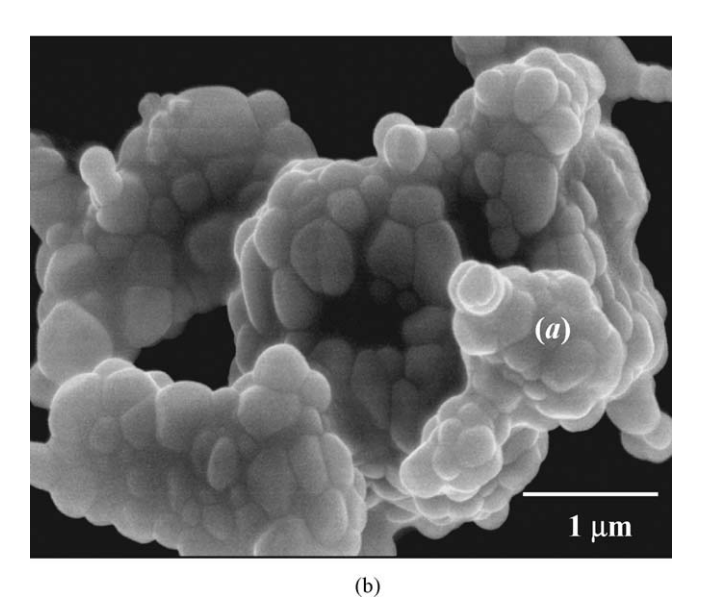


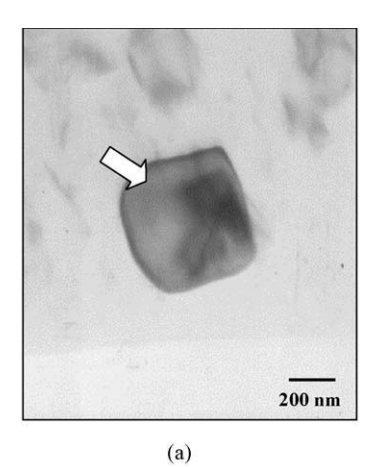
Fig. 8. SEM micrographs of the: (a) columbite- and (b) corundum-route PMN powders after calcined at their optimised conditions.

eters, as also listed in Table 1 (averaged sizes). Even taking in account that the analysis does not reveal the real dimension of single particles (due to agglomeration effects as expected from the SEM results in Fig. 8), a uniform frequency distribution curve was observed for the columbite route whilst narrow distribution curve with tiny kink at front covering the range of  $0.32-1.65~\mu m$  in sizes was found for the corundum route,

Table 1
Particle size data of both PMN powders measured by different techniques

| Measurement techniques                    | Particle size range (average) |                  |  |
|---|-------------------------------|------------------|--|
|   | Columbite route               | Corundum route   |  |
| XRD <sup>a</sup> (nm, ±2.0)               | 26.60                         | 22.50            |  |
| Laser diffraction ( $\mu m$ , $\pm 0.2$ ) | 0.15-7.50 (1.08)              | 0.32-1.65 (0.75) |  |
| SEM ( $\mu$ m, $\pm 0.1$ )                | 0.25-3.00 (1.63)              | 0.20-1.25 (0.73) |  |
| TEM ( $\mu$ m, $\pm 0.01$ )               | 0.25-0.65 (0.45)              | 0.10-0.55 (0.33) |  |

<sup>&</sup>lt;sup>a</sup> Crystallite size.



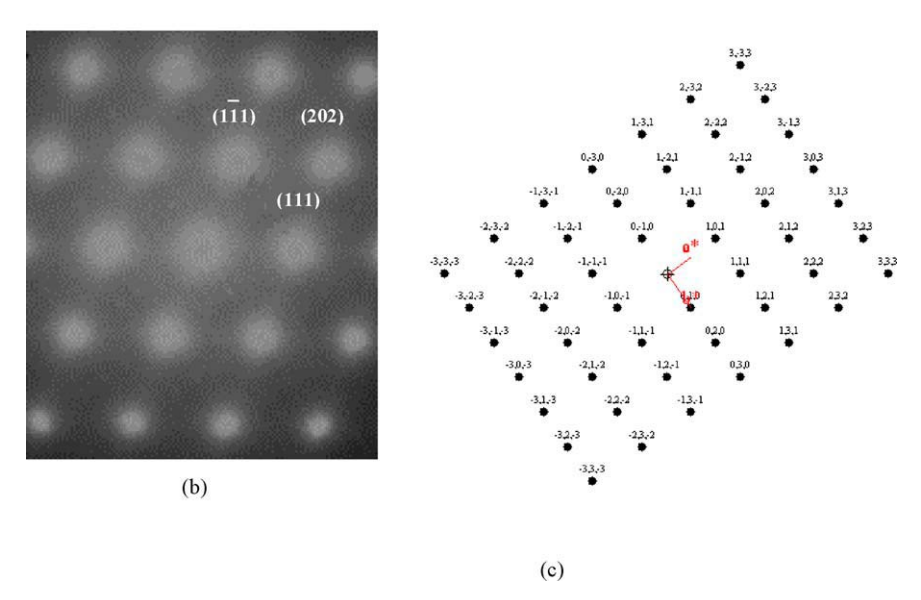
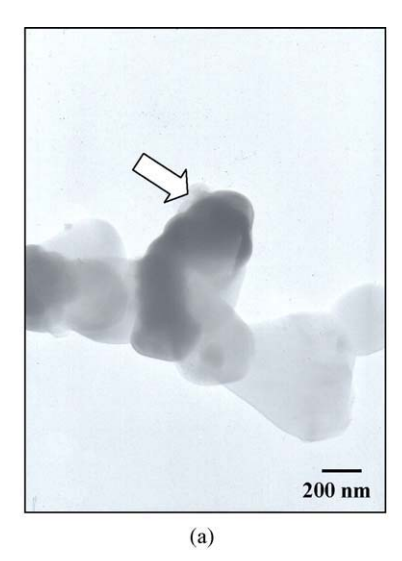


Fig. 9. (a) TEM micrograph with arrow indicates (b) SAED pattern ( $[\bar{1}\ \bar{1}\ 0]$  zone axes) and (c) reciprocal lattice pattern simulation of the columbite-route PMN particles.

reflecting more the size of agglomerates than the real size of particles.

SEM micrographs of the calcined PMN powders derived from columbite- and corundum-precursor methods are shown in Fig. 8(a and b), respectively. In general, the particles are agglomerated and basically irregular in shape, with a substantial variation in particle size. Observed diameters range from 0.25 to 3.00 and 0.20 to 1.25 µm for columbite- and corundumroutes, respectively, in good agreement with the particle size distribution previously determined (Table 1). The primary particles in the agglomerates are, however, submicron in size. This is confirmed by TEM micrographs shown in Figs. 9 and 10. Additionally, the observed morphology reveals considerable difference in homogeneity, uniformity, size and shape between the two PMN powders. It is obviously evident that the columbiteroute powders exhibit more heterogeneous morphology than the corundum-route powders. The columbite-route powders consist mainly of irregular round shape primary particles with a diameter of  $\sim 1 \,\mu m$  or less (Fig. 8(a)). In addition to the primary particles, the powders have another kind of very fine particle (darker particles) with diameter of about 200 nm. A combination of SEM and EDX techniques has demonstrated that pyrochlore and unreacted precursor phases (marked as "y" and "z" in the micrograph in Fig. 8(a)) exist neighbouring the parent PMN phase (marked as "x") (see also Table 2). In general, EDX analysis using a 20 nm probe from a large number of particles of the two calcined powders confirmed the parent composition to be PMN. It is interesting to note that nano-scale MgO and PbO inclusions were also found in the SEM–EDX investigation for the columbite route, in agreement with earlier works [9,29], even though this could not be detected by XRD. It is, therefore, intriguing to note the advantage of a combination between SEM and EDX techniques, which lies in its ability to reveal microstructural features often missed by the XRD method which requires at least 5 wt% of the component [15].

However, it is seen that higher degree of agglomeration with more rounded particle morphology is observed in the powders produced by the corundum route (Fig. 8(b)). The strong interparticle bond within each aggregate is evident by the formation of a well-established necking between neighbouring particles.



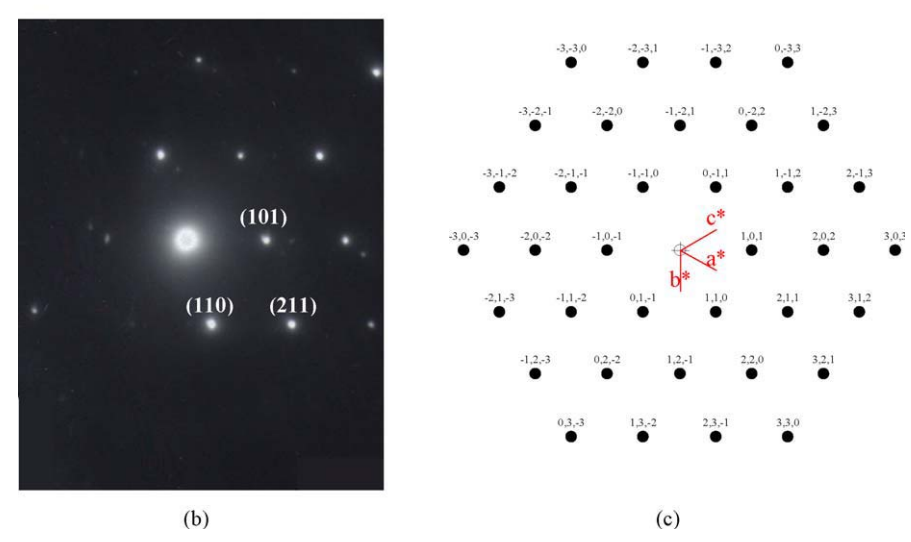


Fig. 10. (a) TEM micrograph with arrow indicates (b) SAED pattern ( $[\bar{1}\ 1\ 1]$  zone axes) and (c) reciprocal lattice pattern simulation of the corundum-route PMN particles.

This observation could be attributed to the mechanism of surface energy reduction of the ultrafine powders, i.e. the smaller the powder the higher the specific surface area [30]. In general, it is seen that primary particle in corundum-route powders is clearly smaller in size than the columbite-route powders. The averaged particle size of corundum-precursor PMN powders with finer particle size is regarded as advantage for better reactivity.

Bright field TEM images of discrete particles of the calcined PMN powders are shown in Figs. 9(a) and 10(a) for the

columbite- and corundum-routes, respectively, indicating the particle sizes and shapes at higher magnifications. The observed morphology reveals the considerable difference in both size and shapes between the two particles. Primary particle in the columbite-route PMN powders is clearly larger in size and also higher in angularity than the corundum-route powders. By employing a combination of both selected area electron diffraction (SAED) and crystallographic analysis, the perovskite phase of cubic PMN was identified for the columbite- and corundum-

Table 2 EDX analysis on PMN powders derived from columbite- and corundum-routes

| EDX positions | Composition | n (at.%) |        | Possible phase(s)   |
|---------------|-------------|----------|--------|---|
|               | Pb (M)      | Mg (K)   | Nb (L) |   |
| x             | 43.12       | 18.87    | 38.01  | Pb(Mg <sub>1/3</sub> Nb <sub>2/3</sub> )O <sub>3</sub>  |
| y             | 8.45        | 84.10    | 7.45   | Pb <sub>1.86</sub> (Mg <sub>0.24</sub> Nb <sub>1.76</sub> )O <sub>6.5</sub> (M), Pb <sub>1.83</sub> (Mg <sub>0.29</sub> Nb <sub>1.71</sub> )O <sub>6.39</sub> (m), MgO (m)          |
| Z             | 5.75        | 89.85    | 4.40   | Pb <sub>1.86</sub> (Mg <sub>0.24</sub> Nb <sub>1.76</sub> )O <sub>6.5</sub> (M), Pb <sub>1.83</sub> (Mg <sub>0.29</sub> Nb <sub>1.71</sub> )O <sub>6.39</sub> (m), MgO (m), PbO (m) |
| a             | 45.04       | 17.75    | 37.21  | $Pb(Mg_{1/3}Nb_{2/3})O_3$   |

M, Majority; m, Minority.

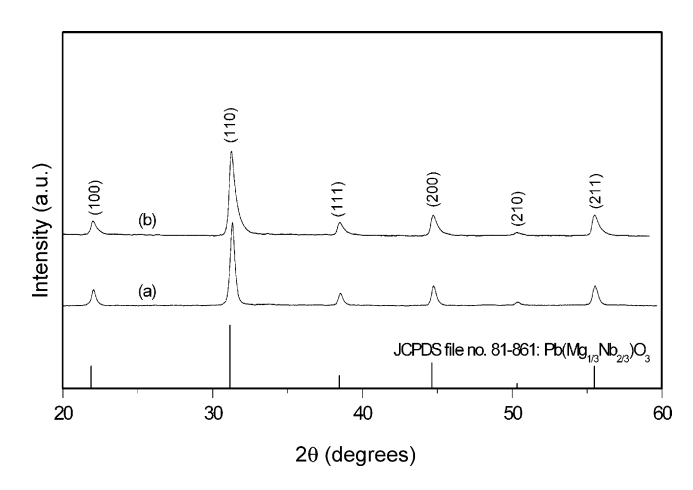


Fig. 11. XRD patterns of PMN ceramics derived from: (a) columbite- and (b) corundum-routes after sintering at  $1225\,^{\circ}\text{C}$  for 2 h.

routes as shown in Figs. 9(b and c) and 10(b and c), respectively, in good agreement with the XRD results.

Preliminary study on the ceramic production from the powders prepared from both routes was also conducted. As shown in Fig. 11, it can be seen that the single-phase perovskite PMN ceramics can be prepared by sintering both PMN powders at 1225 °C for 2 h based upon the firing condition advocated by Ananta and Thomas [5].

## 4. Conclusions

It has been shown that single-phase perovskite PMN powders can be successfully formed by employing either columbite or corundum B-site precursor method via a rapid vibro-milling. Evidence for the formation of a cubic pyrochlore phase, which coexists with the perovskite PMN parent phase, is found at calcination temperture ranging from 800 to 1050 °C. Amongst the two B-site precursor methods, it is seen that lower optimised calcination temperature for the production of pure PMN powders can be obtained by using the columbite route, whereas the smallest obtainable particle size was found in the corundum-route PMN powders.

#### Acknowledgements

The authors gratefully acknowledge the Thailand Research Fund (TRF), the Faculty of Science and the Graduate School, Chiang Mai University for all support.

#### References

- A.J. Moulson, J.M. Herbert, Electroceramics, second ed., Wiley, Chichester, 2003.
- [2] G. Haertling, J. Am. Ceram. Soc. 82 (1999) 797.
- [3] K. Uchino, Piezoelectrics and Ultrasonic Applications, Kluwer, 1998.
- [4] S. Ananta, N.W. Thomas, J. Eur. Ceram. Soc. 19 (1999) 155-163.
- [5] S. Ananta, N.W. Thomas, J. Eur. Ceram. Soc. 19 (1999) 629-635.
- [6] Y.-C. Liou, J.H. Chen, Ceram. Int. 30 (2004) 17-22.
- [7] S.L. Swartz, T.R. Shrout, Mater. Res. Bull. 17 (1982) 1245-1250.
- [8] T.R. Shrout, A. Halliyal, Am. Ceram. Soc. Bull. 66 (1987) 704-711.
- [9] E. Goo, K. Okazaki, J. Am. Ceram. Soc. 69 (1986) C188-C190.
- [10] M. Lejeune, J.P. Boilot, Mater. Res. Bull. 20 (1985) 493–499.[11] P.A. Joy, K. Sreedhar, J. Am. Ceram. Soc. 80 (1997) 770.
- [12] C.H. J. H.C. W. M. J. C. F. D04 (2001) 150
- [12] C.H. Lu, H.S. Yang, Mater. Sci. Eng. B84 (2001) 159.[13] S. Ananta, Mater. Lett. 58 (2004) 2781–2786.
- [14] S. Ananta, Mater. Lett. 58 (2004) 2530-2536.
- [15] H.P. Klug, L.E. Alexander, X-ray Diffraction Procedures, second ed., Wiley, New York, 1974.
- [16] R. Wongmaneerung, R. Yimnirun, S. Ananta, Mater. Lett. 60 (2006) 1447–1452.
- [17] J.P. Guha, J. Mater. Sci. 36 (2001) 5219-5226.
- [18] J. Ryu, J.J. Choi, H.E. Kim, J. Am. Ceram. Soc. 84 (2001) 902.
- [19] A. Udomporn, S. Ananta, Mater. Lett. 58 (2004) 1154-1159.
- [20] Powder Diffraction File No. 81-0861, International Centre for Diffraction Data, Newton Square, PA, 2000.
- [21] M.M.A. Sekar, A. Halliyal, J. Am. Ceram. Soc. 81 (1998) 380-388.
- [22] N.K. Kim, Mater. Lett. 32 (1997) 127-130.
- [23] M. Dambekalne, I. Brante, A. Sternberg, Ferroelectrics 90 (1989) 1-14.
- [24] Powder Diffraction File No. 25-0443, International Centre for Diffraction Data, Newton Square, PA, 2000.
- [25] Powder Diffraction File No. 82-0338, International Centre for Diffraction Data, Newton Square, PA, 2000.
- [26] J.P. Guha, J. Mater. Sci. 34 (1999) 4985-4994.
- [27] L.P. Cruz, A.M. Segadães, J. Rocha, J.D. Pedrosa de Jesus, Mater. Res. Bull. 37 (2002) 1163–1173.
- [28] R. Tipakontitikul, S. Ananta, Mater. Lett. 58 (2004) 449.
- [29] A.L. Costa, G. Fabbri, E. Roncari, C. Capiani, C. Galassi, J. Eur. Ceram. Soc. 21 (2001) 1165–1170.
- [30] J.S. Reeds, Principles of Ceramic Processing, second ed., Wiley, New York, 1995.



#### Available online at www.sciencedirect.com



materials letters

Materials Letters 60 (2006) 2867-2872

www.elsevier.com/locate/matlet

# Effect of calcination conditions on phase formation and particle size of zinc niobate powders synthesized by solid-state reaction

A. Ngamjarurojana, O. Khamman, R. Yimnirun, S. Ananta \*

Department of Physics, Faculty of Science, Chiang Mai University, Chiang Mai 50200, Thailand
Received 26 August 2005; accepted 2 February 2006
Available online 21 February 2006

#### Abstract

A columbite-like phase of zinc niobate,  $ZnNb_2O_6$ , has been synthesized by a solid-state reaction via a rapid vibro-milling technique. The formation of the  $ZnNb_2O_6$  phase in the calcined powders has been investigated as a function of calcination conditions by TG-DTA and XRD techniques. Morphology, particle size and chemical composition have been determined via a combination of SEM and EDX techniques. It has been found that single-phase  $ZnNb_2O_6$  powders were successfully obtained for calcination condition of  $600\,^{\circ}C$  for 2h or  $550\,^{\circ}C$  for 6h with heating/cooling rates of  $30\,^{\circ}C$ /min. Clearly, this study has demonstrated the potentiality of a vibro-milling technique as a significant time-saving method to obtain single-phase  $ZnNb_2O_6$  nanopowders ( $\sim 50-300\,\text{nm}$ ) at low calcination temperature.

Keywords: Zinc niobate; ZnNb<sub>2</sub>O<sub>6</sub>; Columbite; Calcination; Phase formation; Powders; Solid-state reaction

## 1. Introduction

Zinc niobate (ZnNb<sub>2</sub>O<sub>6</sub>, ZN) is one of the binary niobate compounds with excellent dielectric properties at microwave frequencies [1–3]. It has very low loss and high dielectric constant and is a promising candidate for applications in microwave devices [4–6]. This compound with a columbite crystal structure is also a suitable reference material for investigating the defect induced in LiNbO<sub>3</sub> substrates for waveguide fabrication [6,7]. Moreover, recently, it is well established as the key precursor for the successful preparation of single-phase ferroelectric perovskite Pb(Zn<sub>1/3</sub>Nb<sub>2/3</sub>)O<sub>3</sub> (PZN)-based ceramics, which is becoming increasingly important for actuator, transducer and ultrasonic motor applications [8,9].

There has been a great deal of interest in the preparation of single-phase PZN powders as well as in the sintering and piezoelectric properties of PZN-based ceramics [10–14]. In general, the constituents ZnO and  $Nb_2O_5$  are first mixed and reacted together to form zinc niobate (ZnNb $_2O_6$ ), prior to mixing and reacting with PbO in the second step of calcination at

elevated temperature. Interestingly, this mixed oxide route has been employed with minor modifications in the synthesis of ZnNb<sub>2</sub>O<sub>6</sub> itself [10–12]. However, powders prepared by a mixed oxide route have spatial fluctuations in their compositions. The extent of the fluctuation depends on the characteristics of the starting powders as well as on the processing schedule. Generally, the mixed oxide method involves the heating of a mixture of zinc oxide and niobium oxide above 900 °C for long times i.e. 2h [2,5,13], 4h [12,14], 6h [15] and 8h [16]. The optimization of calcination conditions used in the mixed oxide process, however, has not received detailed attention, and the effects of applied dwell time and heating/cooling rates have not yet been studied extensively.

Therefore, the main purpose of this work was to explore a simple mixed oxide synthetic route for the production of ZnNb<sub>2</sub>O<sub>6</sub> (ZN) powders via a rapid vibro-milling technique and to perform a systematic study of the reaction between the starting zinc oxide and niobium oxide precursors. The phase formation and morphology of the powder calcined at various conditions will be studied and discussed. The rapid vibro-milling technique was employed to explore the potentiality in obtaining nano-sized powders, which would in turn lead to lower required firing temperature.

<sup>\*</sup> Corresponding author. Tel.: +66 53 943367; fax: +66 53 943445. E-mail address: Supon@chiangmai.ac.th (S. Ananta).

# 2. Experimental procedure

The starting materials were commercially available zinc oxide, ZnO (Fluka Chemical, 99.9% purity) (JCPDS file number 89-1397) and niobium oxide, Nb<sub>2</sub>O<sub>5</sub> (JCPDS file number 30-873) (Aldrich, 99.9% purity). The two oxide powders exhibited an average particle size in the range of  $3.0-5.0\,\mu m$ . ZnNb<sub>2</sub>O<sub>6</sub> powders were synthesized by the solid-state reaction of thoroughly ground mixtures of ZnO and Nb<sub>2</sub>O<sub>5</sub> powders that were milled in the required stoichiometric ratio. Instead of employing a ball-milling procedure [1,13-15], a McCrone vibro-milling technique was used [17]. In order to combine mixing capacity with a significant time saving, the milling operation was carried out for 0.5h with corundum cylindrical media in isopropyl alcohol (IPA). After drying at 120°C for 2h, the reaction of the uncalcined powders taking place during heat treatment was investigated by themogravimetric and differential thermal analysis (TG-DTA, Shimadzu), using a heating rate of 10°C/min in air from room temperature up to 1000°C. Based on the TG-DTA results, the mixture was calcined at various conditions, i.e. temperatures ranging from 500 to 900°C, dwell times ranging from 0.5 to 8h and heating/cooling rates ranging from 5 to 30°C /min, in closed alumina crucible, in order to investigate the formation of zinc niobate.

Calcined powders were subsequently examined by room temperature X-ray diffraction (XRD; Siemens-D500 diffractometer), using Ni-filtered CuK $_{\alpha}$  radiation to identify the phases formed and optimum calcination conditions for the formation of ZN powders. Powder morphologies and particle sizes were directly imaged, using scanning electron microscopy (SEM; JEOL JSM-840A). The chemical compositions of the phase formed were elucidated by an energy-dispersive X-ray (EDX) analyzer with an ultra-thin window. EDX spectra were quantified with the virtual standard peaks supplied with the Oxford Instruments eXL software.

#### 3. Results and discussion

The TG-DTA simultaneous analysis of a powder mixed in the stoichiometric proportions of ZnNb<sub>2</sub>O<sub>6</sub> is displayed in Fig. 1. In the temperature range from room temperature to ~200 °C, the sample shows both exothermic and endothermic peaks in the DTA curve, consistent with the first weight loss. These observations can be attributed to the decomposition of the organic species from the milling process [17,18]. Increasing the temperature up to ~1000 °C, the solidstate reaction occurred between ZnO and Nb<sub>2</sub>O<sub>5</sub> [2,5,13]. The broad exotherm with several small peaks in the DTA curve represents that reaction, which has a maximum at ~550 and 800°C. These are supported by a second fall in sample weight over the same temperature range. However, it is to be noted that there is no obvious interpretation of these peaks, although it is likely to correspond to a phase transition reported by a number of workers [13-16]. These data were used to define the range of calcination temperatures for XRD investigation between 500 and 900°C.

To further study the phase development with increasing calcination temperature in the powders, they were calcined for 2h in air at various temperatures, up to 900°C, followed by phase analysis using XRD. As shown in Fig. 2, for the uncalcined powder, only X-ray peaks of precursors ZnO (O) and Nb<sub>2</sub>O<sub>5</sub> (●), which could be matched with JCPDS file numbers 89-1397 [19] and 3-873 [20], respectively, are present, indicating that no reaction had yet been triggered during the milling process. It is seen that fine  $ZnNb_2O_6$  crystallites  $(\nabla)$  were developed in the powder at a calcination temperature as low as 500 °C, accompanying with ZnO and Nb2O5 as separated phases. This observation agrees well with those derived from the TG-DTA results and other workers [13,16]. As the temperature increased to 550 °C, the intensity of the columbite-like ZnNb2O6 peaks was further enhanced and became the predominant phase. Upon calcination at 600°C, an essentially monophasic of ZnNb<sub>2</sub>O<sub>6</sub> phase is obtained. This ZN phase was indexable according to an orthorhombic columbite-type structure with lattice parameters  $a=1426\,\mathrm{pm},\,b=572\,\mathrm{pm}$  and  $c=504\,\mathrm{pm},\,\mathrm{space}$ group Pbcn (no. 60), in consistent with JCPDS file numbers 76-1827 [21]. This study also shows that orthorhombic ZN crystallite is the only detectable phase in the powders, after calcination in the range of

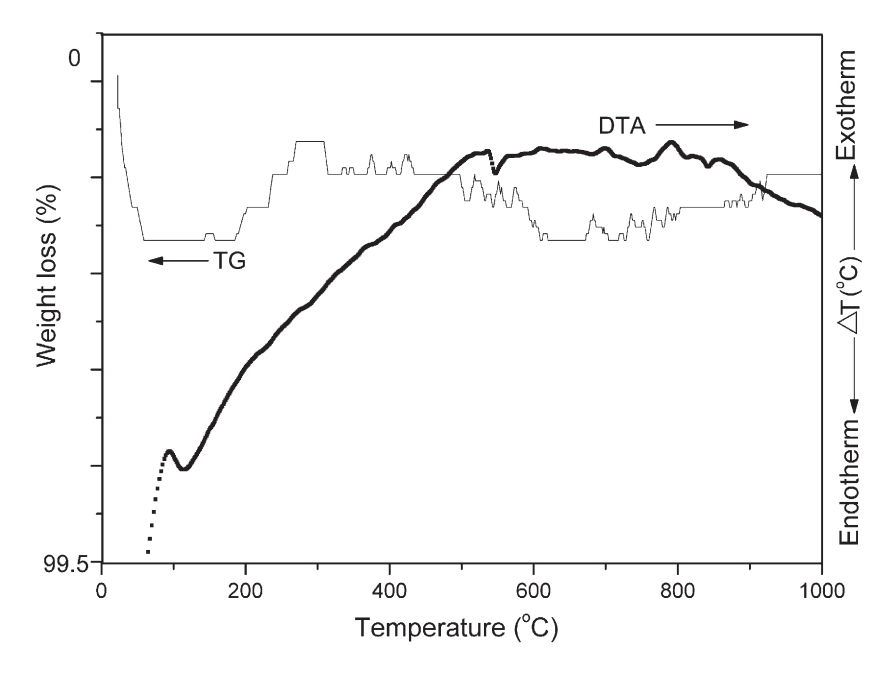


Fig. 1. TG-DTA curves for the mixture of ZnO-Nb<sub>2</sub>O<sub>5</sub> powder.

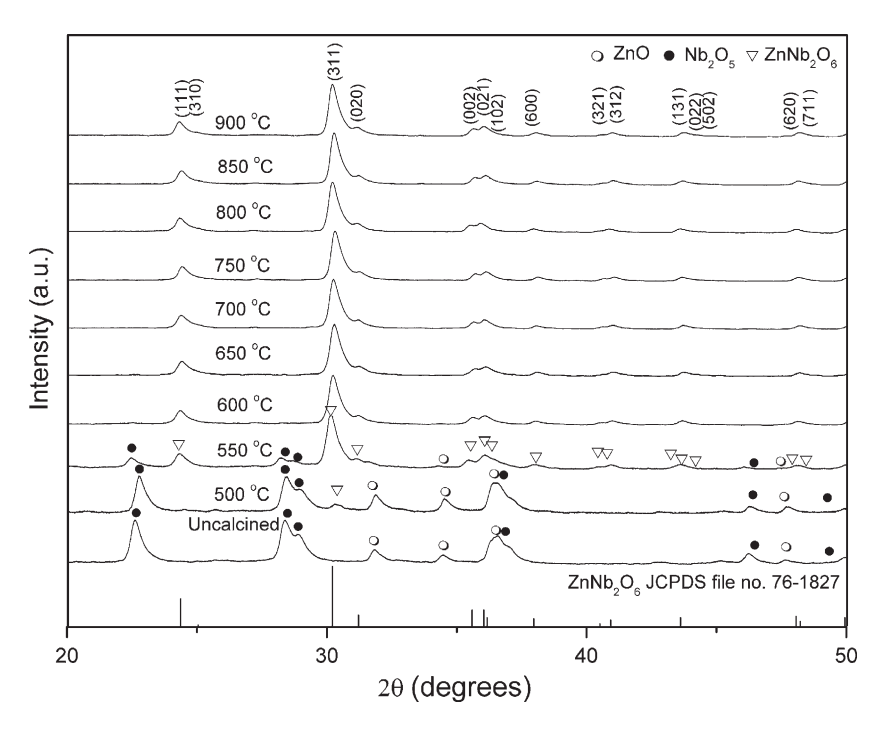


Fig. 2. XRD patterns of ZN powders calcined at various temperatures for 2h with heating/cooling rates of 10 °C/min.

600–900 °C. In earlier works [12–16], long heat treatments at  ${\sim}900-1000$  °C for 2–8h were proposed for the formation of ZnNb<sub>2</sub>O<sub>6</sub> by a conventional mixed oxide synthetic route, although no details on phase formation were provided. However, in the present study, it was found that there are no significant differences between the powders calcined at 600 to 900 °C with dwell time of only 2h, as shown in Fig. 2. This observation would clearly suggest the advantages of a rapid vibromilling technique used in the present study.

Apart from the calcination temperature, the effect of dwell time was also found to be quite significant. From Fig. 3, it can be seen that the single phase of  $ZnNb_2O_6$  (yield of 100% within the limitations of the XRD technique) was found to be possible in powders calcined at

 $600\,^{\circ}\mathrm{C}$  with dwell time of 2h or more. For the present work, there are no significant differences between the powders calcined at  $600\,^{\circ}\mathrm{C}$  with dwell times ranging from 2 to  $8\,h$ . This was apparently a consequence of the enhancement in crystallinity of the  $ZnNb_2O_6$  phase with increasing dwell time. The appearance of ZnO and  $Nb_2O_5$  phases indicated that full crystallization has not occurred at relatively short calcination times. However, in the work reported here, it is to be noted that single phase of  $ZnNb_2O_6$  powder was also successfully obtained for a calcination temperature of  $550\,^{\circ}\mathrm{C}$  with dwell time of at least 6h applied (Fig. 4). This is probably due to the effectiveness of vibro-milling and a carefully optimized reaction. The observation that the dwell time effect may also play an important role in obtaining a single-

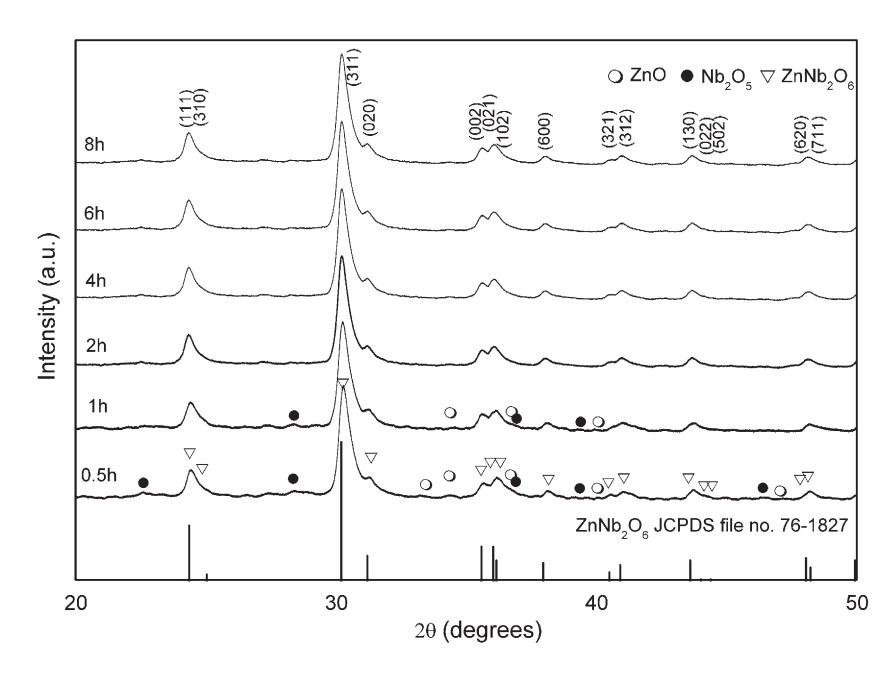


Fig. 3. XRD patterns of ZN powders calcined at 600 °C with heating/cooling rates of 10 °C/min for various dwell times.

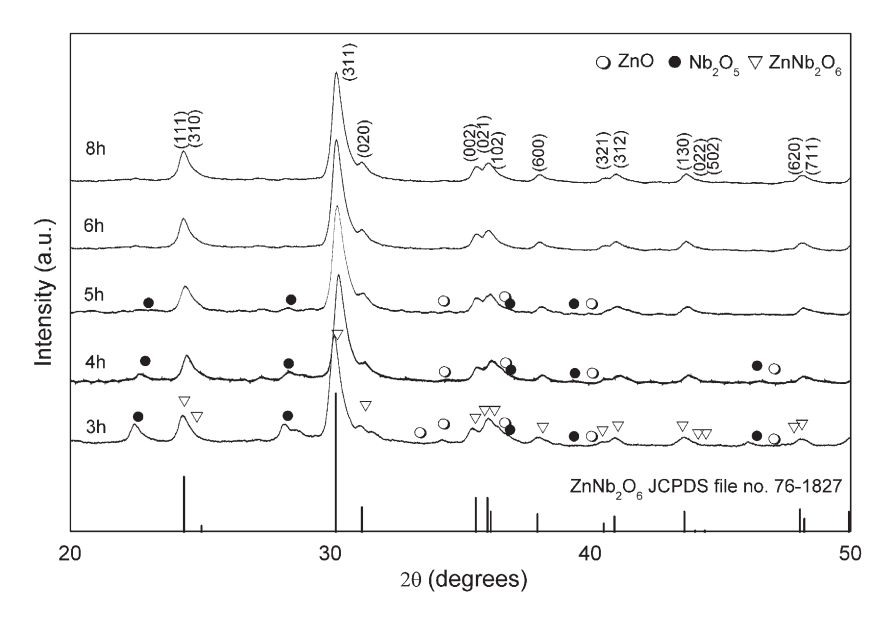


Fig. 4. XRD patterns of ZN powders calcined at 550°C with heating/cooling rates of 10°C/min for various dwell times.

phase columbite product is also consistent with other similar systems [22,23]. It is also very interesting to see that the on-set temperature is approximately 300–400C lower than those reported earlier with a conventional ball-milling method [12–15]. The difference could be attributed to nano-sized mixed powders obtained from a rapid vibro-milling. Most importantly, this study suggests that a rapid vibro-milling method can significantly lower the optimum calcination temperature for formation of single-phase ZN powders.

In the present study, an attempt was also made to calcine ZN powders under various heating/cooling rates (Fig. 5). In this connection, it is shown that the yield of  $ZnNb_2O_6$  phase did not vary significantly with different heating/cooling rates, ranging from 5 to  $30\,C/min$ , in good agreement with early results reported for the mixture of the two kinds of refractory oxides [17,23].

Based on the TG-DTA and XRD data, it may be concluded that, over a wide range of calcination conditions, single-phase  $ZnNb_2O_6$ 

cannot be straightforwardly formed via a solid-state mixed oxide synthetic route, unless a careful design of calcination is performed. It is well documented that powders prepared by a conventional mixed oxide method have spatial fluctuations in their compositions. The extent of the fluctuation depends on the characteristics of the starting powders as well as the processing schedules [13,16,22]. The experimental work carried out here suggests that the optimal calcination conditions for single-phase ZnNb<sub>2</sub>O<sub>6</sub> (with impurities undetected by XRD technique) is 600 °C for 2h or 550 °C for 6h, with heating/cooling rates as fast as 30 °C/min. Moreover, the formation temperature and dwell time for the production of ZnNb<sub>2</sub>O<sub>6</sub> powders observed in this work are also much lower than those reported earlier [14–16]. This clearly emphasizes the advantages of a rapid vibro-milling technique.

Finally, the morphological changes in the  $ZnNb_2O_6$  powders formed by a mixed oxide are illustrated in Fig. 6(a–f) as a function of calcination temperatures, dwell times and heating/cooling rates,

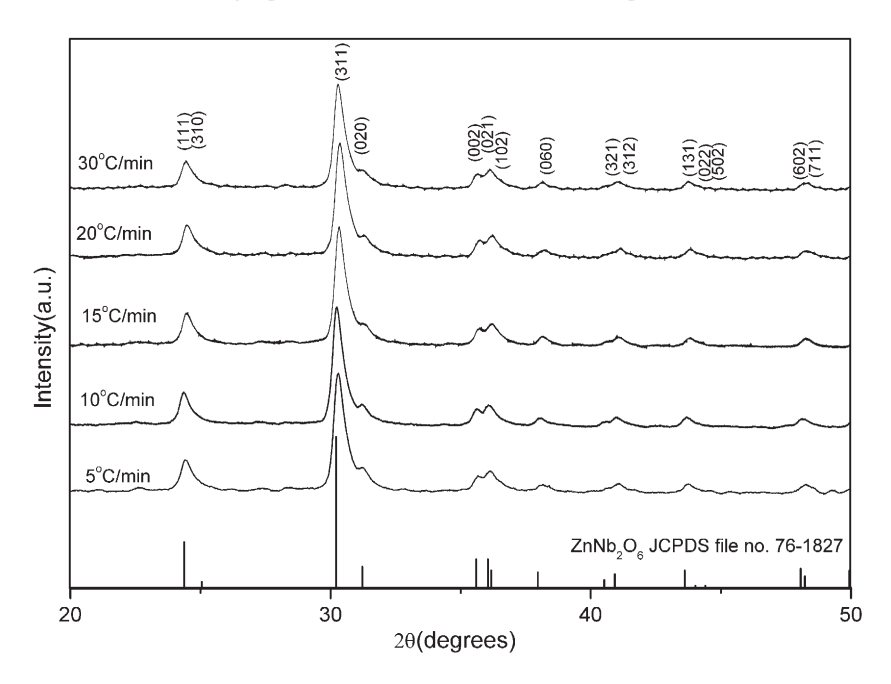


Fig. 5. XRD patterns of ZN powders calcined at 600°C for 2h with various heating/cooling rates.

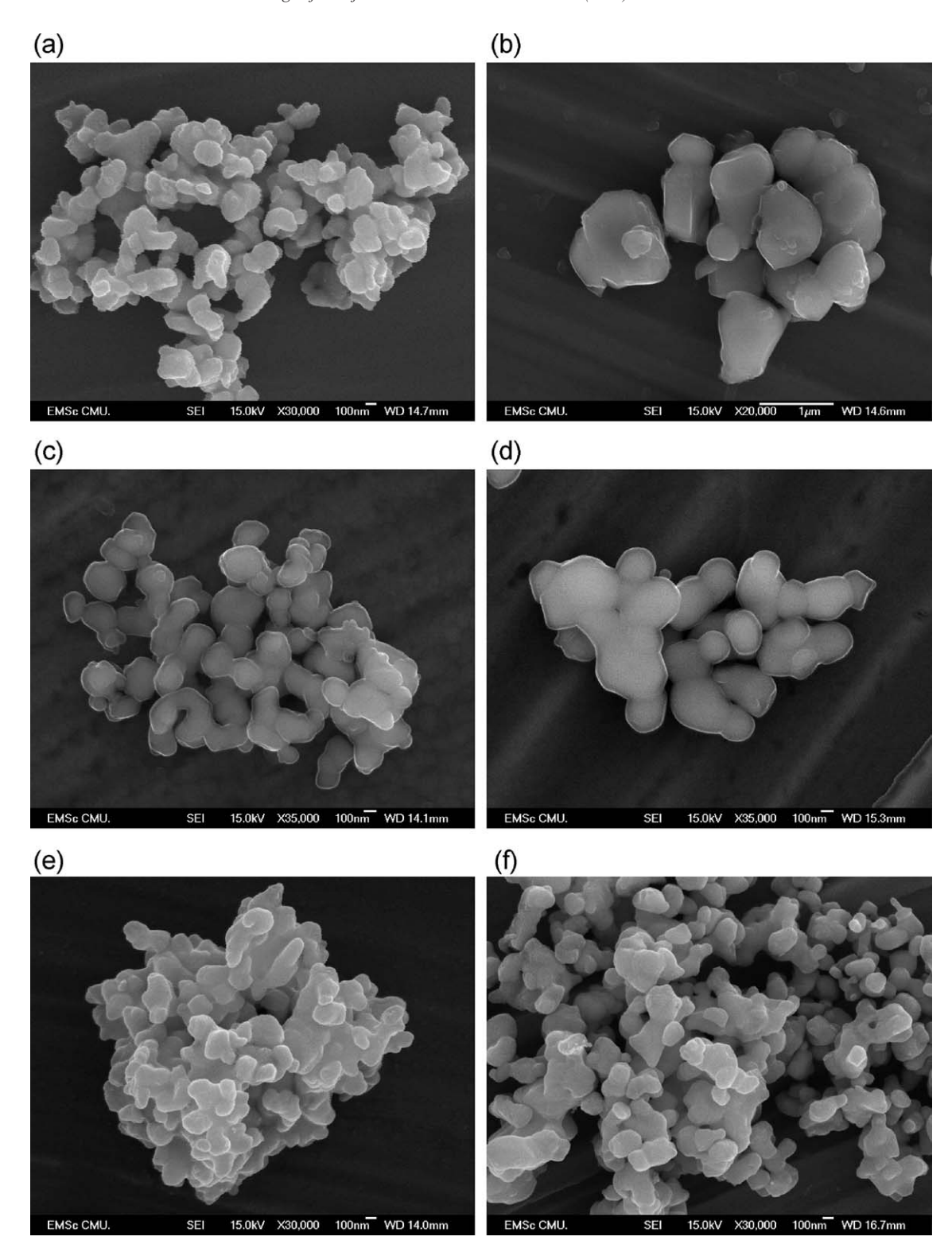


Fig. 6. SEM micrographs of the ZN powders calcined for 2h with heating/cooling rates of 10 °C/min at (a) 600, (b) 900, and at 600 °C with heating/cooling rates of 10 °C/min for (c) 4, (d) 8h, and at 600 °C for 2h with heating/cooling rates of (e) 10 and (f) 30 °C/min.

respectively. The influence of calcination conditions on particle size is given in Table 1. In general, the particles are agglomerated and irregular in shape, with a substantial variation in particle size, particularly in samples calcined at high temperature (Fig. 6(b)) or with fast heating/cooling rates (Fig. 6(e,f)). This finding is also similar to that in  $ZrTiO_4$  powders synthesized by Ananta et al. [17]. The results indicate that

difference in particle size and degree of agglomeration tend to increase with calcination temperatures (Table 1). After calcinations at 900°C (Fig. 6(b)), the powders seem to display a significant level of necking and bonding as if they were in the initial stages of sintering.

The effects of dwell time and heating/cooling rates on the morphology of the calcined powders were also found to be quite significant. As

Table 1 Particle size range of  $ZnNb_2O_6$  powders calcined at various conditions

| Calcination conditions |                |                | Particle                 |  |
|------------------------|----------------|----------------|--------------------------|--|
| Temperature (°C)       | Dwell time (h) | Rates (°C/min) | size<br>range<br>(±10nm) |  |
| 550                    | 6              | 30             | 92-320                   |  |
| 600                    | 2              | 10             | 75-220                   |  |
| 600                    | 4              | 10             | 80-340                   |  |
| 600                    | 6              | 10             | 120-400                  |  |
| 600                    | 8              | 10             | 180-620                  |  |
| 600                    | 2              | 20             | 70-220                   |  |
| 600                    | 2              | 30             | 50-300                   |  |
| 700                    | 2              | 10             | 120-250                  |  |
| 800                    | 2              | 10             | 150-420                  |  |
| 900                    | 2              | 10             | 300-800                  |  |

expected, it is seen that longer heat treatment leads to larger particle sizes and hard agglomeration (Fig. 6(c,d)). As shown in Fig. 6(e,f), by increasing the heating/cooling rates, averaged particle size tends to decrease whilst the degree of agglomeration tends to increase. This observation could be attributed to the mechanism of surface energy reduction of the ultrafine powders, i.e. the smaller the powder the higher the specific surface area [24]. To the author's knowledge, the present data are the first results for the morphology-calcination relationship of ZnNb<sub>2</sub>O<sub>6</sub> powders prepared by the solid-state reaction. It is also of interest to point out that mass production of single-phase ZnNb<sub>2</sub>O<sub>6</sub> nanopowders with the smallest particle size ~50nm (estimated from SEM micrographs) can be achieved by employing a simple solid-state reaction combined with a rapid vibro-milling technique. In addition, EDX analysis using a 20 nm probe on a large number of particles of the calcined powders confirms that the parent composition is ZnNb<sub>2</sub>O<sub>6</sub> powders, in good agreement with XRD results.

The results obtained in this study clearly suggest that a systematic study of the effect of milling parameters such as milling times and milling speed on the phase and morphology evolutions of the  $ZnNb_2O_6$  powders are required for better understanding and verifying the attractiveness of the vibro-milling technique. Further investigation of this relationship is underway and will be reported in the future.

#### 4. Conclusions

The solid-state mixed oxide method via a rapid vibro-milling technique is explored in the preparation of single phase ZN nanopowders. The calcination temperature and dwell time have been found to have a pronounced effect on phase formation and particle size of the calcined  $ZnNb_2O_6$  powders. This work demonstrated that single-phase of zinc niobate powders with particle size ranging from  $50{\text -}300\,\text{nm}$  can be produced via this

technique by using a calcination temperature of 600 °C for 2h or 550 °C for 6h, with heating/cooling rates of 30 °C/min. The resulting ZN powders consist of variety of agglomerated particle sizes, depending on calcination conditions.

#### Acknowledgements

We thank the Thailand Research Fund (TRF), Graduate School and Faculty of Science, Chiang Mai University, and Ministry of University Affairs of Thailand for all support.

#### References

- [1] R.C. Pullar, J.D. Breeze, N.M. Alford, J. Am. Ceram. Soc. 88 (2005) 2466.
- [2] H.J. Lee, S.J. Kim, I.T. Kim, Mater. Res. Bull. 32 (1997) 847.
- [3] D.W. Kim, K.H. Ko, K.S. Hong, J. Am. Ceram. Soc. 84 (2001) 1286.
- [4] Y.C. Zhang, Z.X. Yue, X. Qi, B. Li, Z.L. Gui, L.T. Li, Mater. Lett. 58 (2004) 1392.
- [5] Y.C. Zhang, L.T. Li, Z.X. Yue, Z.L. Gui, Mater. Sci. Eng., B, Solid-State Mater. Adv. Technol. 99 (2003) 282.
- [6] A.Z. Simoes, A.H.M. Gonzalez, A.A. Cavalheiro, M.A. Zaghete, B.D. Stojanovic, J.A. Varela, Ceram. Int. 28 (2002) 265.
- [7] C. Zaldo, M.J. Martin, C. Coya, K. Polgar, A. Peter, J. Paitz, J. Phys., Condens. Matter 7 (1995) 2249.
- [8] Y. Xu, Ferroelectric Materials and Their Applications, Elsevier Science, Amsterdam, The Netherlands, 1991.
- [9] A.J. Moulson, J.M. Herbert, Electroceramics, 2nd ed.Wiley, New York, 2003
- [10] Y. Hou, M.K. Zhu, H. Wang, B. Wang, H. Yan, C.S. Tian, Mater. Lett. 58 (2004) 1508.
- [11] W. Zhu, A.L. Kholkin, P.Q. Mantas, J.L. Baptista, J. Am. Ceram. Soc. 84 (2001) 1740.
- [12] M. Villegas, A.C. Caballero, C. Moure, P. Durán, J.F. Fernández, R.E. Newnham, J. Am. Ceram. Soc. 83 (2000) 141.
- [13] N. Vittayakorn, G. Rujijanagul, T. Tunkasiri, X. Tan, D.P. Cann, Mater. Sci. Eng., B, Solid-State Mater. Adv. Technol. 108 (2004) 258.
- [14] X.J. Lu, X.M. Chen, J. Electroceram, 7 (2001) 127.
- [15] C.L. Li, C.C. Chou, Int. Ferro. 55 (2003) 955.
- [16] L.B. Kong, J. Ma, H. Huang, R.F. Zhang, T.S. Zhang, J. Alloys Compd. 347 (2002) 308.
- [17] S. Ananta, R. Tipakontitikul, T. Tunkasiri, Mater. Lett. 57 (2003) 2637.
- [18] S. Ananta, Mater. Lett. 58 (2004) 2834.
- [19] Powder Diffraction File No. 89-1397. International Centre for Diffraction Data, Newton Square, PA, 2000.
- [20] Powder Diffraction File No. 3-873. International Centre for Diffraction Data, Newton Square, PA, 2000.
- [21] Powder Diffraction File No. 76-1827. International Centre for Diffraction Data. Newton Square. PA. 2000.
- [22] S. Ananta, R. Brydson, N.W. Thomas, J. Eur. Ceram. Soc. 20 (2000) 2325.
- [23] S. Ananta, Mater. Lett. 58 (2004) 2781.
- [24] J.S. Reed, Principles of Ceramic Processing, 2nd ed.Wiley, New York, 1995.

Ferroelectric Letters, 33:137–146, 2006 Copyright © Taylor & Francis Group, LLC ISSN: 0731-5171 print / 1543-5288 online DOI: 10.1080/07315170601014984



# Polarization Behavior in the Two Stage Sintered Lead Titanate Ceramics

R. WONGMANEERUNG,<sup>1,2</sup> R. YIMNIRUN,<sup>1</sup> S. ANANTA,<sup>1</sup> R. GUO,<sup>2</sup> and A. S. BHALLA<sup>2</sup>

<sup>1</sup>Chiang Mai University, Department of Physics, Faculty of Science, Chiang Mai, Thailand <sup>2</sup>Pennsylvania State University, Materials Research Laboratory, University Park, PA 16802, USA

Communicated by Dr. George W. Taylor

(Received July 24, 2006)

Polarization behavior in lead titanate, prepared by the two stage sintering approach, is determined by using the dilatometer thermal expansion data. We report the temperature-dependent measurements of the strain, the magnitude of polarization,  $\sqrt{\bar{P}}_s^2$ , deduced from the sets of data gathered from the thermal expansion values. The calculated values of the electric polarization,  $P_s$ , on the two stage sintered lead titanate ceramics show the simple approach to determine the temperature dependence of the polarization below and around the transition temperature. Various aspects of our understanding of the polarization behavior and other effects in the ferroelectric are discussed.

Keywords: polarization behavior; thermal expansion; lead titanate

# INTRODUCTION

The high Curie temperature of lead titanate, PbTiO<sub>3</sub>, ceramics has long qualified these materials for potential high-temperature and high frequency applications [1–3]. For PbTiO<sub>3</sub>, above the ferroelectric transition temperature,  $T_C$ , the structure is cubic and below  $T_C$  it becomes tetragonal with a spontaneous polarization  $P_S$ . In general, the value of  $P_S$  is difficult to measure due to its high coercive field and  $T_C \approx 490^{\circ}C$  [1]. However, the change in polarization with temperature can be observed through thermal expansion (or strain) measurements and from the data, spontaneous polarization and

 $* Corresponding \ author. \ E-mail: as b 2@psu.edu$ 

its temperature dependence can be computed. Some authors [4, 5] suggest the value of  $P_S$  at room temperature to be greater than 50  $\mu$ C/cm<sup>2</sup>. Shirane [6] and Jona [7] give the value of  $P_S = 80 \mu$ C/cm<sup>2</sup>.

It is always a challenge to measure the temperature-dependence of the polarization of the high  $T_C$  ferroelectric over the entire temperature range. In general with the increase in temperature and due to the increase in losses in the PbTiO<sub>3</sub> samples it hinders the real spontaneous polarization and its ( $P_S$ ) temperature dependence measurements at higher temperature by using the hysteresis and pyroelectric techniques. Therefore, some alternate approaches have to be made in order to extract some useful data on PbTiO<sub>3</sub> for the polarization versus temperature behavior. From the phenomenological approach we know that the  $P_S$  values can be extracted by using the relation [8];

$$x_{ij} = \frac{\Delta l}{l} = Q_{ijkk} P_k^2 \tag{1}$$

where  $x_{ij}$  is the strain,  $\Delta l/l$  is thermal expansion,  $Q_{ijkk}$  is the electrostrictive coefficient. Q coefficients are determined in paraelectric phase and considered constant. And  $P_k^2$  is the polarization.

Also, by knowing the  $\Delta l/l$  and its temperature dependence,  $P_k$  versus temperature as well as the transition temperature of PbTiO<sub>3</sub> and the nature of the transition can be studied.

In this paper, we report the  $P_S$  versus temperature behavior of PbTiO<sub>3</sub> samples prepared and sintered under various conditions. Thermal expansion versus temperature behavior has been measured and the values of polarization at various temperatures have been computed. Measurements have also been extended on the unpoled, poled and depoled samples and compared. As clear from the equation (1) that  $\Delta l/l$  is directly related to the square of polarization and thus the measurements do not specifically require the poled samples.

# EXPERIMENTAL PROCEDURE

Commercially available powders of PbO and TiO<sub>2</sub> (anatase form), (Fluka, >99% purity) were used as starting materials. PbTiO<sub>3</sub> powders were synthesized by a simple mixed oxide method. Ceramic fabrication was achieved by adding 3 wt% polyvinyl alcohol binder, prior to pressing as pellets in a pseudo-uniaxial die press at 100 MPa. Each pellet was placed in an alumina

crucible together with an atmosphere powder of identical chemical composition. Sintering was carried out with a dwell time of 2 h at each step, with constant heating/cooling rates of 1°C/min [9]. Three sets of the first sintering temperature were assigned for the two stage sintering [10] case: 700, 800 and 900°C. The second sintering temperature was set at 1200°C.

For thermal expansion measurement, the PbTiO<sub>3</sub> samples were cut in bar shapes (5 mm long and 1 mm thick). The sample was placed inside a fused silica holder and the thermal expansion was measured as a function of temperature using a linear voltage-differential transformer (LVDT) dilatometer. The samples were heated at a rate of  $2^{\circ}$ C/min from room temperature to 600°C. The LVDT has an advantage over the other transformer; it gives a linear output for every unit displacement.

#### RESULTS AND DISCUSSION

The thermal expansion behaviors of PbTiO<sub>3</sub> ceramics synthesized under various sintering condition and with unpoled, poled and depoled states were measured by a high-sensitivity dilatometer, Table I summarizes the various important features of these measurements. The results are shown in Figs. 1a, 1b and 1c, respectively. It should be noted that the thermal expansion measurements were made during the first heating from room temperature after poling. The results show the thermal expansion of PbTiO<sub>3</sub> ceramics sintered at 700/1200°C, 800/1200°C and 900/1200°C, respectively in Figs. 1a, b and c. The thermal expansion behaviors of these samples are linear at temperatures above 500°C, i.e., above Curie temperature.

The change of strain at the Curie point may be easily seen in the thermal contraction curves. The phase transition temperatures are in good agreement with the published values [11, 12]. The curves on the depoled samples are parallel to the curve for the unpoled sample, essentially restoring the sample

**TABLE I** Summary of the various important features of the thermal expansion measurements

|   | T <sub>C</sub> (°C) |                   |                   |                         | lates $P_S$ at erature ( $\mu C$ |                         |
|---|---------------------|-------------------|-------------------|-------------------------|----------------------------------|-------------------------|
| Sample  | Unpoled             | Poled 11          | Poled ⊥           | Unpoled                 | Poled 11                         | Poled ⊥                 |
| 1 PbTiO <sub>3</sub> 700/1200°C<br>2 PbTiO <sub>3</sub> 800/1200°C<br>3 PbTiO <sub>3</sub> 900/1200°C | 489<br>481<br>478   | 482<br>478<br>477 | 489<br>482<br>476 | 74.99<br>75.49<br>76.85 | 75.76<br>72.28<br>74.62          | 69.47<br>72.06<br>75.81 |

dimension to the prepoled value. Effect of poling on thermal expansion properties was also determined. It can be noted that the strain values for both perpendicular and parallel (w.r.t. length direction) poled sampled can be reduced or changed by the surface charge. Moreover, it is indicated that the transition temperature is comparatively decreased from the Curie point of the unpoled ceramics.

The high temperature data in the cubic phase, above  $T_C$ , can be approximated by a straight line. The deviation from this linear high temperature behavior occurs at approximately the same temperature ( $\sim 500^{\circ}$ C). On analyzing the deviation of the strain from the high temperature linear behavior and by using Eq. (1) the  $P_S$  values can be obtained at various temperatures. Using the values of  $Q_{11} = 8.9 \times 10^{-2} \, \text{m}^4/\text{C}^2$  and  $Q_{12} = -2.6 \times 10^{-2} \, \text{m}^4/\text{C}^2$  [13], the  $P_S$  can be calculated. The results for various samples are plotted in

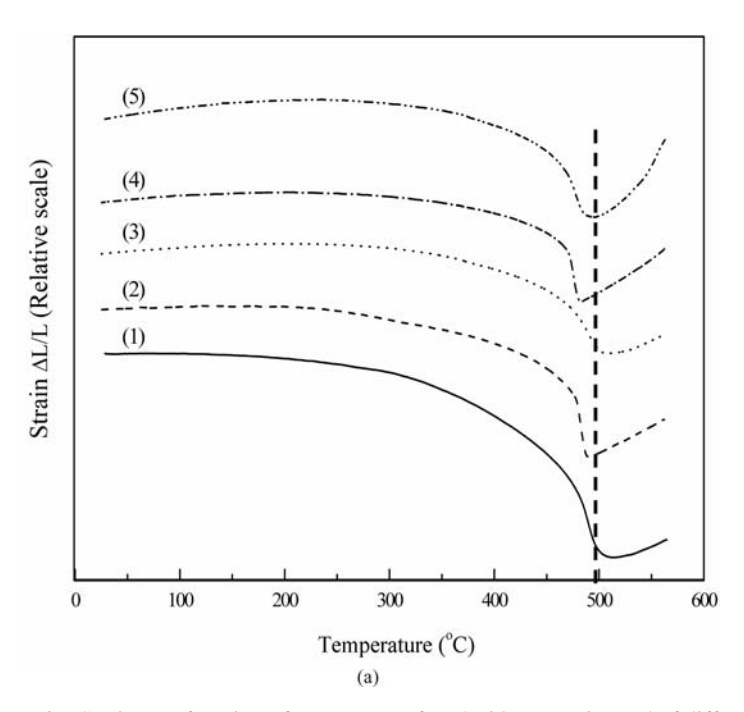


**Figure 1.** Strain as a function of temperature for PbTiO<sub>3</sub> ceramics and of different poling states: (1) unpoled, (2) poled parallel to the length direction, (3) poled perpendicular to the length direction, (4) depoled parallel to the length direction and (5) depoled perpendicular to the length direction (all measurements are in heating cycles and along the length direction); Figures a, b, c are for (a) sintered at 700/1200°C, (b) sintered at 800/1200°C and (c) sintered at 900/1200°C. (*Continued*)

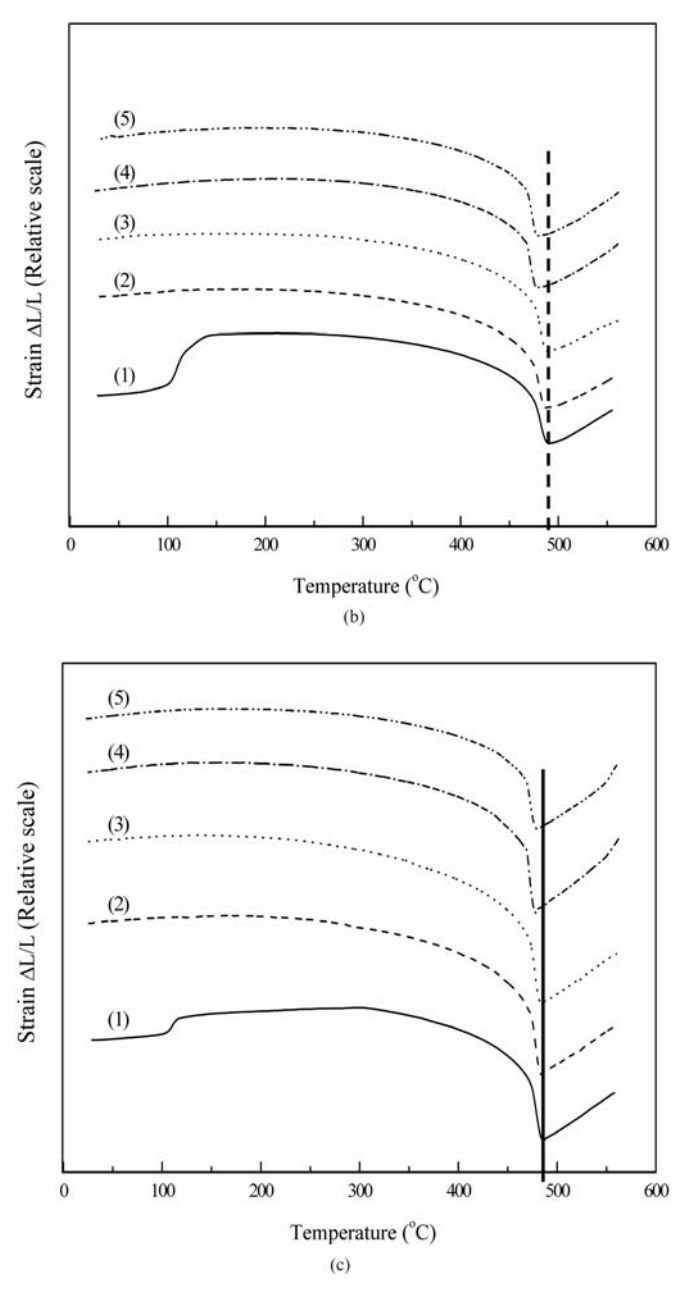
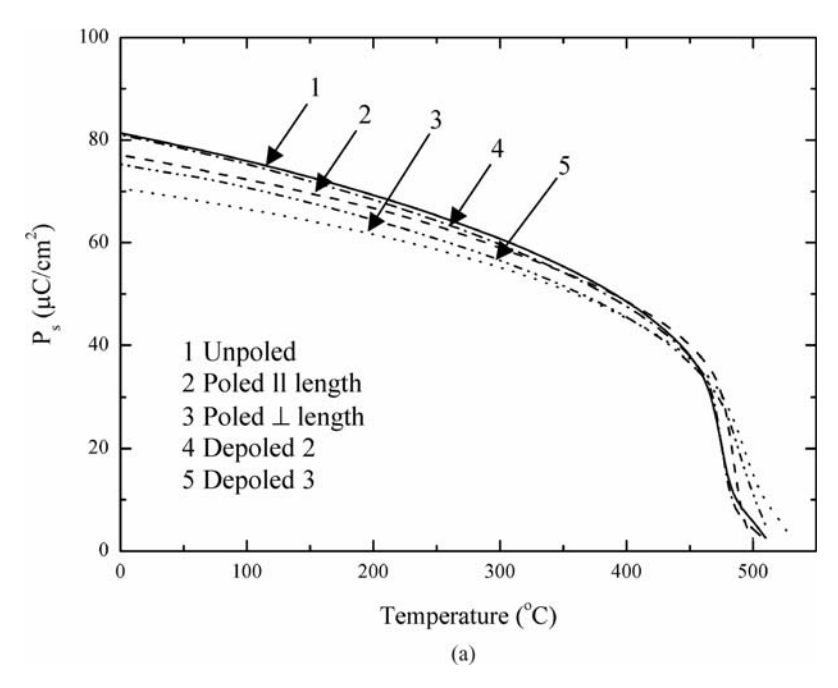


Figure 1. (Continued)

Figs. 2a, 2b and 2c, respectively. When calculating the spontaneous strains of the tetragonal at a particular temperature, the cubic cell constant should be extrapolated to that temperature accounting for the thermal expansion. A linear extrapolation from above the transition can be made over a narrow range with fairly good accuracy.

In Figures 2a, 2b and 2c are shown the  $P_s = \sqrt{\bar{P}_S^2}$  values calculated from the thermal expansion data. The agreement in the  $P_S$  values is excellent. The values are also in good agreement not only in magnitude but also in the  $T_C$  values with the earlier reported results [6, 7]. Figure 2a, shows the  $P_S$  value versus temperature of PbTiO<sub>3</sub> ceramic sintered at 700/1200°C. The  $P_S$  value in the case of unpoled sample is slightly higher than those of both parallel and perpendicular poled samples in temperature range below Curie point, and is caused by the  $P_S$  of the poled ceramics. Also the  $P_S$  is smaller than the value in thermally depoled sample. Similar trends have



**Figure 2.**  $P_S$  as a function of temperature for PbTiO<sub>3</sub> ceramics with and without poling: (1) unpoled, (2) poled parallel to the length direction, (3) poled perpendicular to the length direction, (4) depoled parallel to the length direction and (5) depoled perpendicular to the length direction; figures a, b, c are for (a) sintered at 700/1200°C, (b) sintered at 800/1200°C and (c) sintered at 900/1200°C. (*Continued*)

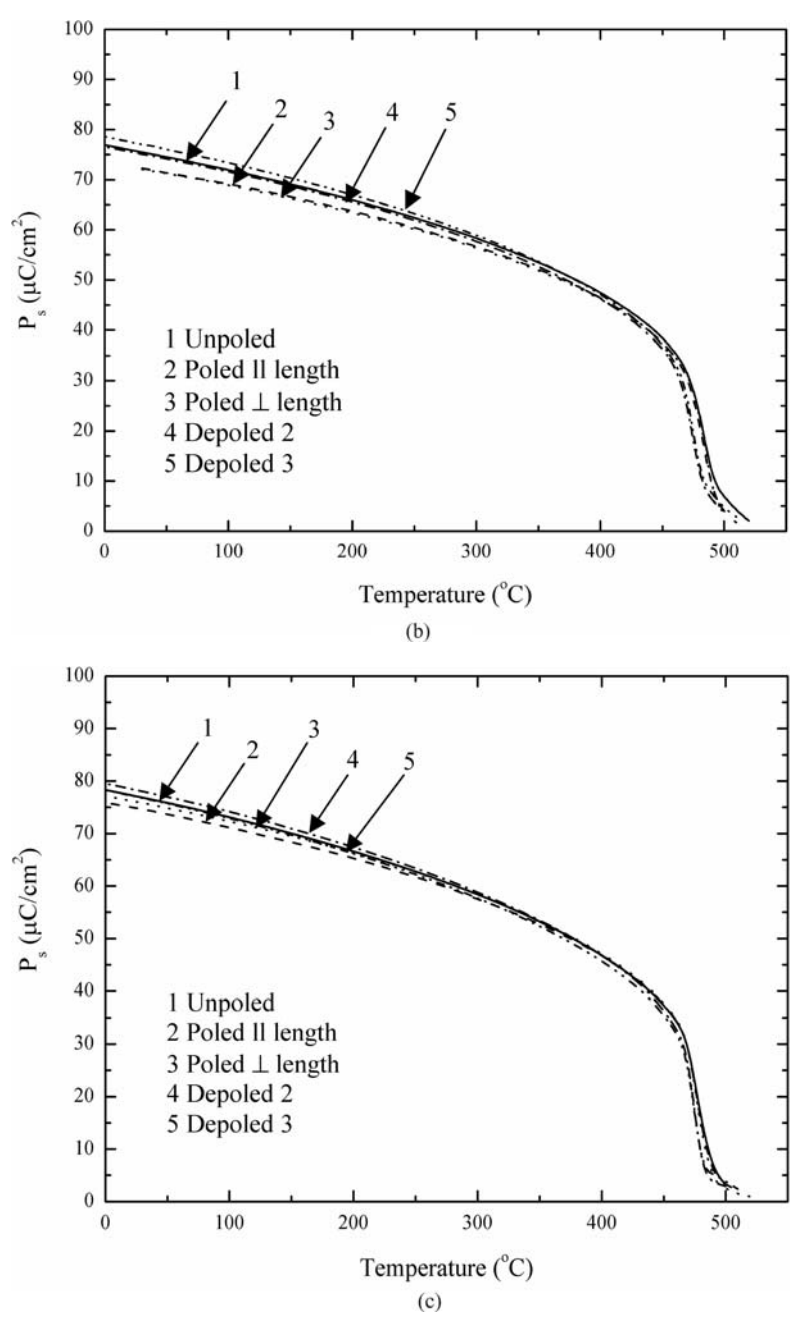


Figure 2. (Continued)

been noticed in the samples sintered under different processing conditions. There are a few factors which could be influencing the measurements. First, there are some sources of contributions to the strain in ferroelectrics, i.e., in addition to the structural component which is present at all temperatures, a component associated with the appearance of spontaneous polarization in the case of ferroelectric state is also present. The contribution of the spontaneous polarization to strain is due to electrostrictive coupling. Second, after poling it is also possible to have some residual surface charge on the surfaces which can affect the net strain. For perpendicular poling conditions, the net thermal strain might be more along the length due to the positive expansion of a-axis. Therefore, the strain along the length direction can be affected differently in the parallel and perpendicular poled samples. At temperature near T<sub>C</sub>, it is seen that the P<sub>S</sub> values of both poled samples are sharper compare to those of unpoled and depoled samples. For the other two samples sintered under different conditions, the polarization behaviors are slightly different, however, the magnitude of P<sub>S</sub> and trend of polarization behavior are similar to that of 700/1200°C PbTiO<sub>3</sub> ceramic. The sharpness of the transition increases and the hyteresis space gradually decreases for the samples sintered at higher temperature in first step of the two stage sintering process.

# **CONCLUSIONS**

We investigated the polarization behavior of PbTiO<sub>3</sub> ceramics in unpoled, poled and depoled states by using the thermal expansion data. The room temperature  $P_S = 75~\mu\text{C/cm}^2$  is in good agreement with the reported values and also suggesting that thermal strain data can be used for estimating the reliable polarization and its temperature dependence in the case of high  $T_C$  ferroelectrics or where the high conductivity of the samples interferes with the electrical measurements. Some important conclusions are made as follow:

- (i) The temperature dependence of thermal strain of unpoled and poled ceramics showed nonlinearity and large anomalies resulting from polarization.
- (ii) The unpoled and depoled samples synthesized under the different two stage sintering conditions exhibited similar behavior in strain versus temperature and the poled samples tend to increase the sharpness of the transition. The polarization behavior shows a sharp first-order phase transition.

- (iii) Hysteresis of T<sub>C</sub> in heating and cooling cycles is larger in the samples sintered at lower temperature (data not shown here).
- (iv) On poling hysteresis of  $T_{\text{C}}$  (cooling and heating cycles) in general decreases.
- (v) Transitions with parallel poled samples are sharper.
- (vi) The polarization versus temperature and its decay, above  $T_C$ , is less dispersive for the high temperature sintered or the high density ceramics.
- (vii) In the case of higher density samples, all the T<sub>C</sub> (unpoled, poled and depoled) are approximately the same.

# **ACKNOWLEDGMENT**

We thank the Thailand Research Fund (TRF), the Graduate School of Chiang Mai University and NSF Relaxor program, Materials Research Laboratory and MRI of Penn State University for all the support during this work.

#### REFERENCES

- [1] B. Jaffe, W. R. Cook, and H. Jaffe, *Piezoelectric Ceramics* (New York, Academic Press, 1971).
- [2] G. H. Haertling, Ferroelectric Ceramics: History and Ttechnology, J. Am. Ceram. Soc., 82(4), 797–818 (1999).
- [3] T. Takahashi, Lead Titanate Ceramics with Large Piezoelectric Anisotropy and Their Applications, Am. Ceram. Soc. Bull. 69, 691–695 (1990).
- [4] G. Burns and B.A. Scott, Lattice Modes in Ferroelectric Perovskite: PbTiO<sub>3</sub>, *Phys. Rev. B* 7, 3087–3101 (1973).
- [5] F. G. Fesenko, V. G. Gavrilyachenko, and E. V. Zarochencev, Izv, Akad. Nauk SSSR, 34, 2541 (1970).
- [6] V. G. Gavrilyachenko, R. I. Spinko, M. A. Martynenko, and E. G. Fesenko, Fiz. Tverd. Tela 12, 1532 (1970); Sov. Phys. Solid State (English Transl.) 12, 1203 (1970).
- [7] F. Jona and G. Shirane, Ferroelectric Crystal (Oxford, Pergamon Press, 1962).
- [8] A. S. Bhalla, R. Guo, and L. E. Cross, Measurements of Strain and the Optical Indices in the Ferroelectric Ba<sub>0.4</sub>Sr<sub>0.6</sub>Nb<sub>2</sub>O<sub>6</sub>: Polarization Effects, *Phys. Rev. B.* 36, 2030–2035 (1987).
- [9] A. Udomporn, K. Pengpat, and S. Ananta, Highly Dense Lead Titanate Ceramics from Refined Processing, *J. Eur. Ceram. Soc.* 24, 185–188 (2004).
- [10] S. Ananta and N.W. Thomas, Fabrication of PMN and PFN Ceramics by a Two-Stage Sintering Technique, J. Eur. Ceram. Soc. 19, 2917–2930 (1999).

- [11] G. Shirane and S. Hoshino, On the Phase Transition in Lead Titanate, J. Phys. Soc. Jpn. 6, 265–270 (1951).
- [12] G. Shirane, R. Pepinsky, and B. C. Frazer, X-Ray and Neutron Diffraction Study of Ferroelectric PbTiO<sub>3</sub>, Acta Crystallogr., 9, 131–140 (1956).
- [13] M. J. Huan, E. Furman, S. J. Jang, H. A. McKinstry and L. E. Cross, Thermodynamic Theory of PbTiO<sub>3</sub>, J. Appl. Phys. 62, 3331–3338 (1987).



Available online at www.sciencedirect.com



materials letters

Materials Letters 61 (2007) 639-643

www.elsevier.com/locate/matlet

# Effect of calcination conditions on phase formation and particle size of nickel niobate powders synthesized by solid-state reaction

O. Khamman, R. Yimnirun, S. Ananta\*

Department of Physics, Faculty of Science, Chiang Mai University, Chiang Mai 50200, Thailand

Received 31 March 2006; accepted 14 May 2006

Available online 6 June 2006

#### Abstract

The solid-state mixed oxide method via a rapid vibro-milling technique is explored in the preparation of single-phase nickel niobate (NiNb<sub>2</sub>O<sub>6</sub>) powders. The formation of the NiNb<sub>2</sub>O<sub>6</sub> phase in the calcined powders has been investigated as a function of calcination conditions by TG-DTA and XRD techniques. Morphology, particle size and chemical composition have been determined via a combination of SEM and EDX techniques. It has been found that the minor phases of unreacted NiO and Nb<sub>2</sub>O<sub>5</sub> precursors and the Ni<sub>4</sub>Nb<sub>2</sub>O<sub>9</sub> phase tend to form together with the columbite NiNb<sub>2</sub>O<sub>6</sub> phase, depending on calcination conditions. More importantly, it is seen that optimization of calcination conditions can lead to a single-phase NiNb<sub>2</sub>O<sub>6</sub> in an orthorhombic phase.

© 2006 Elsevier B.V. All rights reserved.

Keywords: Nickel niobate; NiNb<sub>2</sub>O<sub>6</sub>; Columbite; Calcination; Phase formation; Powders solid-state reaction

## 1. Introduction

Lead nickel niobate, Pb(Ni<sub>1/3</sub>Nb<sub>2/3</sub>)O<sub>3</sub>, or PNN, is one of the perovskite relaxor ferroelectric materials which have been investigated extensively as potential candidates for electroceramic components such as multilayer ceramic capacitor, electrostrictor and actuator applications [1–3]. However, a practical limitation to the utilization of this compound in device applications has been the lack of a simple, reproducible preparation technique for a pure perovskite phase with consistent properties. The formation of PNN is often accompanied by the occurrence of one or more undesirable phases, which significantly degrade the properties of PNN [4–6].

In order to eliminate the unwanted phases, the two-stage columbite method [5–7] has been widely used. In this process, the constituents NiO and Nb<sub>2</sub>O<sub>5</sub> are first mixed and reacted together to form nickel niobate (NiNb<sub>2</sub>O<sub>6</sub>), prior to mixing and reacting with PbO in the second step of calcination at elevated temperature. Interestingly, this mixed oxide route has been employed with minor modifications in the synthesis of NiNb<sub>2</sub>O<sub>6</sub> itself [5–7].

However, powders prepared by a mixed oxide route have spatial fluctuations in their compositions. The extent of the fluctuation depends on the characteristics of the starting powders as well as on the processing schedule. Generally, the mixed oxide method involves heating of a mixture of nickel oxide and niobium oxide at 1000 °C or above for long times, i.e. 6 h [8] and 12 h [9]. The optimization of calcination conditions used in the mixed oxide process, however, has not received detailed attention, and the effects of applied dwell time and heating/cooling rates have not yet been studied extensively.

Therefore, the main purpose of this work was to explore a simple mixed oxide synthetic route for the production of NiNb $_2$ O $_6$  (NN) powders via a rapid vibro-milling technique and to perform a systematic study of the reaction between the starting nickel oxide and niobium oxide precursors. The phase formation and morphology of the powders calcined at various conditions will be studied and discussed.

#### 2. Experimental procedure

The starting materials were commercially-available nickel oxide, NiO (JCPDS file number 73-1519) and niobium oxide, Nb<sub>2</sub>O<sub>5</sub> (JCPDS file number 30-0873) (Aldrich, 99.9% purity).

<sup>\*</sup> Corresponding author. Tel.: +66 53 943367; fax: +66 53 943445. *E-mail address*: Suponananta@yahoo.com (S. Ananta).

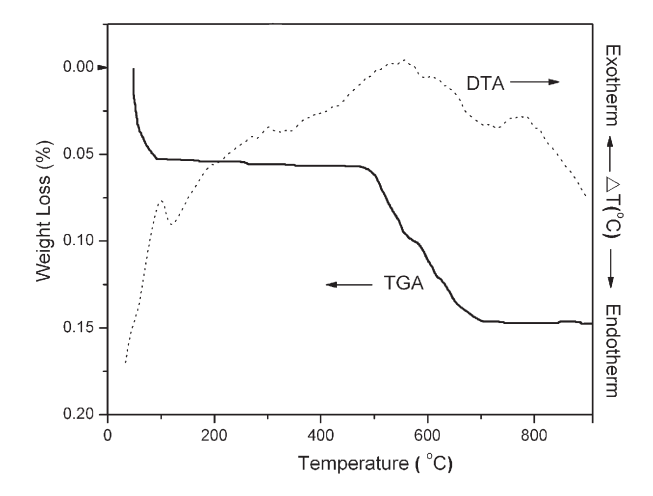


Fig. 1. TG-DTA curves for the mixture of NiO-Nb $_2$ O $_5$  powder.

The two oxide powders exhibited an average particle size in the range of  $3.0-5.0 \, \mu m$ . NiNb<sub>2</sub>O<sub>6</sub> powders were synthesized by the solid-state reaction of thoroughly ground mixtures of NiO and Nb<sub>2</sub>O<sub>5</sub> powders that were milled in the required stoichiometric ratio. Instead of employing a ball-milling procedure [6,8], a McCrone vibro-milling technique was used [10]. In order to combine mixing capacity with a significant time saving, the mil-

ling operation was carried out for 1 h (instead of 6 h [7] or 12 h [3]) with corundum cylindrical media in isopropyl alcohol (IPA). After drying at 120 °C for 2 h, the reaction of the uncalcined powders taking place during heat treatment was investigated by themogravimetric and differential thermal analysis (TG-DTA, Shimadzu), using a heating rate of 10 °C/min in air from room temperature up to 1000 °C. Based on the TG-DTA results, the mixture was calcined at various conditions, in closed alumina crucible, in order to investigate the formation of nickel niobate.

Calcined powders were subsequently examined by room temperature X-ray diffraction (XRD; Siemen-D500 diffractometer), using Ni-filtered  $\text{CuK}_{\alpha}$  radiation to identify the phases formed and optimum calcination conditions for the formation of NiNb<sub>2</sub>O<sub>6</sub> powders. Powder morphologies and particle sizes were directly imaged, using scanning electron microscopy (SEM; JEOL JSM-840A). The chemical compositions of the phase formed were elucidated by an energy-dispersive X-ray (EDX) analyzer with an ultra-thin window. EDX spectra were quantified with the virtual standard peaks supplied with the Oxford Instruments eXL software.

#### 3. Results and discussion

The TG-DTA simultaneous analysis of a powder mixed in the stoichiometric proportions of  $NiNb_2O_6$  is displayed in Fig. 1. In the

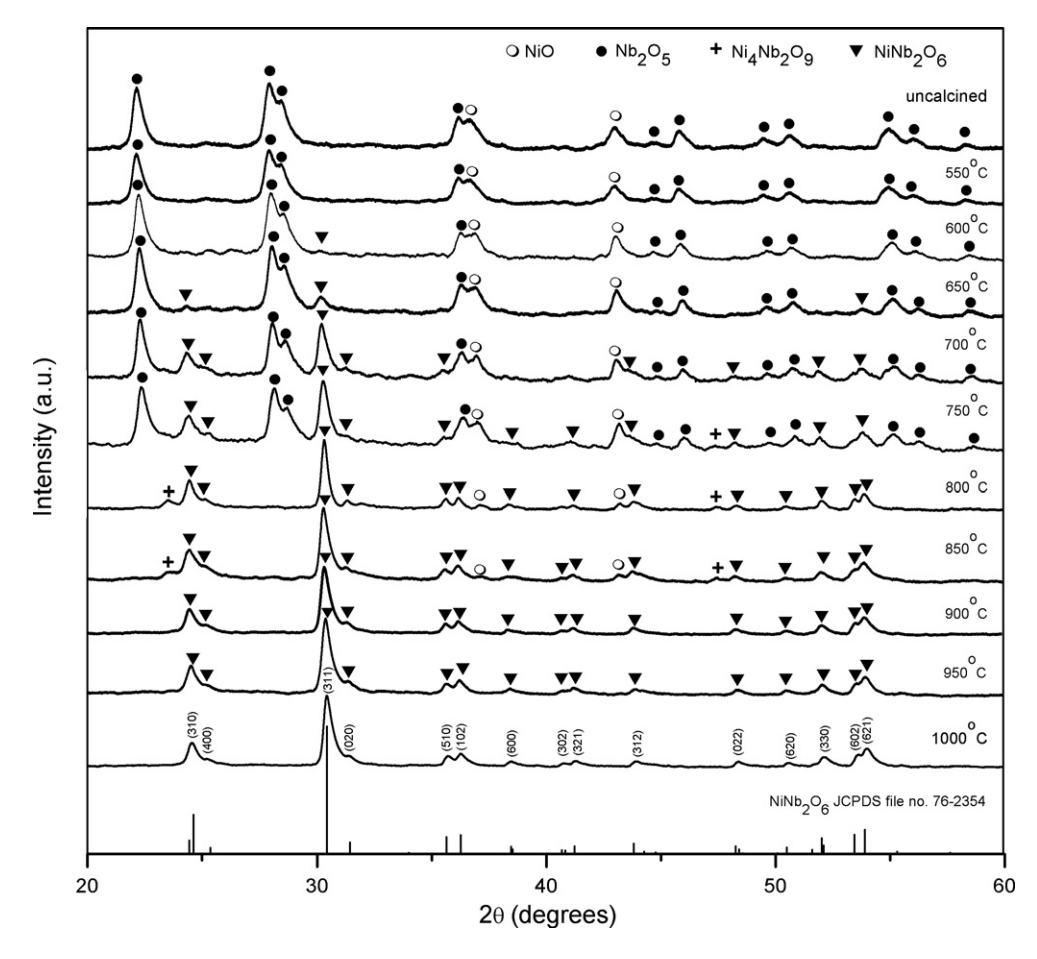


Fig. 2. XRD patterns of NN powders calcined at various temperatures for 4 h with heating/cooling rates of  $10 \, ^{\circ}\text{C/min}$ .

temperature range from room temperature to  $\sim150\,^{\circ}\mathrm{C}$ , the sample shows both exothermic and endothermic peaks in the DTA curve, consistent with the first weight loss. These observations can be attributed to the decomposition of the organic species from the milling process [10]. Increasing the temperature up to  $\sim1000\,^{\circ}\mathrm{C}$ , the solid-state reaction occurred between NiO and Nb<sub>2</sub>O<sub>5</sub> [3,6]. The broad exotherm with several peaks in the DTA curve represents that reaction, which has a maximum at  $\sim550\,^{\circ}\mathrm{C}$  and 800 °C. These are supported by a second fall in sample weight over the same temperature range. However, it is to be noted that there is no obvious interpretation of these peaks, although it is likely to correspond to a phase transition reported earlier [6,11]. These data were used to define the range of calcination temperatures for XRD investigation between 550 and 1000 °C.

To further study the phase development with increasing calcination temperature in the powders, they were calcined for 4 h in air at various temperatures, up to 1000 °C, followed by phase analysis using XRD. As shown in Fig. 2, for the uncalcined powders and the powders calcined at 550 °C, only X-ray peaks of precursors NiO (o) and Nb<sub>2</sub>O<sub>5</sub> (●), which could be matched with JCPDS file numbers 73-1519 [12] and 30-0873 [13], respectively, are present, indicating that no reaction had yet been triggered during the vibro-milling and low firing processes. However, it is seen that little crystalline phase of the desired NiNb<sub>2</sub>O<sub>6</sub> crystallites (▼) was found as separated phases in the powders calcined at 600 °C, and became the predominant phase in the powder calcined at 700 °C. As the temperature increased to 800 °C, the intensity of the NiNb2O6 peaks was further enhanced whereas some new peaks (+) of the Ni<sub>4</sub>Nb<sub>2</sub>O<sub>9</sub> reported by Ehrenberg et al. [14] started to appear, mixing with NiNb<sub>2</sub>O<sub>6</sub> and NiO phases. It is seen that the peaks corresponding to Nb<sub>2</sub>O<sub>5</sub> phase were completely eliminated after calcination above 750 °C. This observation is associated to the DTA peaks found at the same temperature range within the broad exothermic effects in Fig. 1. To a first approximation, this Ni<sub>4</sub>Nb<sub>2</sub>O<sub>9</sub> phase has a corundum-type structure with an orthorhombic unit cell (a=505.4 pm, b=876.8 pm and c=1430.4 pm, space group Pcan (no. 60), consistent with JCPDS file numbers 77-2409 [15]. This observation could be attributed mainly to the poor reactivity of nickel and niobium species [6]. Upon calcination at 900 °C, a single-phase of NiNb<sub>2</sub>O<sub>6</sub> is already formed. For the present work, there are no significant differences between the powders calcined at temperatures ranging from 900 to 1000 °C. This NiNb<sub>2</sub>O<sub>6</sub> phase (JCPDS file numbers 76-2354 [16]) has a columbite structure with an orthorhombic unit cell (a=1403 pm, b=568.7 pm and c=503.3 pm, space group Pbcn (no. 60), in agreement with literature [11].

Apart from the calcination temperature, the effect of dwell time was also found to be quite significant. From Fig. 3, it can be seen that the single phase of NiNb<sub>2</sub>O<sub>6</sub> (yield of 100% within the limitations of the XRD technique) was found to be possible in powders calcined at 900 °C with dwell time of at least 4 h (Fig. 3(c, d)) or 950 °C with dwell time of at least 3 h (Fig. 3(g, h)) applied. This is probably due to the effectiveness of vibro-milling and a carefully optimized reaction. The observation that the dwell time may also play an important role in obtaining a single-phase columbite product is also consistent with other similar systems [10,17]. It is also very interesting to see that the on-set temperature is approximately 100-200 °C lower than those reported earlier with a conventional ball-milling method [6,8]. The difference could be attributed to nano-sized mixed powders obtained from a rapid vibro-milling. Most importantly, this study suggests that a rapid vibromilling method can significantly lower the optimum calcination temperature for the formation of single-phase NiNb<sub>2</sub>O<sub>6</sub> powders.

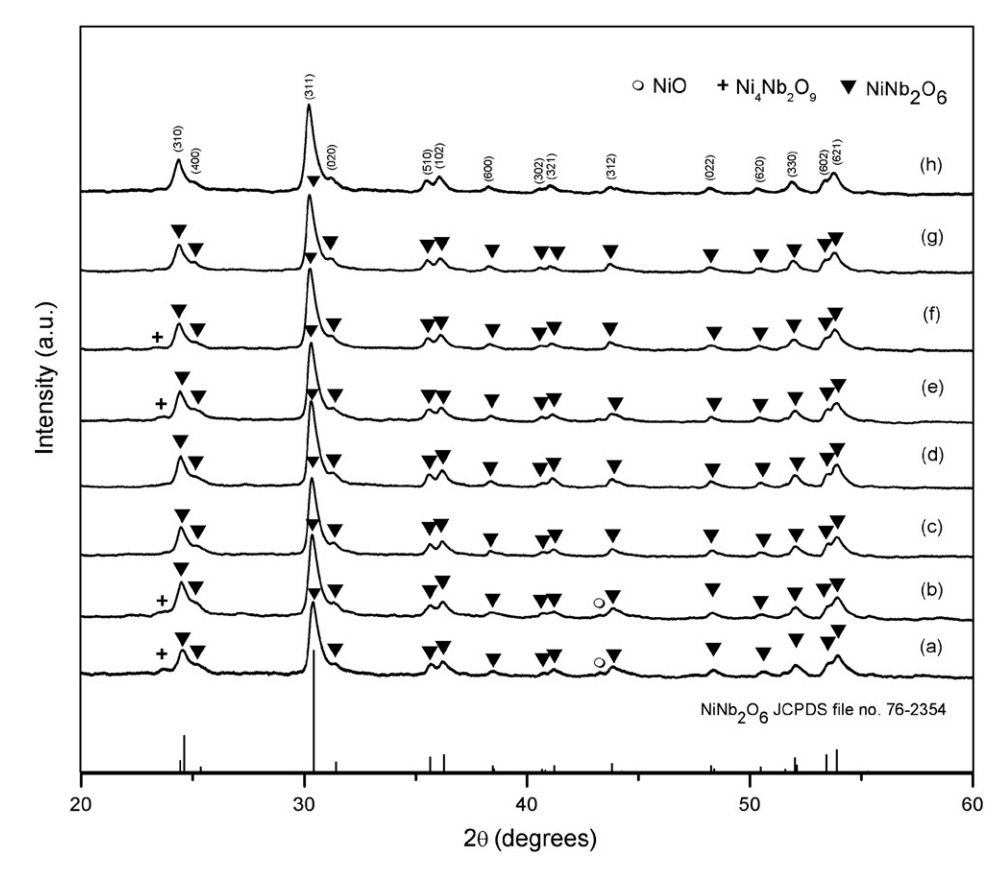


Fig. 3. XRD patterns of NN powders calcined with heating/cooling rates of 10 °C/min at 900 °C for (a) 2, (b) 3, (c) 4 and (d) 6 h, and at 950 °C for (e) 1, (f) 2, (g) 3 and (h) 4 h.

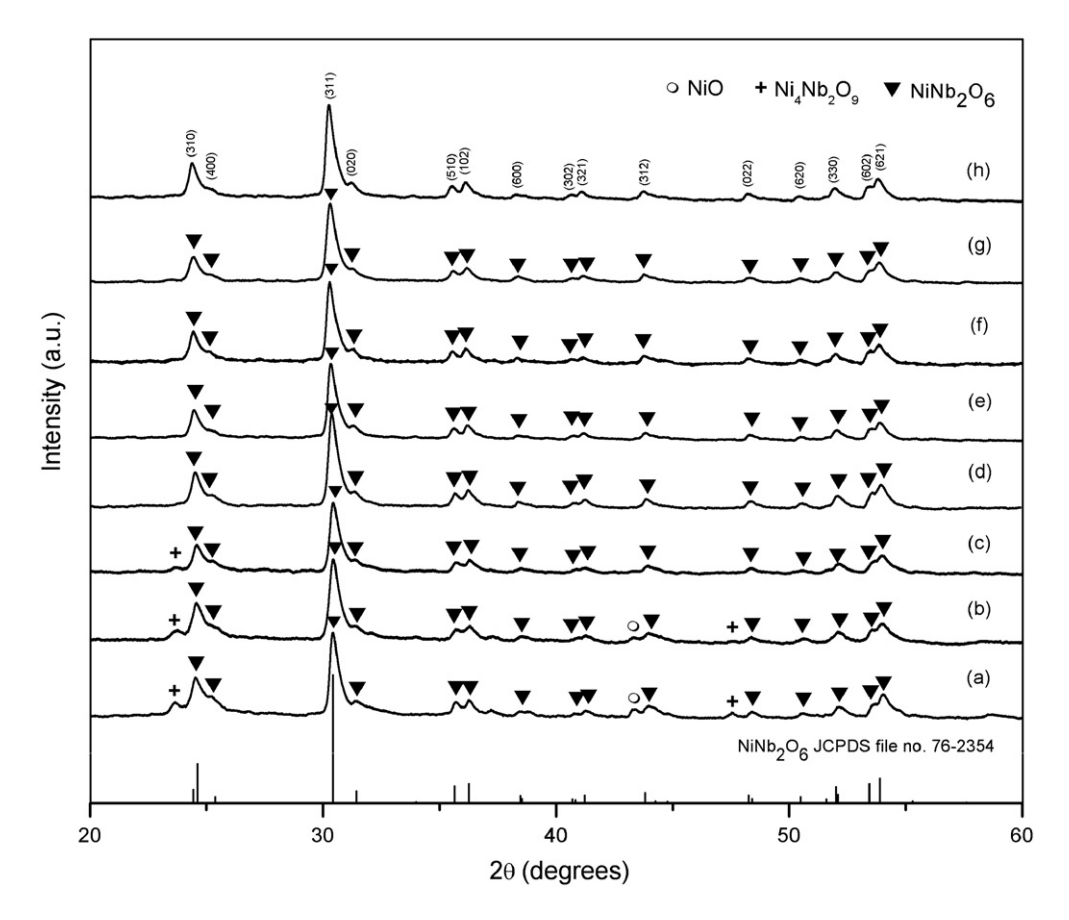


Fig. 4. XRD patterns of NN powders calcined at 900 °C for 4 h with heating/cooling rates of (a) 5, (b) 10, (c) 15, (d) 20 and (e) 30 °C/min, and at 950 °C for 3 h with heating/cooling rates of (f) 10, (g) 20 and (h) 30 °C/min.

In the present study, an attempt was also made to calcine  $NiNb_2O_6$  powders under various heating/cooling rates (Fig. 4). In this connection, it is shown that faster heating/cooling rates can lead to better crystallization of  $NiNb_2O_6$  phase. Based on the TG-DTA and XRD data, it may be concluded that, over a wide range of calcination conditions, single-phase  $NiNb_2O_6$  cannot be straightforwardly formed via a solid-state mixed oxide synthetic route, unless a careful design of calcination is performed. The experimental work carried out here suggests that the optimal calcination conditions for single-phase  $NiNb_2O_6$  (with impurities undetected by XRD technique) is 900 °C for 4 h or 950 °C for 3 h, with heating/cooling rates as fast as 30 °C/min. Moreover, the formation temperature and dwell time for the production of  $NiNb_2O_6$  powders observed in this work are also much lower than those reported earlier [6,8,9]. This clearly emphasizes the advantages of a rapid vibro-milling technique.

Finally, the morphological changes in the NiNb<sub>2</sub>O<sub>6</sub> powders formed by a mixed oxide are illustrated in Fig. 5(a-f) as a function of calcination temperatures, dwell times and heating/cooling rates, respectively. The influence of calcination conditions on particle size is given in Table 1. In general, the particles are agglomerated and irregular in shape, with a substantial variation in particle size, particularly in samples calcined at high temperature (Fig. 5(b, c)) or with fast heating/cooling rates (Fig. 5(e, f)). This finding is also similar to that in Mg<sub>4</sub>Nb<sub>2</sub>O<sub>9</sub> powders [10]. The results indicate that average particle size and degree of agglomeration tend to increase with calcination temperatures, dwell times or heating/cooling rates (Table 1). All powders seem to display a significant level of necking and bonding as if they were in the initial stages of sintering. This observation could be attributed to the mechanism of surface energy reduction of the ultrafine powders, i.e. the smaller the powder the higher

the specific surface area [18]. To the authors' knowledge, the present data are the first results for the morphology—calcination relationship of NiNb<sub>2</sub>O<sub>6</sub> powders prepared by the solid-state reaction. It is also of interest to point out that mass production of single-phase NiNb<sub>2</sub>O<sub>6</sub> nanopowders with the smallest particle size  $\sim 100$  nm (estimated from SEM micrographs) can be achieved by employing a simple solid-state reaction combined with a rapid vibro-milling technique. In addition, EDX analysis using a 20 nm probe on a large number of particles of the calcined powders confirms that the parent composition is NiNb<sub>2</sub>O<sub>6</sub>, in good agreement with XRD results.

#### 4. Conclusions

This study has demonstrated the potential of a rapid vibromilling technique as a significant time saving method to obtain

Table 1 Particle size range of NiNb $_2$ O $_6$  powders calcined at various conditions

| Calcination condition | Particle       |                |                        |  |
|-----------------------|----------------|----------------|------------------------|--|
| Temperature (°C)      | Dwell time (h) | Rates (°C/min) | size range<br>(±10 nm) |  |
| 900                   | 4              | 10             | 100-750                |  |
| 900                   | 4              | 20             | 100-850                |  |
| 900                   | 4              | 30             | 100-900                |  |
| 950                   | 3              | 10             | 200-1000               |  |
| 950                   | 4              | 10             | 300-1150               |  |
| 1000                  | 2              | 10             | 800-1200               |  |

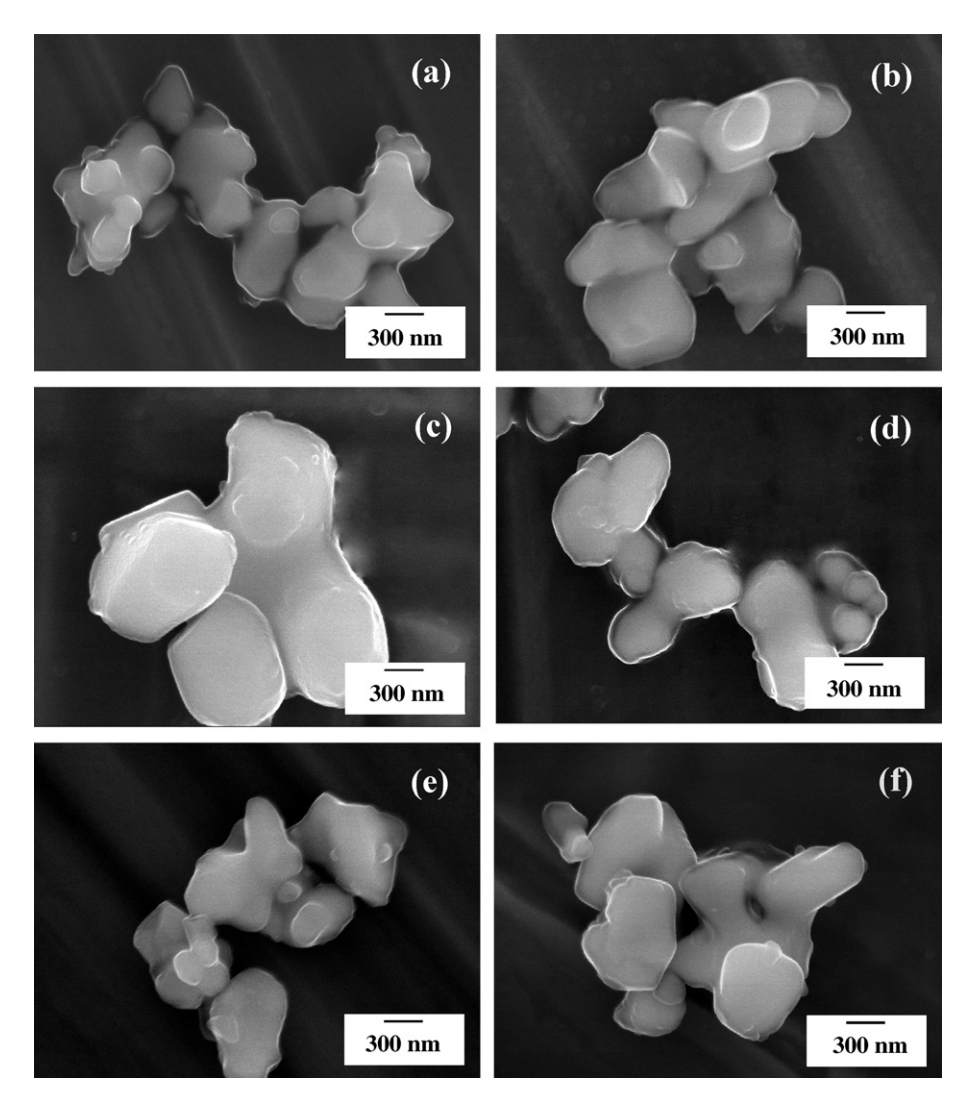


Fig. 5. SEM micrographs of NN powders calcined for 4 h with heating/cooling rates of 10 °C/min at (a) 900, (b) 950 and (c) 1000 °C; (d) at 950 °C for 3 h with heating/cooling rates of 10 °C/min; and at 900 °C for 4 h with heating/cooling rates of (e) 20 and (f) 30 °C/min.

single-phase NiNb $_2$ O $_6$  nanopowders at low calcination temperatures. The calcination conditions have been found to have a pronounced effect on phase formation and particle size of the calcined NiNb $_2$ O $_6$  powders. The resulting NiNb $_2$ O $_6$  powders consist of a variety of agglomerated particle sizes, depending on calcination conditions.

# Acknowledgements

This work was supported by the Thailand Research Fund (TRF), the Royal Golden Jubilee Ph.D. Program, the Faculty of Science and the Graduate School, Chiang Mai University.

# References

- K. Niwa, M. Kondo, M. Hida ad, K. Kurihara, Jpn. Ceram. Trans. 150 (2004) 401.
- [2] A.J. Moulson, J.M. Herbert, Electroceramics, 2nd ed., Wiley, Chichester, 2003.
- [3] E.F. Alberta, A.S. Bhalla, Mater. Lett. 54 (2002) 47-54.
- [4] C.H. Lu, J.F. Wu, J. Mater. Res. 11 (1996) 3064.

- [5] L. Veitch, B.S. Thesis, Pennsylvania State University, University Park, PA, 1982.
- [6] C.H. Lu, H.J. Hwang, Ceram. Int. 22 (1996) 373.
- [7] N. Vittayakorn, G. Rujijanagul, X. Tan, M.A. Marquardt, D.P. Cann, J. Appl. Phys. 96 (2004) 5103.
- [8] C. Lei, K. Chen, X. Zhang, J. Electroceram. 10 (2003) 233.
- [9] M. Pastor, P.K. Bajpai, R.N.P. Choudhary, Bull. Mater. Sci. 28 (2005) 199.
- [10] S. Ananta, Mater. Lett. 58 (2004) 2781.
- [11] R. Wichmann, H. Mueller-Buschbaum, Z. Anorg. Allg. Chem. 539 (1986) 203.
- [12] Powder Diffraction File No. 73-1519. International Centre for Diffraction Data, Newton Square, PA, 2000.
- [13] Powder Diffraction File No. 30-0873. International Centre for Diffraction Data, Newton Square, PA, 2000.
- [14] H. Ehrenberg, G. Wltschek, H. Weitzel, F. Trouw, J.H. Buettner, T. Kroener, H. Fuess, Phys. Rev., B 52 (1995) 9595.
- [15] Powder Diffraction File No. 77-2409. International Centre for Diffraction Data, Newton Square, PA, 2000.
- [16] Powder Diffraction File No. 76-2354. International Centre for Diffraction Data, Newton Square, PA, 2000.
- [17] S. Ananta, R. Brydson, N.W. Thomas, J. Eur. Ceram. Soc. 20 (2000) 2325.
- [18] J.S. Reed, Principles of Ceramic Processing, 2nd ed., Wiley, New York, 1995.



Available online at www.sciencedirect.com



materials letters

Materials Letters 61 (2007) 2565-2570

www.elsevier.com/locate/matlet

# Phase and morphology evolution of corundum-type Ni<sub>4</sub>Nb<sub>2</sub>O<sub>9</sub> powders synthesized by solid-state reaction

O. Khamman, R. Yimnirun, S. Ananta\*

Department of Physics, Faculty of Science, Chiang Mai University, Chiang Mai 50200, Thailand

Received 2 May 2006; accepted 28 September 2006

Available online 16 October 2006

#### Abstract

The solid-state mixed oxide method via a rapid vibro-milling technique is explored in the preparation of single-phase nickel diniobate  $(Ni_4Nb_2O_9)$  powders. The formation of the  $Ni_4Nb_2O_9$  phase in the calcined powders has been investigated as a function of calcination conditions by TG-DTA and XRD techniques. Morphology, particle size and chemical composition have been determined via a combination of SEM and EDX techniques. It has been found that minor phases of unreacted NiO and  $Nb_2O_5$  precursors and  $NiNb_2O_6$  phase tend to form together with the  $Ni_4Nb_2O_9$  phase, depending on calcination conditions. It is seen that optimization of calcination conditions can lead to a single-phase  $Ni_4Nb_2O_9$  in an orthorhombic phase.

© 2006 Elsevier B.V. All rights reserved.

Keywords: Nickel diniobate; Calcination; Phase formation; Vibro-milling; Powders solid-state reaction

## 1. Introduction

It is known that various compositions are possible in the Ni–Nb–O system e.g. NiNb<sub>2</sub>O<sub>6</sub>, Ni<sub>4</sub>Nb<sub>2</sub>O<sub>9</sub>, Ni<sub>3</sub>Nb<sub>2</sub>O<sub>8</sub>, NiNb<sub>14</sub>O<sub>36</sub>, Ni<sub>0.66</sub>Nb<sub>11.33</sub>O<sub>29</sub>, etc. [1–3]. Amongst these compounds, nickel niobate (NiNb<sub>2</sub>O<sub>6</sub>) is one of the most well-known materials, which has recently gained considerable attention [4,5]. This compound is very well-known as the key precursor for the successful preparation of single-phase perovskite lead nickel niobate, Pb(Ni<sub>1/3</sub>Nb<sub>2/3</sub>)O<sub>3</sub>, or PNN, which is becoming increasingly important for multilayer ceramic capacitor, electrostrictor and actuator applications [6,7]. In general, production of single-phase NiNb<sub>2</sub>O<sub>6</sub> is not straightforward, as minor concentration of Ni<sub>4</sub>Nb<sub>2</sub>O<sub>9</sub> is sometimes formed alongside the major phase of NiNb<sub>2</sub>O<sub>6</sub> [8,9].

In contrast, very little is known about Ni<sub>4</sub>Nb<sub>2</sub>O<sub>9</sub>, since no work has been dedicated to the synthesis of this compound. Much of the work concerning the Ni<sub>4</sub>Nb<sub>2</sub>O<sub>9</sub> compound has been directed towards determining crystal structure and magnetic properties [10]. Wichmann et al. [11,12] reported

that Ni<sub>4</sub>Nb<sub>2</sub>O<sub>9</sub> exhibits orthorhombic symmetry with 2 different point groups (i.e. Fd2d and Pbcn). Its crystal structure can be represented as a network of edge- and corner-sharing NiO<sub>6</sub> and NbO<sub>6</sub> octahedra dimers. Moreover, to date, the potential of the Ni<sub>4</sub>Nb<sub>2</sub>O<sub>9</sub> as a possible alternative precursor for the preparation of PNN has not yet been reported. Interestingly, the mixed oxide route for the production of Ni<sub>4</sub>Nb<sub>2</sub>O<sub>9</sub> powders has not received detailed attention, and the effects of calcination conditions (i.e. applied firing temperature, dwell time and heating/cooling rates) have not yet been studied extensively. Therefore, the main purpose of this work was to explore a simple mixed oxide synthetic route for the production of Ni<sub>4</sub>Nb<sub>2</sub>O<sub>9</sub> powders via a rapid vibro-milling technique and to perform a systematic study of the reaction between the starting nickel oxide and niobium oxide precursors. The phase formation and morphology of the powder calcined at various conditions will be studied and discussed. The study also forms a possible basis for a further survey of PNN preparation.

# 2. Experimental procedure

The starting materials were commercially available nickel oxide, NiO (JCPDS file number 73-1519) and niobium oxide,

<sup>\*</sup> Corresponding author. Tel.: +66 53 943367; fax: +66 53 943445. *E-mail address*: Suponananta@yahoo.com (S. Ananta).

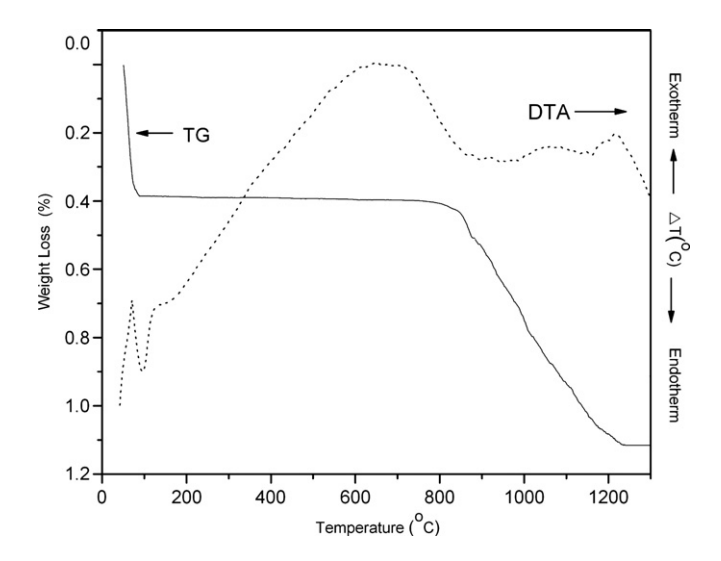


Fig. 1. TG-DTA curves for the mixture of NiO-Nb<sub>2</sub>O<sub>5</sub> powder.

Nb<sub>2</sub>O<sub>5</sub> (JCPDS file number 30-0873) (Aldrich, 99.9% purity). The two oxide powders exhibited an average particle size in the range of 3.0–5.0  $\mu$ m. Ni<sub>4</sub>Nb<sub>2</sub>O<sub>9</sub> powders were synthesized by the solid-state reaction of thoroughly ground mixtures of NiO and Nb<sub>2</sub>O<sub>5</sub> powders that were milled in the required stoichiometric ratio. In order to combine mixing capacity with a significant time saving, a McCrone vibro-milling technique [13,14] was carried out for 0.5 h with corundum cylindrical media in isopropyl alcohol (IPA). After drying at 120 °C for 2 h, the reaction of the uncalcined powders taking place during heat

treatment was investigated by themogravimetric and differential thermal analysis (TG-DTA, Shimadzu), using a heating rate of 10 °C/min in air from room temperature up to 1300 °C. Based on the TG-DTA results, the mixture was calcined at various conditions, in closed alumina crucible, in order to investigate the formation of nickel diniobate.

Calcined powders were subsequently examined by room temperature X-ray diffraction (XRD; Siemen-D500 diffractometer), using Ni-filtered  $CuK_{\alpha}$  radiation to identify the phases formed and optimum calcination conditions for the formation of Ni<sub>4</sub>Nb<sub>2</sub>O<sub>9</sub> powders. Powder morphologies and particle sizes were directly imaged, using scanning electron microscopy (SEM; JEOL JSM-840A). The chemical compositions of the phase formed were elucidated by an energy-dispersive X-ray (EDX) analyzer with an ultra-thin window. EDX spectra were quantified with the virtual standard peaks supplied with the Oxford Instruments eXL software.

#### 3. Results and discussion

The TG-DTA simultaneous analysis of a powder mixed in the stoichiometric proportions of  $Ni_4Nb_2O_9$  is displayed in Fig. 1. In the temperature range from room temperature to  $\sim 150$  °C, the sample shows both exothermic and endothermic peaks in the DTA curve, consistent with the first weight loss. These observations can be attributed to the decomposition of the organic species from the milling process [13]. Increasing the temperature up to  $\sim 1300$  °C, the solid-state reaction occurred between NiO and  $Nb_2O_5$  [8,9]. The broad exotherm with several peaks in the DTA curve represents that reaction,

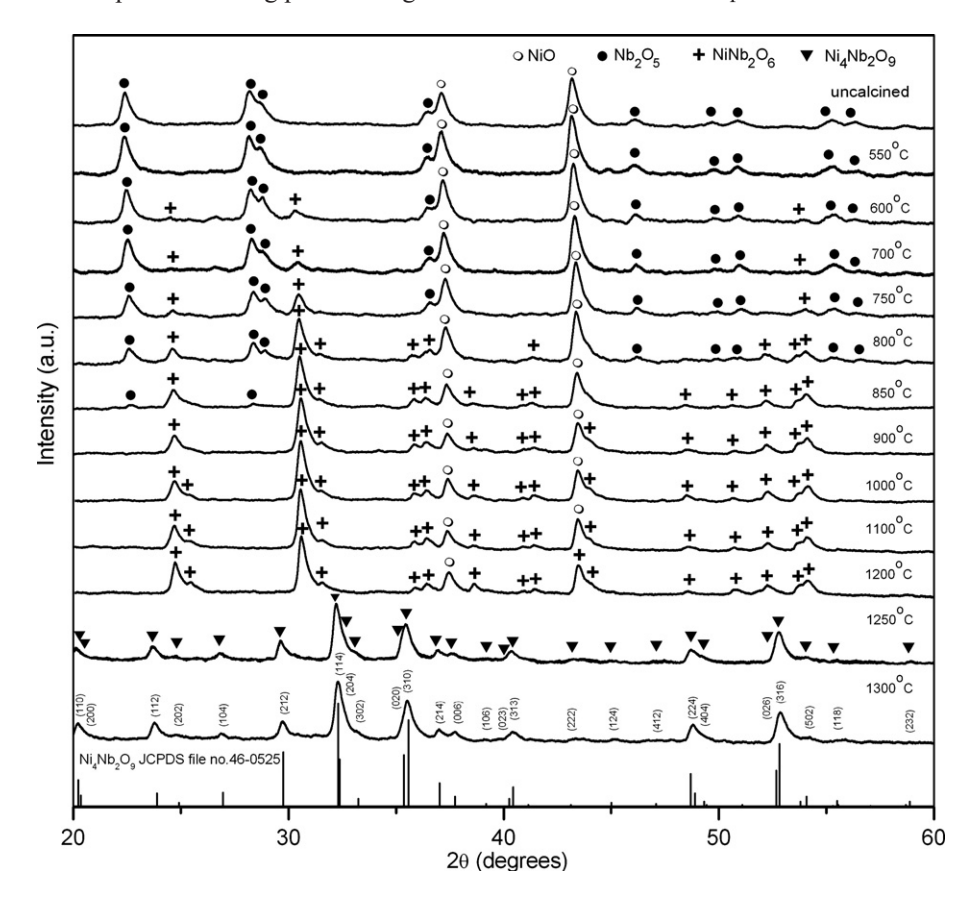


Fig. 2. XRD patterns of  $Ni_4Nb_2O_9$  powders calcined at various temperatures for 2 h with heating/cooling rates of 10 °C/min.

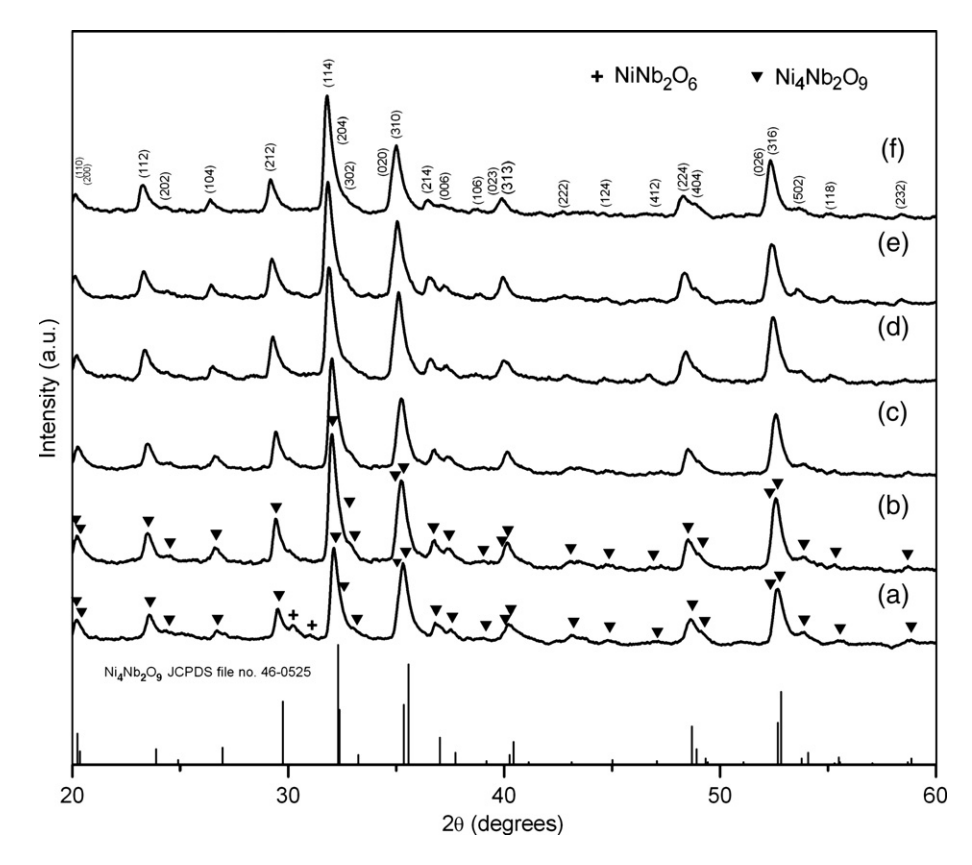


Fig. 3. XRD patterns of  $Ni_4Nb_2O_9$  powders calcined with heating/cooling rates of 10 °C/min at 1250 °C for (a) 1, (b) 2 and (c) 3 h, and at 1300 °C for (d) 0.5, (e) 1 and (f) 2 h.

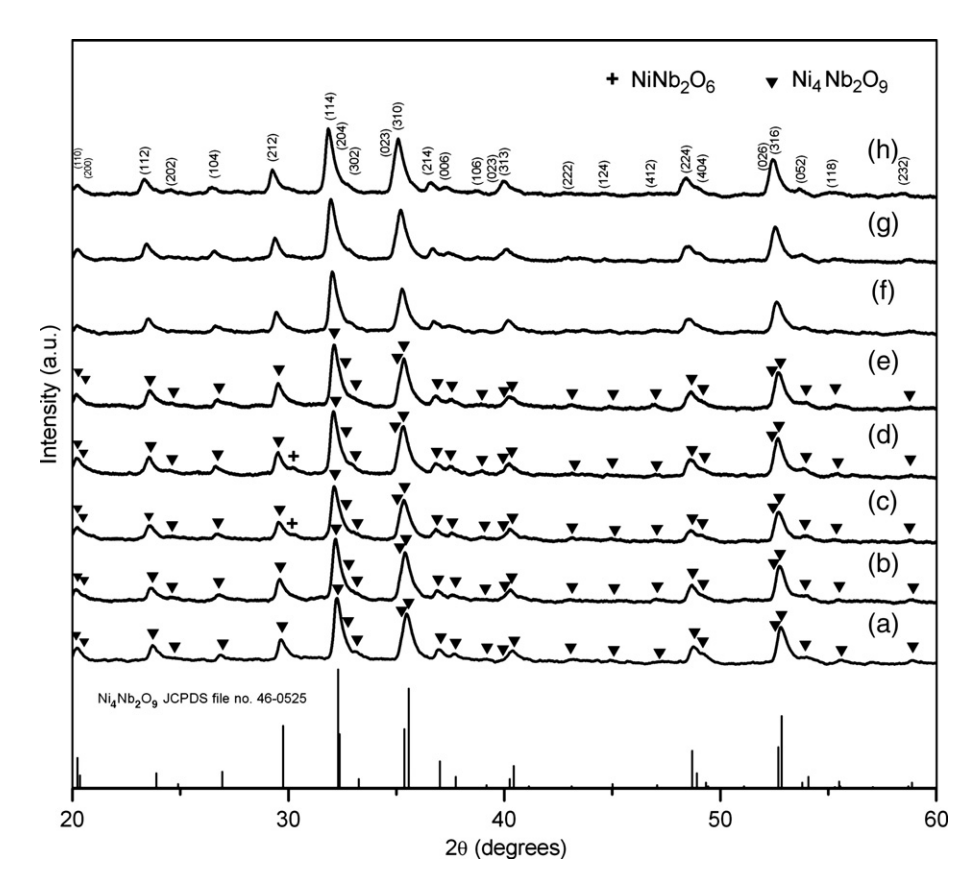


Fig. 4. XRD patterns of  $Ni_4Nb_2O_9$  powders calcined at 1250 °C for 2 h with heating/cooling rates of (a) 10, (b) 20, (c) 25 and (d) 30 °C/min, and at 1300 °C for 0.5 h with heating/cooling rates of (e) 5, (f) 10, (g) 20 and (h) 30 °C/min.

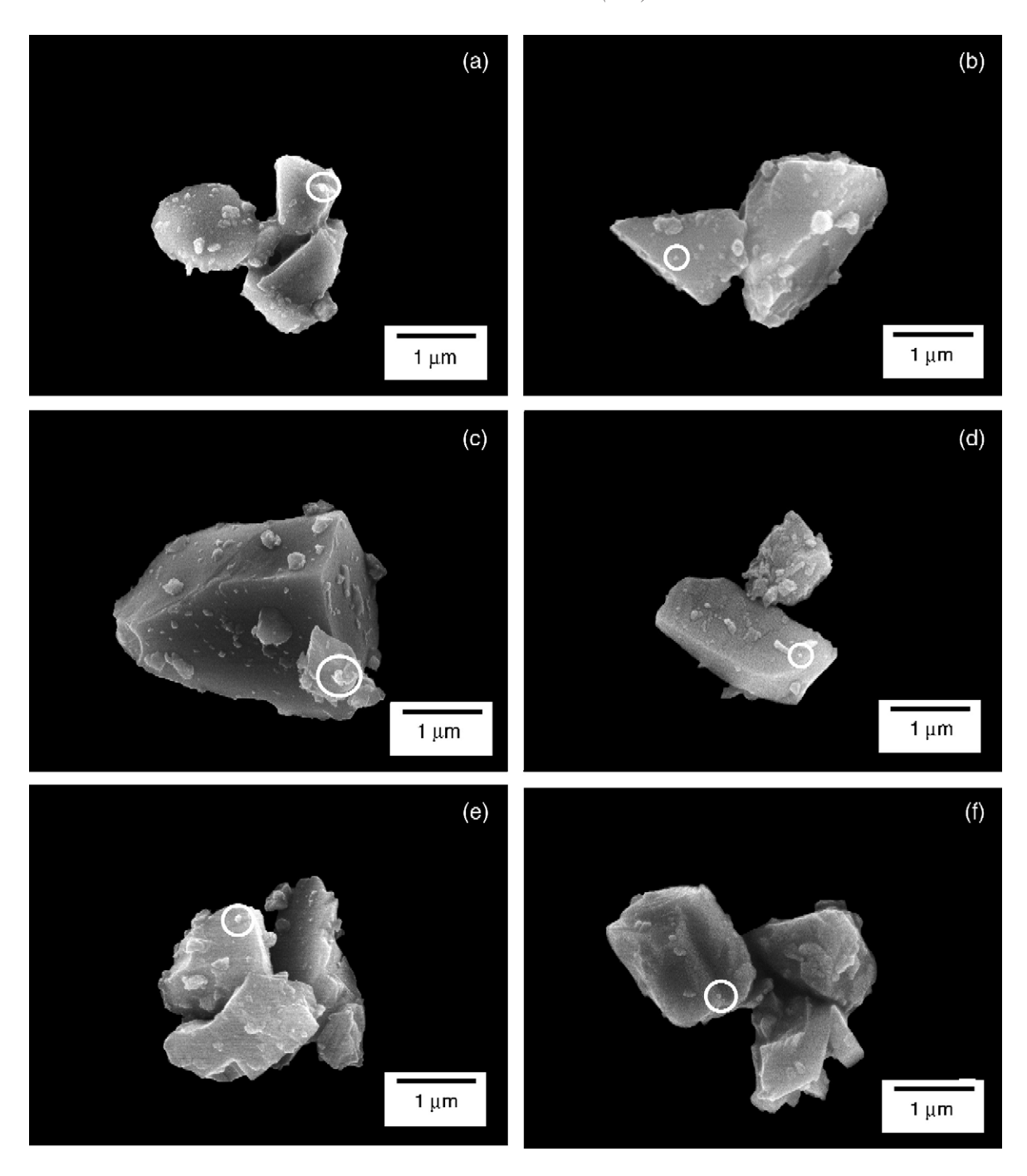


Fig. 5. SEM micrographs of  $Ni_4Nb_2O_9$  powders calcined for 2 h with heating/cooling rates of 10 °C/min at (a) 1250, (b) 1300 and (c) 1400 °C; (d) at 1300 °C for 0.5 h with heating/cooling rates of 10 °C/min; and at 1250 °C for 2 h with heating/cooling rates of (e) 20 and (f) 30 °C/min.

which has a maximum at  $\sim\!600\,^{\circ}\mathrm{C}$ ,  $1050\,^{\circ}\mathrm{C}$  and  $1200\,^{\circ}\mathrm{C}$ . These are supported by a second fall in sample weight over the same temperature range. However, it is to be noted that there is no obvious interpretation of these peaks, although they are likely to correspond to phase transitions reported earlier [3,9]. These data were used to define the range of calcination temperatures for XRD investigation between 550 and 1300  $^{\circ}\mathrm{C}$ .

To further study the phase development with increasing calcination temperature in the powders, they were calcined for 2 h in air at various temperatures, up to 1300 °C, followed by phase analysis using XRD. As shown in Fig. 2, for the uncalcined powders and the powders

calcined at 550 °C, only X-ray peaks of precursors NiO (O) and Nb<sub>2</sub>O<sub>5</sub> ( $\bullet$ ), which could be matched with JCPDS file numbers 73-1519 [15] and 30-0873 [16], respectively, are present, indicating that no reaction had yet been triggered during the vibro-milling and low firing processes. However, it is seen that the columbite-type NiNb<sub>2</sub>O<sub>6</sub> crystallites (+) reported by many workers [8,9] were found as separated phases in the powders calcined at 600 °C. As the temperature increased to 1200 °C, the intensity of the NiNb<sub>2</sub>O<sub>6</sub> peaks was further enhanced, and became the predominant phase in the powder calcined above 800 °C, mixing with NiO and Nb<sub>2</sub>O<sub>5</sub> phases. It is seen that the peaks corresponding to Nb<sub>2</sub>O<sub>5</sub> phase were completely eliminated after

Table 1
Particle size range of Ni<sub>4</sub>Nb<sub>2</sub>O<sub>9</sub> powders calcined at various conditions

| Calcination condition | Particle             |          |                          |
|-----------------------|----------------------|----------|--------------------------|
| Temperature (°C)      | Dwell time rates (h) | (°C/min) | size range<br>(±0.01 μm) |
| 1250                  | 2                    | 10       | 1.00-1.55                |
| 1250                  | 2                    | 20       | 1.00 - 2.00              |
| 1250                  | 2                    | 30       | 1.36 - 1.91              |
| 1300                  | 0.5                  | 10       | 1.10-2.09                |
| 1300                  | 2                    | 10       | 1.90 - 2.45              |
| 1400                  | 2                    | 10       | 1.00 - 3.27              |

calcinations above 850 °C. This observation is associated to the DTA peaks found at the same temperature range within the broad exothermic effects in Fig. 1. To a first approximation, this NiNb<sub>2</sub>O<sub>6</sub> phase (JCPDS file numbers 76-2354 [17]) has a columbite structure with an orthorhombic unit cell (a=1403 pm, b=568.7 pm and c=503.3 pm, space group Pbcn (no. 60)). This study shows that minor amounts of the NiO phase tend to co-exist along with the NiNb<sub>2</sub>O<sub>6</sub> phase, after calcinations in the range 600-1200 °C. This observation could be attributed mainly to the poor reactivity of nickel and niobium species [6]. It is of interest to point out that upon calcination at 1250 °C, a single-phase of Ni<sub>4</sub>Nb<sub>2</sub>O<sub>9</sub> (**▼**) is already formed. For the present work, there are no significant differences between the powders calcined at temperatures ranging from 1250 to 1300 °C. This Ni<sub>4</sub>Nb<sub>2</sub>O<sub>9</sub> phase has a corundum-type structure with an orthorhombic unit cell (a=871.9 pm, b=507.2 pm and c=1428.9 pm, space group *Pbcn* (no. 60)), consistent with JCPDS file numbers 46-0525 [18].

Apart from the calcination temperature, the effect of dwell time was also found to be quite significant. From Fig. 3, it can be seen that the single-phase of Ni<sub>4</sub>Nb<sub>2</sub>O<sub>9</sub> (yield of 100% within the limitations of the XRD technique) was found to be possible in powders calcined at 1250 °C with dwell time of at least 2 h (Fig. 3(b, c)) or 1300 °C with dwell time of at least 0.5 h (Fig. 3(d-f)) applied. This is probably due to the effectiveness of vibro-milling and a carefully optimized reaction. The observation that the dwell time may also play an important role in obtaining a single-phase corundum product is also consistent with other similar systems [13,19]. It is also very interesting to see that the on-set temperature is approximately 100-200 °C lower than those reported earlier [6,8]. The difference could be attributed to powders with better degree of mixing obtained from a rapid vibro-milling [13,14]. Most importantly, this study suggests that a rapid vibro-milling method can significantly lower the optimum calcination temperature for the formation of single-phase Ni<sub>4</sub>Nb<sub>2</sub>O<sub>9</sub> powders.

In the present study, an attempt was also made to calcine  $Ni_4Nb_2O_9$  powders under various heating/cooling rates (Fig. 4). In this connection, it is shown that slower heating/cooling rates can lead to better crystallization of  $Ni_4Nb_2O_9$  phase, probably because there is enough time for the diffusion of NiO and  $Nb_2O_5$  species to complete their solid-state reaction process. Based on the TG-DTA and XRD data, it may be concluded that, over a wide range of calcination conditions, single-phase  $Ni_4Nb_2O_9$  cannot be straightforwardly formed via a solid-state mixed oxide synthetic route, unless a careful design of calcination is performed. The experimental work carried out here suggests that the optimal calcination conditions for single-phase  $Ni_4Nb_2O_9$  (with impurities undetected by XRD technique) is 1250 °C for 2 h or 1300 °C for 0.5 h, with heating/cooling rates of 20 °C/min.

Finally, the morphological changes in the  $Ni_4Nb_2O_9$  powders formed by a mixed oxide are illustrated in Fig. 5(a–f) as a function of calcination temperatures, dwell times and heating/cooling rates,

respectively. The influence of calcination conditions on particle size is given in Table 1. In general, the particles are agglomerated and irregular in shape, with a substantial variation in particle size, particularly in samples calcined at high temperature (Fig. 5(b, c)) or with fast heating/cooling rates (Fig. 5(e, f)). The results indicate that average particle size and degree of agglomeration tend to increase with calcination temperatures, dwell times or heating/cooling rates (Table 1). All powders seem to display a significant level of grain angularity. This observation could be attributed to a relatively high firing temperature required for achieving Ni<sub>4</sub>Nb<sub>2</sub>O<sub>9</sub> powders prepared by the solid-state reaction [20].

In addition, EDX analysis using a 20 nm probe on a large number of particles of the calcined powders confirms that the parent composition is  $Ni_4Nb_2O_9$ , in good agreement with XRD results. A combination of SEM and EDX techniques has demonstrated that a NiOrich phase (spherical particle with diameter  $\sim 50-100$  nm) exists near the  $Ni_4Nb_2O_9$  parent phase, as small circles in Fig. 5. Moreover, a variation of the Ni/Nb ratio was also found, similar to that of MgNb<sub>2</sub>O<sub>6</sub> powders [13]. The existence of discrete nano-sized NiO phase points to the poor reactivity of NiO, although the concentration is too low for detection by XRD [21], similar with other niobate compounds [13,19].

#### 4. Conclusions

The solid-state mixed oxide synthetic route via a rapid vibro-milling technique is explored in the preparation of single-phase Ni<sub>4</sub>Nb<sub>2</sub>O<sub>9</sub> powders. The calcination conditions have been found to have a pronounced effect on phase formation and particle size of the calcined Ni<sub>4</sub>Nb<sub>2</sub>O<sub>9</sub> powders. Evidence gained from XRD and SEM revealed that the single-phase of corundum Ni<sub>4</sub>Nb<sub>2</sub>O<sub>9</sub> powders with particle size ranging from  $\sim 1$  to 2  $\mu m$  has been obtained in this study by using a calcination temperature of 1250 °C for 2 h or 1300 °C for 0.5 h, with heating/cooling rates of 20 °C/min.

#### Acknowledgements

This work was supported by the Thailand Research Fund (TRF), the Commission on Higher Education (CHE), the Faculty of Science and the Graduate School, Chiang Mai University.

# References

- R.S. Roth, Phase Diagrams for Electronic Ceramics I, The American Ceramic Society, Ohio, 2003.
- $[2]\,$  U. Lehmann, H. Mueller-Buschbaum, Monatsh. Chem. 111 (1980) 1225.
- [3] R. Wichmann, H. Mueller-Buschbaum, Z. Anorg. Allg. Chem. 503 (1983) 101.
- [4] N. Vittayakorn, G. Rujijanagul, X. Tan, M.A. Marquardt, D.P. Cann, J. Appl. Phys. 96 (2004) 5103.
- [5] M. Pastor, P.K. Bajpai, R.N.P. Choudhary, Bull. Mater. Sci. 28 (2005) 199.
- [6] G. Haertling, J. Am. Ceram. Soc. 82 (1999) 797.
- [7] A.J. Moulson, J.M. Herbert, Electroceramics, 2nd ed.Wiley, Chichester, 2003.
- [8] L. Veitch, B.S. Thesis, Pennsylvania State University, University Park, PA, 1982.
- [9] C.H. Lu, H.J. Hwang, Ceram. Int. 22 (1996) 373.
- [10] H. Ehrenberg, G. Wltschek, H. Weitzel, F. Trouw, J.H. Buettner, T. Kroener, H. Fuess, Phys. Rev., B 52 (1995) 9595.
- [11] R. Wichmann, H. Mueller-Buschbaum, Z. Anorg. Allg. Chem. 525 (1985) 135.

- [12] R. Wichmann, H. Mueller-Buschbaum, Z. Anorg. Allg. Chem. 539 (1986) 203.
- [13] S. Ananta, Mater. Lett. 58 (2004) 2781.
- [14] R. Wongmaneerung, R. Yimnirun, S. Ananta, Mater. Lett. 60 (2006) 1447.
- [15] Powder Diffraction File No. 73-1519. International Centre for Diffraction Data, Newton Square, PA, 2000.
- [16] Powder Diffraction File No. 30-0873. International Centre for Diffraction Data, Newton Square, PA, 2000.
- [17] Powder Diffraction File No. 76-2354. International Centre for Diffraction Data, Newton Square, PA, 2000.
- [18] Powder Diffraction File No. 46-0525. International Centre for Diffraction Data, Newton Square, PA, 2000.
- [19] S. Ananta, Mater. Lett. 58 (2004) 2530.
- [20] J.S. Reed, Principles of Ceramic Processing, 2nd ed.Wiley, New York, 1995.
- [21] H. Klug, L. Alexander, X-ray Diffraction Procedures for Polycrystalline and Amorphous Materials, 2nd ed.Wiley, New York, 1974.

# Temperature scaling of dynamic hysteresis in soft lead zirconate titanate bulk ceramic

R. Yimnirun, <sup>a)</sup> R. Wongmaneerung, S. Wongsaenmai, A. Ngamjarurojana, S. Ananta, and Y. Laosiritaworn

Department of Physics, Faculty of Science, Chiang Mai University, Chiang Mai 50200, Thailand

(Received 15 November 2006; accepted 8 February 2007; published online 13 March 2007)

The temperature scaling of the dynamic hysteresis was investigated in soft ferroelectric bulk ceramic. The power-law temperature scaling relations were obtained for hystersis area  $\langle A \rangle$  and remnant polarization  $P_r$ , while the coercivity  $E_C$  was found to scale linearly with temperature T. The three temperature scaling relations were also field dependent. At fixed field amplitude  $E_0$ , the scaling relations take the forms of  $\langle A \rangle \propto T^{-1.1024}$ ,  $P_r \propto T^{-1.2322}$ , and  $(E_{C0} - E_C) \propto T$ . Furthermore, the product of  $P_r$  and  $E_C$  also provides the same scaling law on the T dependence in comparison with  $\langle A \rangle$ . © 2007 American Institute of Physics. [DOI: 10.1063/1.2713336]

Soft lead zirconate titanate [Pb(Zr<sub>1-x</sub>Ti<sub>x</sub>)O<sub>3</sub> or PZT] ceramics have been employed extensively in sensors and actuators. In these applications, the dynamic hysteresis characteristics have become an important consideration. Theoretical studies have been carried out to understand the dynamic response of hysteresis curves in spin and polarization systems.<sup>2–5</sup> In particular, attention is focused on scaling law  $\langle A \rangle \propto f^m E_0^n$  (where  $\langle A \rangle$  is hysteresis area,  $E_0$  is field amplitude, f is frequency, and m and n are exponents that depend on the dimensionality and symmetry of the system). Experimental investigations on a few thin-film systems have also been reported. 6-12 Recently, the scaling relation for soft PZT bulk ceramic was reported in the form of  $\langle A \rangle$  $\propto f^{-0.25}E_0$ . We also reported the stress-dependent scaling relation in the form of  $\langle A-A_{\sigma=0}\rangle \propto f^{-0.25}E_0\sigma^{0.44}$ , which indicates the difference of the energy dissipation between the under stress and stress-free conditions. 14 More importantly, it is well known that the size and shape of the hysteresis loop in the ferroelectric state depend strongly on temperature  $T^{1,15}$  The temperature dependence of ferroelectric properties is of interest in view not only of technological applications, but also in a fundamental sense. <sup>16–22</sup> The theoretical investigation by Rao et al.2 has already proposed a temperature scaling for ferromagnetic materials, which indicates that the hysteresis area decreases with increasing temperature. Experimental results on ferromagnetic thin films have revealed various temperature scaling relations. 2,3,6,8 Interestingly, there has been no report on the temperature scaling of dynamic hysteresis in ferroelectrics, both theoretically and experimentally. It is therefore the aim of this study to experimentally establish the temperature scaling of the ferroelectric hysteresis for soft PZT bulk ceramic.

The polarization–electric field (P-E) hysteresis loops of commercial soft PZT ceramic disks (APC-855, APC International, Ltd., USA) with diameter of 8 mm and thickness of 1 mm were obtained by a standardized ferroelectric testing unit, RT66A (Radiant Technologies Inc., NM), over the temperature range 298–453 K with  $E_0$  up to 40 kV/cm (f was fixed at 4 Hz). The measurements were performed on three ceramic disks. The Curie temperature ( $T_C$ ) of the soft PZT

used was experimentally determined from dielectric measurement to be 523 K. Other basic properties provided by the supplier are dielectric constant (1 kHz)  $\varepsilon_r$ =3400, piezoelectric strain constants  $d_{33}$ =600 pm/V and  $d_{31}$ =-276 pm/V, planar coupling factor  $k_p$ =0.68, and mechanical quality factor  $Q_m$ =65. It should also be noted that after being subjected to the hysteresis measurements, the samples showed a reduction of 10% in  $\varepsilon_r$  value and of 30% in  $d_{33}$  value.

Figure 1 displays the hysteresis loop profile for various electric field amplitudes  $E_0$  at a fixed T=373 K [Fig. 1(a)] and for various temperatures at a fixed  $E_0$ =40 kV/cm [Fig. 1(b)]. From the P-E loops, it is obvious that both  $E_0$  and T play a crucial role on the hysteresis area  $\langle A \rangle$ . Similar observations have been reported in many other ferroelectric systems.  $^{12,18,20,22}$  More interestingly, the observed temperature dependence of these hysteresis parameters prompts a question of whether there exist temperature scaling relations for these parameters.

Figure 2 shows the relation between  $\langle A \rangle$  and T in a double logarithmic form, where good linear fits are apparent  $(R^2$  close to 1). This implies a power-law relation between the hysteresis area and temperature, i.e.,  $\langle A \rangle \propto T^{\gamma}$ , and for each  $E_0$ , the exponent  $\gamma$  can be extracted from the slope, i.e.,  $\gamma = d \ln \langle A \rangle / d \ln T$ . However, both the slope  $\gamma$  and the y intercept seem to vary with  $E_0$ . Thus, to prove this  $E_0$  dependence, both the slope  $\gamma$  and the y intercept are plotted as a function of  $E_0$  (insets in Fig. 2), and the linear dependences on  $E_0$  are noticeable. The linear least square fits of both slopes and y intercepts with  $E_0$  give y=-0.0332x-1.1024with  $R^2$ =0.9983 for the slope (lower inset) and y=0.0769x+6.0137 with  $R^2=0.9966$  for the y intercept (upper inset). However, the y intercept refers to the value of  $\ln\langle A \rangle$  at the limit  $\ln T$  approaching zero, and from the fitting,  $\ln \langle A \rangle$  is not ceased at this limit, which is not really sound because at low temperatures the dynamics of the dipoles or domain walls is frozen. This could be due to the fact that the domain wall motion at high temperature is very different from those at very low temperature. 23,24 Consequently, this study does not imply if there is a finite hysteresis area at T approaching zero (i.e., in this case  $\ln T=0$  or T=1), but the quantity  $\ln \langle A \rangle$  at  $\ln T = 0$  here comes from an empirical fit to fulfill the validity of the linear fit. Therefore, based on the proposed assump-

a) Author to whom correspondence should be addressed; electronic mail: rattikornyimnirun@yahoo.com

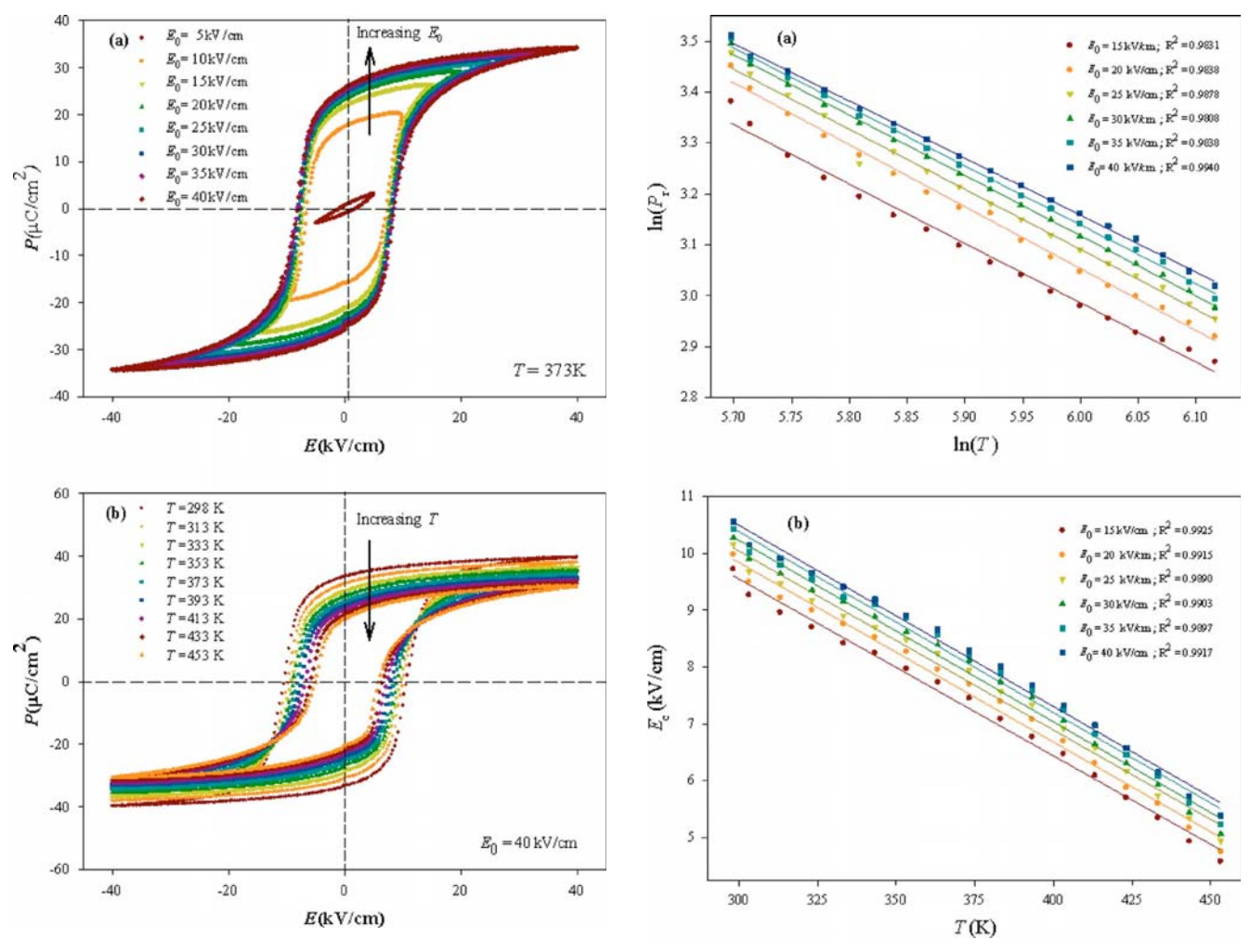


FIG. 1. Hysteresis loops for soft PZT ceramic (a) at T=373 K with varying  $E_0$ , and (b) at  $E_0$ =40 kV/cm with varying T.

FIG. 3. (a) Double logarithmic plot between  $ln(P_r)$  and ln(T), and (b) linear plot between  $E_C$  and T.

tions and fitting techniques, and by integrating all the relevant fits, it is found that

$$\langle A \rangle = \exp(0.0769E_0 + 6.0137)T^{-(0.0332E_0 + 1.1024)}.$$
 (1)

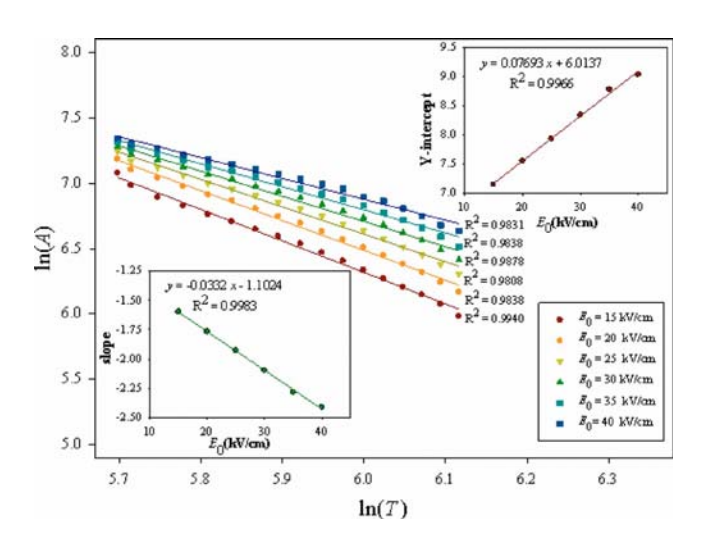


FIG. 2. Double logarithmic plot between ln(A) and ln(T) for various  $E_0$ , where the linear relations are found but the y intercepts and slopes seem to

Through similar mathematical treatment performed on  $\langle A \rangle$ , temperature-dependent relations for remnant polarization  $(P_r)$  and coercivity  $(E_C)$  are also obtained. Figure 3(a) shows the relation between  $P_r$  and T in a double logarithmic plot. As being evident, the power-law relation seems suitable for the fit since good  $R^2$  are attained. It is found that

$$P_r = \exp(-0.0068E_0 + 10.305)T^{(0.0022E_0 - 1.2322)}.$$
 (2)

The relation between  $E_C$  and T is shown in Fig. 3(b). Surprisingly, linear relations are apparent so an approximation on y=ax+b could be used to fit the data. Nonlinear fits between  $E_C$  and T are also performed (not shown) and the linear dependence of  $E_C$  and T is confirmed. Therefore, it could be estimated that

$$E_C = (-0.000\ 03E_0 - 0.030\ 85)T + (0.0459E_0 + 18.319).$$

The temperature dependences of  $\langle A \rangle$ ,  $P_r$ , and  $E_C$  shown in Eqs. (1)–(3) are also slightly  $E_0$  dependent. Obviously, small coefficients to  $E_0$  (for the whole range of  $E_0$  used in this study) suggests that at fixed  $E_0$ 

$$\langle A \rangle \propto T^{-1.1024},$$
 (4)

 $P_r \propto T^{-1.2322}$ be  $E_0$  dependent. The insets show those linear relations with  $E_0$ .  $P_r \propto T^{-1.2322}$ , Downloaded 19 Sep 2007 to 202.28.27.3. Redistribution subject to AIP license or copyright, see http://apl.aip.org/apl/copyright.jsp

$$(E_{C0} - E_C) \propto T. \tag{6}$$

 $E_{C0}$  in Eq. (6) can be viewed as the coercivity at  $T \sim 0$  K. However, as  $T \rightarrow 0$ , thermal energy is low, causing a nonsymmetric hysteresis loop; hence,  $E_{C0}$  cannot be meaningfully defined. Here  $E_{C0}$  is used for proposing the fit, which is valid for the experimental range in this study.

More importantly, Eqs. (4)–(6) present simple relations for the temperature scaling of ferroelectric hysteresis parameters. It should be noted that there have only been few theoretical treatments to include a temperature term in the dynamic hysteresis scaling of ferromagnetics. 2,3,25 Considering relatively successful applications of the treatments to E- and f-dependent ferroelectric hysteresis, 2-5 it would be worthwhile to compare our experimental results with the theoretically derived scaling. Theoretical scaling relations have been proposed as  $\langle A \rangle \propto T^{-\gamma}$ , with  $\gamma$  being 0.7, 1.18, and 1.98 for continuum three-dimensional (3D) ( $(\Phi^2)^2$ , two-dimensional, and 3D Ising models, respectively.  $^{2,3,25}$  An explanation for the variation may come from the different polarizationinteraction terms as considered in these models. It could be seen that our experimentally obtained temperature scaling of  $\langle A \rangle$  (with  $\gamma \sim 1.1$ ) falls between the values obtained from the models. The difference could be attributed to additional contributions from depolarizing effects within the ceramics (arisen from domain walls, grain boundaries, space charges, immobile defects, etc.), <sup>13,14</sup> as compared to physically oversimplified polarization interaction proposed in the theoretical models.<sup>2,3</sup>

Furthermore, the relation  $E_C \propto (T-T_C)^{-0.35}$  drawn from the 3D  $((\Phi^2)^2 \text{ model}^2)$  is significantly different from the linear relation obtained from our study, which further clarifies that the theoretical models cannot be applied to ferroelectric bulk ceramics. This study clearly serves as a survey to show that more improvement of the theoretical approach is needed to predict the scaling behavior in bulk ferroelectric ceramics. Interestingly, different forms of temperature scaling of  $E_C$  extracted from the previous experimental data on PZT thin films also indicate dimensional dependence of the coercivity, as reported in previous investigations.  $^{8,26,27}$ 

In approaching the saturation, the hysteresis area can be roughly estimated with  $(2P_r)(2E_C)$ . It is also interesting to check if the product of  $P_r$  and  $E_C$  would provide the same scaling law on the T dependence in comparison with  $\langle A \rangle$ . So, by substituting the  $E_0$  dependence on both  $E_C$  and  $P_r$  [Eqs. (2) and (3)], it is found that

$$(2E_C)(2P_r) = 4[(-0.000\ 03E_0 - 0.030\ 85)T + (0.0459E_0 + 18.319)] \times [\exp(-0.0068E_0 + 10.305)T^{(0.0022E_0 - 1.2322)}]. \tag{7}$$

Since all coefficients to  $E_0$  are small, by taking an approximation that  $E_0$  is fixed (or not very high), the  $(2P_r)$  × $(2E_C)$  reduces to

$$(2E_C)(2P_r) \approx 4(9.2 \times 10^2 T^{-0.2322} + 5.5 \times 10^5 T^{-1.2322}).$$
 (8)

As can be seen, the term  $T^{-1.2322}$  strongly decays in temperature than the term  $T^{-0.2322}$ , but  $T^{-1.2322}$  has a much larger coefficient. However, by substituting all temperatures used in

this study, it is found that  $T^{-1.2322}$  should be a principal term. Therefore, the scaling of "area" in this way on the temperature should have the exponent  $\gamma$  closer to -1.2322. In comparison with those extracted from the  $\ln\langle A \rangle$  and  $\ln T$  plot (in which the exponent  $\gamma$  has a value of -1.1024), these two scaling methods seem to agree. So once the scaling of area to the temperature is found, it is possible to guess how the  $E_C$  would scale with T if the scaling relation between  $P_r$  and T is known or vice versa. Similarly, a scaling of area to frequency has also been reported in a previous investigation.

In summary, the power-law temperature scaling relations have been found for hystersis area  $\langle A \rangle$  and remnant polarization  $P_r$ , while the coercivity  $E_C$  scales linearly with temperature. The three temperature scaling relations are also field dependent. At fixed  $E_0$ , the scaling relations take the forms of  $\langle A \rangle \propto T^{-1.1024}$ ,  $P_r \propto T^{-1.2322}$ , and  $(E_{C0} - E_C) \propto T$ . Furthermore, the product of  $P_r$  and  $E_C$  also provides the same scaling law on the T dependence in comparison with  $\langle A \rangle$ .

Financial support from the Thailand Research Fund (TRF) and the Commission on Higher Education (CHE) are gratefully acknowledged.

<sup>1</sup>K. Uchino, Ferroelectric Devices (Dekker, New York, 2000).

<sup>2</sup>M. Rao, H. R. Krishnamurthy, and R. Pandit, Phys. Rev. B **42**, 856 (1990).

<sup>3</sup>M. Acharyya and B. K. Chakrabarti, Phys. Rev. B **52**, 6560 (1995).

<sup>4</sup>L.-F. Wang and J.-M. Liu, J. Appl. Phys. **98**, 064106 (2005).

<sup>5</sup>J.-M. Liu, H. L. W. Chan, C. L. Choy, and C. K. Ong, Phys. Rev. B **65**, 014416 (2001).

<sup>6</sup>Q. Jiang, H. N. Yang, and G. C. Wang, Phys. Rev. B **52**, 14911 (1995).
 <sup>7</sup>Y.-H. Kim and J.-J. Kim, Phys. Rev. B **55**, R11933 (1997).

<sup>8</sup>J. S. Suen and J. L. Erskine, Phys. Rev. Lett. **78**, 3567 (1997).

<sup>9</sup>J.-M. Liu, H. P. Li, C. K. Ong, and L. C. Lim, J. Appl. Phys. **86**, 5198 (1999).

<sup>10</sup>B. Pan, H. Yu, D. Wu, X. H. Zhou, and J.-M. Liu, Appl. Phys. Lett. 83, 1406 (2003).

<sup>11</sup>J.-H. Park, C.-S. Kim, B.-C. Choi, B. K. Moon, J. H. Jeong, and I. W. Kim, Appl. Phys. Lett. **83**, 536 (2003).

<sup>12</sup>J.-M. Liu, B. Pan, H. Yu, and S. T. Zhang, J. Phys.: Condens. Matter 16, 1189 (2004).

<sup>13</sup>R. Yimnirun, Y. Laosiritaworn, S. Wongsaenmai, and S. Ananta, Appl. Phys. Lett. **89**, 162901 (2006).

<sup>14</sup>R. Yimnirun, S. Wongsaenmai, S. Ananta, and Y. Laosiritaworn, Appl. Phys. Lett. 89, 242901 (2006).

<sup>15</sup>M. E. Lines and A. M. Glass, Principles and Applications of Ferroelectrics and Related Materials (Clarendon, Oxford, 1977).

<sup>16</sup>T. Mihara, H. Watanabe, and C. A. Araujo, Jpn. J. Appl. Phys., Part 1 33, 3996 (1994).

<sup>17</sup>Q. Tan, J. Li, and D. Viehland, Appl. Phys. Lett. **75**, 418 (1999).

<sup>18</sup>G. L. Yuan, J.-M. Liu, S. T. Zhang, D. Wu, Y. P. Wang, Z. G. Liu, H. L. W. Chan, and C. L. Choy, Appl. Phys. Lett. **84**, 954 (2004).

<sup>19</sup>B. S. Li, G. R. Li, Q. R. Yin, Z. G. Zhu, A. L. Ding, and W. W. Cao, J. Phys. D 38, 1107 (2005).

Lin, D. Xiao, J. Zhu, and P. Yu, Appl. Phys. Lett. 88, 062901 (2006).
 W. Chang, A. H. King, and K. Bowman, Appl. Phys. Lett. 88, 242901 (2006).

<sup>22</sup>S. K. Pandey, O. P. Thakur, A. Kumar, C. Prakash, R. Chatterjee, and T. C. Goel, J. Appl. Phys. **100**, 014104 (2006).

<sup>23</sup>A. Gruverman, O. Auciello, and H. Tokumoto, Annu. Rev. Mater. Sci. 28, 101 (1998).

<sup>24</sup>K. Lee and S. Baik, Annu. Rev. Mater. Res. **36**, 81 (2006).

<sup>25</sup>M. Rao and R. Pandit, Phys. Rev. B **43**, 3373 (1991).

<sup>26</sup>O. Lohse, D. Bolten, S. Tiedke, T. Schneller, and R. Waser, Proceedings of the IEEE-ISAF 98 (IEEE, Piscataway, NJ, 1998), Vol. 1, p. 27.

<sup>27</sup>H. Maiwa and N. Ichinose, Ferroelectrics **293**, 89 (2003).

<sup>28</sup>J.-M. Liu, W. M. Wang, Z. G. Liu, H. L. Chan, and C. L. Choy, Appl. Phys. A: Mater. Sci. Process. **75**, 507 (2002).

# Dynamic hysteresis and scaling behavior of hard lead zirconate titanate bulk ceramics

R. Yimnirun, <sup>a)</sup> R. Wongmaneerung, S. Wongsaenmai, A. Ngamjarurojana, S. Ananta, and Y. Laosiritaworn

Department of Physics, Faculty of Science, Chiang Mai University, Chiang Mai 50200, Thailand

(Received 20 November 2006; accepted 9 February 2007; published online 14 March 2007)

The scaling relation of ferroelectric hysteresis area  $\langle A \rangle$  against frequency f and field amplitude  $E_0$  for the saturated loops of the hard lead zirconate titanate bulk ceramic takes the form of  $\langle A \rangle \propto f^{-0.28} E_0^{0.89}$ , while that for the minor loops takes the form of  $\langle A \rangle \propto f^{-0.43} E_0^{3.19}$ . In both cases, the scaling relations are similar to those of its soft counterpart. This indicates that the dynamic behaviors and scaling relations in bulk ceramics are mainly governed by the domain states and structures, while the distinct types of complex defects contribute mainly to the difference in the coercive field observed in hard and soft ceramics. © 2007 American Institute of Physics.

[DOI: 10.1063/1.2713769]

Lead zirconate titanate  $[Pb(Zr_{1-x}Ti_x)O_3 \text{ or } (PZT)]$  ceramics are among the lead-based complex perovskites that have been investigated extensively both from academic and commercial viewpoints with various applications. However, PZT ceramics are usually modified with dopants. Generally, donor (higher-valency) additives induce "soft" piezoelectric behaviors with higher dielectric and piezoelectric activities, while acceptor (lower-valency) additives result in "hard" piezoelectric behaviors.

In many applications, the dynamic hysteresis, i.e., hysteresis area  $\langle A \rangle$  as a function of the field amplitude  $E_0$  and frequency f, has become an important consideration. <sup>1-5</sup> Hence, there have been reports on the scaling behavior of the dynamic hysteresis in ferromagnetic and ferroelectric thin films. <sup>6-13</sup> Many theoretical studies have been focused on the scaling law,

$$\langle A \rangle \propto f^{\alpha} E_0^{\beta}$$
 (1)

(where  $\alpha$  and  $\beta$  are exponents that depend on the dimensionality and symmetry of the system), of hysteresis curves in polarization systems.<sup>6–8</sup> Earlier investigations<sup>6–8,13</sup> have reported the scaling relations for the high-f region with  $\alpha$  and  $\beta$  values, respectively, of -1 and 2 for  $(\Phi^2)^2$  and  $(\Phi^2)^3$  models and of -0.33 and 3 for a PZT thin film. We also reported the scaling relation for soft PZT bulk ceramics with  $\alpha$  and  $\beta$ values, respectively, of -0.25 and 1 for saturated loops. Interestingly, the scaling form for the minor loops is identical to that of the PZT thin film. The difference in the scaling relations has been attributed to the different domain dynamics. <sup>14</sup> Generally, the domain dynamics differs depending on the composition and the doping type. 15,16 In this point of view, the domain dynamics in hard and soft PZT ceramics, which contain distinct types of complex defects, should be very different. 16 Since our earlier work has already shown unique scaling relations for the soft PZT bulk ceramics, 14 it will be of interest to investigate the scaling behavior of the hard PZT bulk ceramic, as the direct comparison will help extracting roles of complex defects to the dynamic hysteresis behavior. Thus, we present in this letter the results on the

scaling behaviors of the dynamic hysteresis of a hard PZT bulk ceramic. As will be seen, the dynamic hysteresis and scaling behaviors of the hard ceramic are surprisingly very similar to those of the soft one.

The dynamic hysteresis (P-E) loops of commercial hard PZT ceramic disks (APC-840, APC International, Ltd., USA) with a diameter of 8 mm and a thickness of 1 mm were characterized at room temperature (298 K) by using a modified Sawyer-Tower circuit with f covering from 1 to 100 Hz and  $E_0$  from 0 to 40 kV/cm. The electric field was applied to a sample by a high voltage ac amplifier (Trek 610D) with the input sinusoidal signal from a function generator (HP 3310A). The P-E loops were recorded by a digital oscilloscope (HP 54645A, 100 MHz). Each loop was obtained after 20 sampling cycles to average out the noise deformation. The hysteresis loop obtained was very consistent with that obtained by a standardized ferroelectric testing unit, RT66A (Radiant Technologies Inc., NM), which ensures the reliability of the measurements. It should be noted that the exact compositional formulation for APC-840 is proprietary to APC International, Ltd., but our elemental analysis showed multiple lower valent substituents, such as Na, Ni, Co, and Ga, which are known to produce hard properties through the formation of complex defects. 1,2,4,15,16

The hysteresis loops of unpoled samples at different f but fixed  $E_0$  (40 kV/cm) and at different  $E_0$  but fixed f (20 Hz) are shown in Fig. 1. The loop area  $\langle A \rangle$ , remanent polarization  $(P_r)$ , and coercive field  $(E_c)$  decrease with an increase of frequency, as shown in Fig. 1(a). The dependence of the hysteresis loop on  $E_0$  is depicted in Fig. 1(b). For small fields (10 and 15 kV/cm), the loops do not saturate. With further increase in  $E_0$ ,  $\langle A \rangle$ ,  $P_r$ , and  $E_c$  increase until a well saturated loop is achieved. Similar observations have been reported in thin films and ceramics.  $^{8,10,13,14}$ 

To investigate the scaling behavior for unpoled hard PZT bulk ceramics, we followed the scaling relation reported earlier for soft PZT bulk ceramics in the form of  $\langle A \rangle \propto f^{-0.25} E_0$ . <sup>14</sup> The data are shown in Fig. 2 and the solid line represents the fitting. Surprisingly, it is revealed that the high *E*-field (saturated loops) data can be fitted reasonably well ( $R^2 \sim 0.97$ ) with the scaling relation obtained experimentally for the soft PZT bulk ceramics. However, some deviation is still ob-

a) Author to whom correspondence should be addressed; electronic mail: rattikornyimnirun@yahoo.com

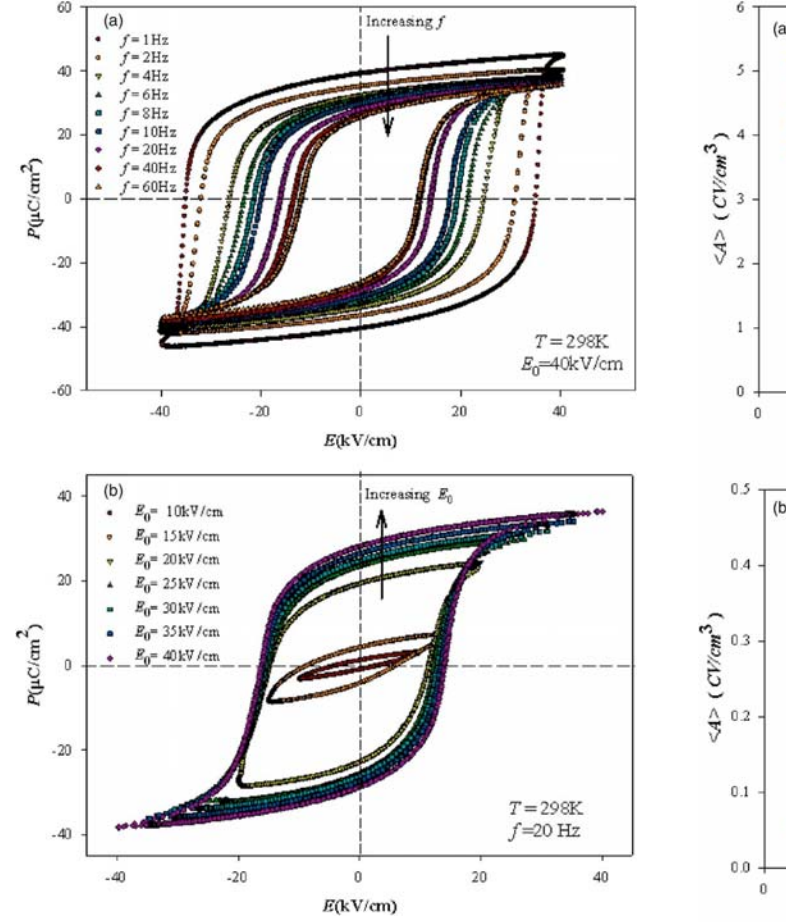


FIG. 1. (Color online) Hysteresis loops for hard PZT bulk ceramic (a) at various f and  $E_0$ =40 kV/cm and (b) at various  $E_0$  and f=20 Hz.

served, particularly for low *E*-field (minor loops) data. This was also the case for the soft PZT bulk ceramics, as reported earlier, <sup>14</sup> in which the different scaling relations were obtained for the saturated and minor loops. Apparently, a similar situation is also observed in the hard PZT bulk ceramics.

Attempt to obtain better scaling can be done by fitting the data with  $\langle A \rangle \propto f^m E_0^n$ , where m and n are exponents to be determined directly from the experimental data. By plotting  $\langle A \rangle$  against f at fixed  $E_0$ , one obtains the exponent m. On the

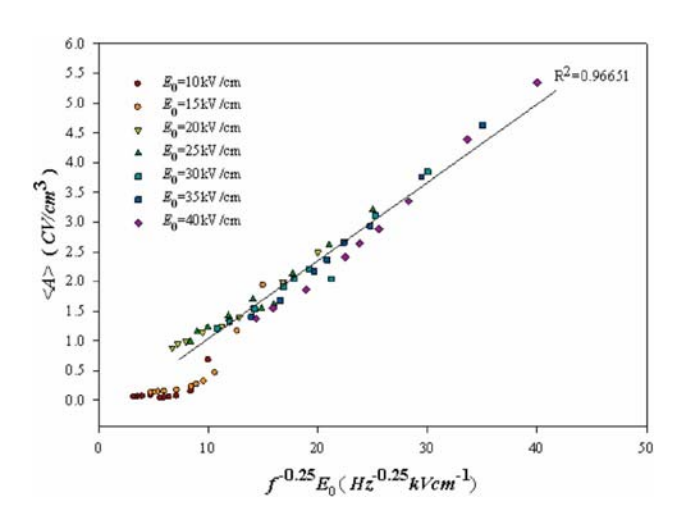


FIG. 2. (Color online) Scaling of hysteresis area  $\langle A \rangle$  against  $f^{-0.25}E_0$  for hard

Downloaded 19 Sep 2007 to 202.28.27.3. Redistribution subject to AIP license or copyright, see http://apl.aip.org/apl/copyright.jsp

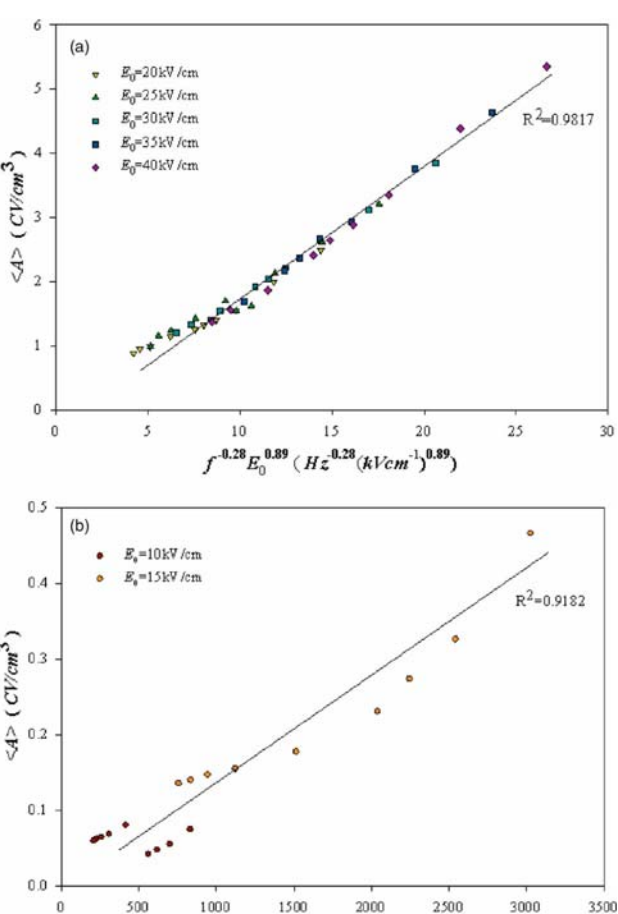


FIG. 3. (Color online) Scaling of hysteresis for hard PZT bulk ceramic. (a) Area  $\langle A \rangle$  against  $f^{-0.28}E_0^{0.89}$  for the saturated loops; (b) area  $\langle A \rangle$  against  $f^{-0.43}E_0^{3.19}$  for the minor loops.

 $f^{-0.43}E_0^{-3.18} (Hz^{-0.43}(kVcm^{-1})^{3.18})$ 

other hand, the exponent n can be obtained from plotting  $\langle A \rangle$  against  $E_0$  at fixed f. By least-squares-fitting method, for the high E-field data (saturated loops) the exponents  $m=-0.28\pm0.01$  and  $n=0.89\pm0.05$  were obtained. As plotted in Fig. 3(a), it is revealed that the high E-field data can be fitted only slightly better  $(R^2\sim0.98)$ , within the measured uncertainty, by

$$\langle A \rangle \propto f^{-0.28} E_0^{0.89}. \tag{2}$$

Furthermore, the exponents  $m=-0.43\pm0.08$  and  $n=3.19\pm0.56$  were obtained and fitted reasonably well  $(R^2\sim0.92)$  for the minor loop data, as plotted in Fig. 3(b). Therefore, the scaling relation for minor loops of hard PZT bulk ceramic takes the form of

$$\langle A \rangle \propto f^{-0.43} E_0^{3.19}. \tag{3}$$

The scaling relation obtained in Eq. (2) for the saturated loops of the hard PZT bulk ceramic indicates that  $\langle A \rangle$  decays more slowly with f and grows more slowly with  $E_0$  than that theoretically predicted and that observed in the PZT thin film, as listed in Table I and discussed in an earlier publication. <sup>14</sup>

As listed in Table I, it is even more interesting to observe that the scaling behaviors for the hard PZT bulk ceramic are to some extent similar to those of the soft counterpart. By a direct comparison, the exponents *m* and *n* for the two ceraman and the light see http://apl.aip.org/apl/converght.ep.

TABLE I. Dynamic scaling exponents for different systems [refer to Eq. (1)].

| System   | α                | β               | References |
|--|------------------|-----------------|------------|
| $\Phi^2$ and $\Phi^2$ model  | -1               | 2               | 6 and 7    |
| 1–3 composite  | -1               | 2               | 17         |
| Nd-doped Bi <sub>4</sub> Ti <sub>3</sub> O <sub>12</sub> thin film | -0.66            | 2               | 18         |
| SBT thin film  | -0.33            | 2               | 19         |
| PZT thin film  | -0.33            | 3               | 13         |
| Soft PZT bulk ceramic  |                  |                 |            |
| -Saturated loops   | -0.25            | 1               | 14         |
| -Minor loops   | -0.33            | 3               | 14         |
| Hard PZT bulk ceramic  |                  |                 |            |
| -Saturated loops   | $-0.28 \pm 0.01$ | $0.89 \pm 0.05$ | This work  |
| -Minor loops   | $-0.43 \pm 0.08$ | $3.19 \pm 0.56$ | This work  |

ics are not significantly different. As well known, the major difference between the two types of ceramic is the complex defects. 1,3,4,15,16 In the hard PZT, the oxygen vacancies are introduced, are trapped at the domain walls, and then form electric dipoles with the acceptor atoms. These dipoles called complex defects act as pinning points for the domain wall, and the domain wall motion is reduced. The complex defects are absent in the soft PZT ceramics; hence the domain walls can move more easily. Therefore, hard PZT ceramics typically show higher  $E_C$  than soft ones. Other dielectric and piezoelectric properties of the two types of ceramics are also significantly different. However, the similar scaling behaviors for the two types of ceramics suggest that though the complex defects contribute greatly to the difference on the electrical properties, they contribute only slightly to the dynamic behaviors. At high fields (saturated loops), one can picture that beyond the critical field, i.e.,  $E_C$  which is different between the hard and soft ceramics, the dynamic hysteresis behavior of the PZT bulk ceramics is mainly governed by the available domain states for polarization switching, while the contribution the complex defects is very minimal; hence the scaling behavior is nearly similar between the hard and soft PZT ceramics. However, at lower fields (minor loops), the complex defects still play limited roles in controlling the dynamic behavior, as can be observed from the relatively larger differences in the values of m and n between the soft and hard PZT ceramics.

More importantly, all these observations suggest that bulk PZT ceramics with similar domain structures should have very comparable dynamic hysteresis and scaling behavior. As also listed in Table I, it is interesting to observe that models and thin films of different materials, which contain similar domain structures, show comparable scaling behaviors (with only a slight difference in exponents m and n). It could be stated that the dynamic hysteresis (hence the scaling behavior) is mainly controlled by available domain states and polarization switching mechanism. Therefore, the scaling relations obtained theoretically and experimentally from models, thin films, and bulks with distinct types of domain structures and mechanisms should be noticeably different (hence different universality classes among them), as shown

in Table I. Our opinion on the contribution of the domain states in controlling the dynamic hysteresis behavior may be strengthened by a further study of the domain states in different materials, particularly in soft and hard PZT ceramics. Previous transmission electron microscopy studies have already shown fine "wavy" domains in hard PZT, while irregular domain morphologies have been reported in soft PZT. PZT. Thus, giving the complexity of the dopant types and concentrations in the commercial hard and soft PZT ceramics, it may be too complicated to evaluate the domain state contribution to the dynamic behavior in these ceramics. It is more suitable to compare the domain states in undoped PZT and single-element soft- and hard-doped PZT ceramics. <sup>15,23</sup>

In summary, the scaling relation for the saturated hysteresis loops of the hard PZT ceramic takes the form of  $\langle A \rangle \propto f^{-0.28} E_0^{0.89}$ , while that for the minor loops takes the form of  $\langle A \rangle \propto f^{-0.43} E_0^{3.19}$ . The two scaling relations are very similar to those of soft PZT bulk ceramics, suggesting that the scaling behaviors of the two types of bulk ceramics are in the same universality class.

This work was supported by the Thailand Research Fund (TRF), Commission on Higher Education (CHE), and Faculty of Science and Graduate School of Chiang Mai University.

<sup>1</sup>B. Jaffe, W. R. Cook, and H. Jaffe, *Piezoelectric Ceramics* (Academic, New York, 1971), p. 271.

<sup>2</sup>Y. H. Xu, Ferroelectric Materials and Their Applications (North Holland, Los Angeles, 1991), p. 121.

<sup>3</sup>K. Uchino, Ferroelectric Devices (Dekker, New York, 2000), p. 145.

<sup>4</sup>A. J. Moulson and J. M. Herbert, *Electroceramics* (Wiley-Interscience, New York, 2003), p. 358.

<sup>5</sup>J. F. Scott, Ferroelectr. Rev. 1, 1 (1998).

<sup>6</sup>M. Rao, H. R. Krishnamurthy, and R. Pandit, Phys. Rev. B **42**, 856 (1990).

<sup>7</sup>M. Acharyya and B. K. Chakrabarti, Phys. Rev. B **52**, 6560 (1995).

<sup>8</sup>J.-M. Liu, H. L. W. Chan, C. L. Choy, Y. Y. Zhu, S. N. Zhu, Z. G. Liu, and N. B. Ming, Appl. Phys. Lett. **79**, 236 (2001).

Q. Jiang, H. N. Yang, and G. C. Wang, Phys. Rev. B 52, 14911 (1995).
 B. Pan, H. Yu, D. Wu, X. H. Zhou, and J.-M. Liu, Appl. Phys. Lett. 83, 1406 (2003).

<sup>11</sup>Y.-H. Kim and J.-J. Kim, Phys. Rev. B **55**, R11933 (1997).

<sup>12</sup>J.-H. Park, C.-S. Kim, B.-C. Choi, B. K. Moon, J. H. Jeong, and I. W. Kim, Appl. Phys. Lett. **83**, 536 (2003).

 J.-M. Liu, H. L. W. Chan, and C. L. Choy, Mater. Lett. **52**, 213 (2002).
 R. Yimnirun, Y. Laosiritaworn, S. Wongsaenmai, and S. Ananta, Appl. Phys. Lett. **89**, 162901 (2006).

<sup>15</sup>Q. Tan, J. Li, and D. Viehland, Appl. Phys. Lett. **75**, 418 (1999).

<sup>16</sup>W. Chang, A. H. King, and K. J. Bowman, Appl. Phys. Lett. 88, 242901 (2006)

<sup>17</sup>B. Pan, Y. Yang, L. C. Yu, J. M. Liu, K. Li, Z. G. Liu, and H. L. W. Chan, Mater. Sci. Eng., B **B99**, 179 (2005).

<sup>18</sup>J.-M. Liu, B. Pan, H. Yu, and S. T. Zhang, J. Phys.: Condens. Matter 16, 1189 (2004).

<sup>19</sup>J.-M. Liu, B. Pan, K. F. Wang, and H. Yu, Ceram. Int. **30**, 1471 (2004).

Q. Tan, Z. Xu, J. F. Li, and D. Viehland, J. Appl. Phys. **80**, 5866 (1996).
 J. F. Li, X. H. Dai, A. Chow, and D. Viehland, J. Mater. Res. **10**, 926 (1995).

<sup>22</sup>W. Cao and C. A. Randall, J. Phys. Chem. Solids **37**, 1499 (1996).

<sup>23</sup>T. Granzow, E. Suvaci, H. Kungl, and M. J. Hoffmann, Appl. Phys. Lett. 89, 262908 (2006).



Available online at www.sciencedirect.com



materials letters

www.elsevier.com/locate/matlet

Materials Letters 61 (2007) 3873 - 3877

# Effect of calcination conditions on phase formation and particle size of Zn<sub>3</sub>Nb<sub>2</sub>O<sub>8</sub> powders synthesized by solid-state reaction

A. Prasatkhetragarn, R. Yimnirun, S. Ananta\*

Department of Physics, Faculty of Science, Chiang Mai University, Chiang Mai 50200, Thailand

Received 19 October 2006; accepted 21 December 2006

Available online 30 December 2006

#### Abstract

The solid-state mixed oxide method via a rapid vibro-milling technique is explored in the preparation of single-phase  $Zn_3Nb_2O_8$  powders. The formation of the  $Zn_3Nb_2O_8$  phase in the calcined powders has been investigated as a function of calcination conditions by TG-DTA and XRD techniques. Morphology, particle size and chemical composition have been determined via a combination of SEM and EDX techniques. It has been found that the minor phases of unreacted ZnO and  $Nb_2O_5$  precursors and the columbite  $ZnNb_2O_6$  phase tend to form together with the  $Zn_3Nb_2O_8$  phase, depending on calcination conditions. It is seen that optimization of calcination conditions can lead to a single-phase  $Zn_3Nb_2O_8$  in a monoclinic phase.

© 2007 Elsevier B.V. All rights reserved.

Keywords: Zn<sub>3</sub>Nb<sub>2</sub>O<sub>8</sub>; Calcination; Phase formation; Particle size; Nanopowders

## 1. Introduction

The quest for optimal powder characteristics (controlled chemical composition, homogeneity, reactivity, particle size and shape) in the fabrication of materials has directed attention particularly towards powder production techniques. It is known that various compositions are possible in the Zn-Nb-O system [1,2]. To date, three possible zinc niobium oxides have been identified: ZnNb<sub>2</sub>O<sub>6</sub>, Zn<sub>2</sub>Nb<sub>34</sub>O<sub>87</sub> and Zn<sub>3</sub>Nb<sub>2</sub>O<sub>8</sub> [1,2]. Amongst these compounds, zinc niobate (ZnNb<sub>2</sub>O<sub>6</sub>) is one of the most well-known materials, which has recently gained considerable attention [3,4]. This compound is very well known as the key precursor for the successful preparation of singlephase perovskite lead zinc niobate, Pb(Zn<sub>1/3</sub>Nb<sub>2/3</sub>)O<sub>3</sub>, or PZNbased materials, which are becoming increasingly important for multilayer ceramic capacitor, electrostrictor and actuator applications [5,6]. In general, production of single-phase ZnNb<sub>2</sub>O<sub>6</sub> is not straightforward, as a minor concentration of

In contrast, very little is known about Zn<sub>3</sub>Nb<sub>2</sub>O<sub>8</sub>, since no work has been dedicated to the synthesis of this compound.

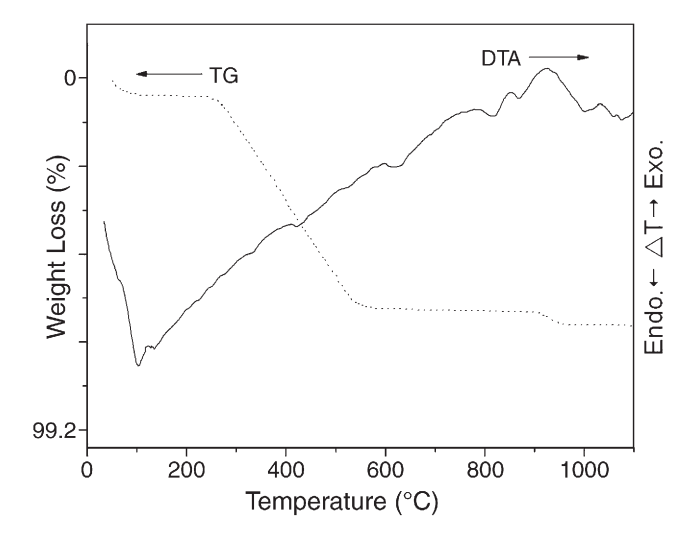


Fig. 1. TG-DTA curves for the mixture of 3ZnO-Nb<sub>2</sub>O<sub>5</sub> powder.

the ZnO is sometimes formed alongside the major phase of  $ZnNb_2O_6$  [7,8].

<sup>\*</sup> Corresponding author. Tel.: +66 53 943367; fax: +66 53 943445. *E-mail address*: Suponananta@yahoo.com (S. Ananta).

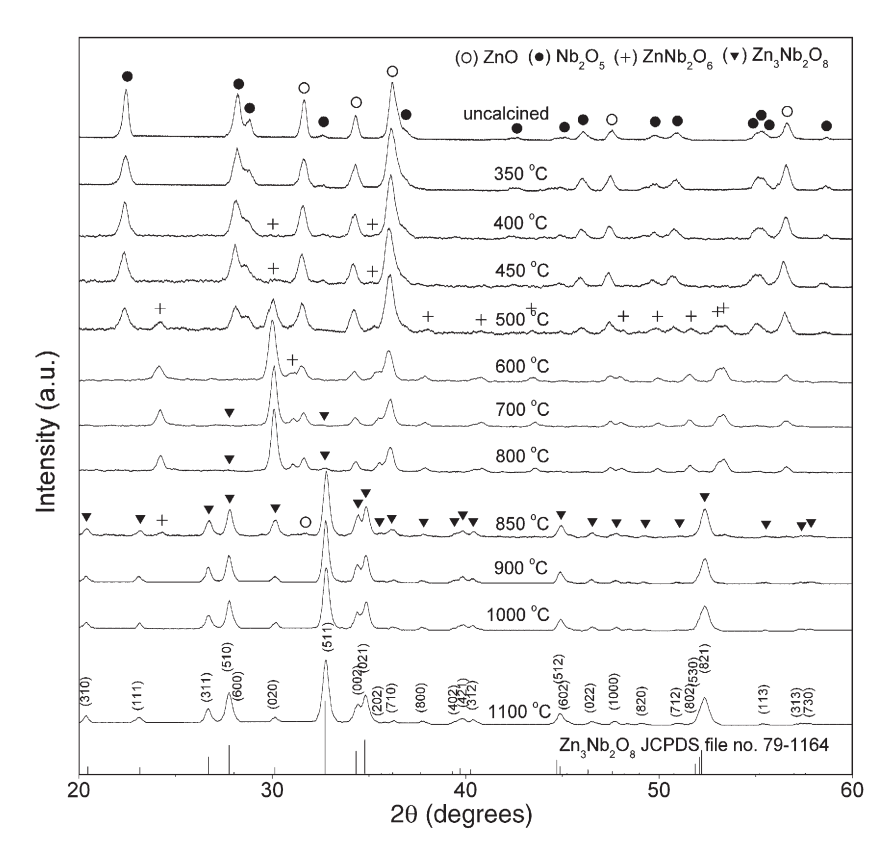


Fig. 2. XRD patterns of ZN powders calcined at various temperatures for 5 h with heating/cooling rates of 10 °C/min.

Much of the work concerning the  $Zn_3Nb_2O_8$  compound has been directed towards determining crystal structure and microwave dielectric properties [9–11]. Kasper [10] and Isobe et al. [11] reported that the structure of  $Zn_3Nb_2O_8$  is closely related to the columbite structure of  $ZnNb_2O_6$ . Its crystal structure can be represented as an order super-structure of  $\alpha$ -PbO<sub>2</sub> [12]. Moreover, to date, the potential of  $Zn_3Nb_2O_8$  as a

possible alternative precursor for the preparation of PZN has not yet been reported. Interestingly, the mixed oxide route for the production of Zn<sub>3</sub>Nb<sub>2</sub>O<sub>8</sub> powders has not received detailed attention, and the effects of calcination conditions (*i.e.* applied firing temperature, dwell time and heating/cooling rates) have not yet been studied extensively. Therefore, the main purpose of this work was to explore a simple mixed oxide synthetic route

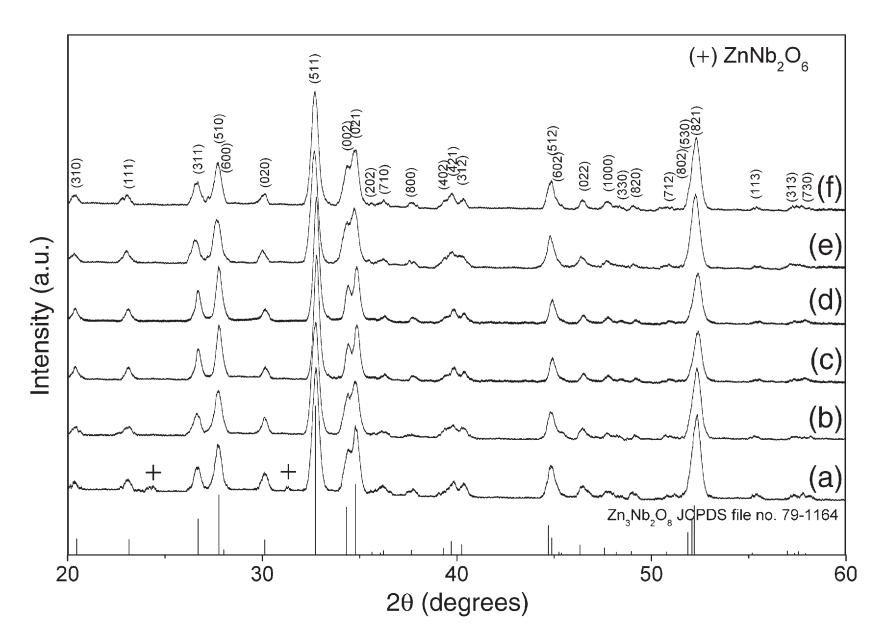


Fig. 3. XRD patterns of ZN powders calcined at 900 °C for (a) 0.5, (b) 1, (c) 2 and (d) 3 h, with heating/cooling rates of 10 °C/min and for 1 h with heating/cooling rates of (e) 20 and (f) 30 °C/min.

for the production of  $Zn_3Nb_2O_8$  powders via a rapid vibromilling technique and to perform a systematic study of the reaction between the starting zinc oxide and niobium oxide precursors. The phase formation and morphology of the powder calcined at various conditions will be studied and discussed. The study also forms a possible basis for a further survey on PZN preparation.

### 2. Experimental procedure

The starting materials were commercially available zinc oxide, ZnO (JCPDS file number 89-1397) and niobium oxide, Nb<sub>2</sub>O<sub>5</sub> (JCPDS file number 30-0873) (Aldrich, 99.9% purity).

The two oxide powders exhibited an average particle size in the range 3.0–5.0 μm. Zn<sub>3</sub>Nb<sub>2</sub>O<sub>8</sub> powders were synthesized by the solid-state reaction of thoroughly ground mixtures of ZnO and Nb<sub>2</sub>O<sub>5</sub> powders that were milled in the required stoichiometric ratio. In order to combine mixing capacity with a significant time saving, a McCrone vibro-milling technique [8,13] was carried out for 0.5 h with corundum cylindrical media in isopropyl alcohol (IPA). After drying at 120 °C for 2 h, the reaction of the uncalcined powders taking place during heat treatment was investigated by thermogravimetric and differential thermal analyses (TG–DTA, Shimadzu), using a heating rate of 10 °C/min in air from room temperature up to 1100 °C. Based on the TG–DTA results, the mixture was calcined at

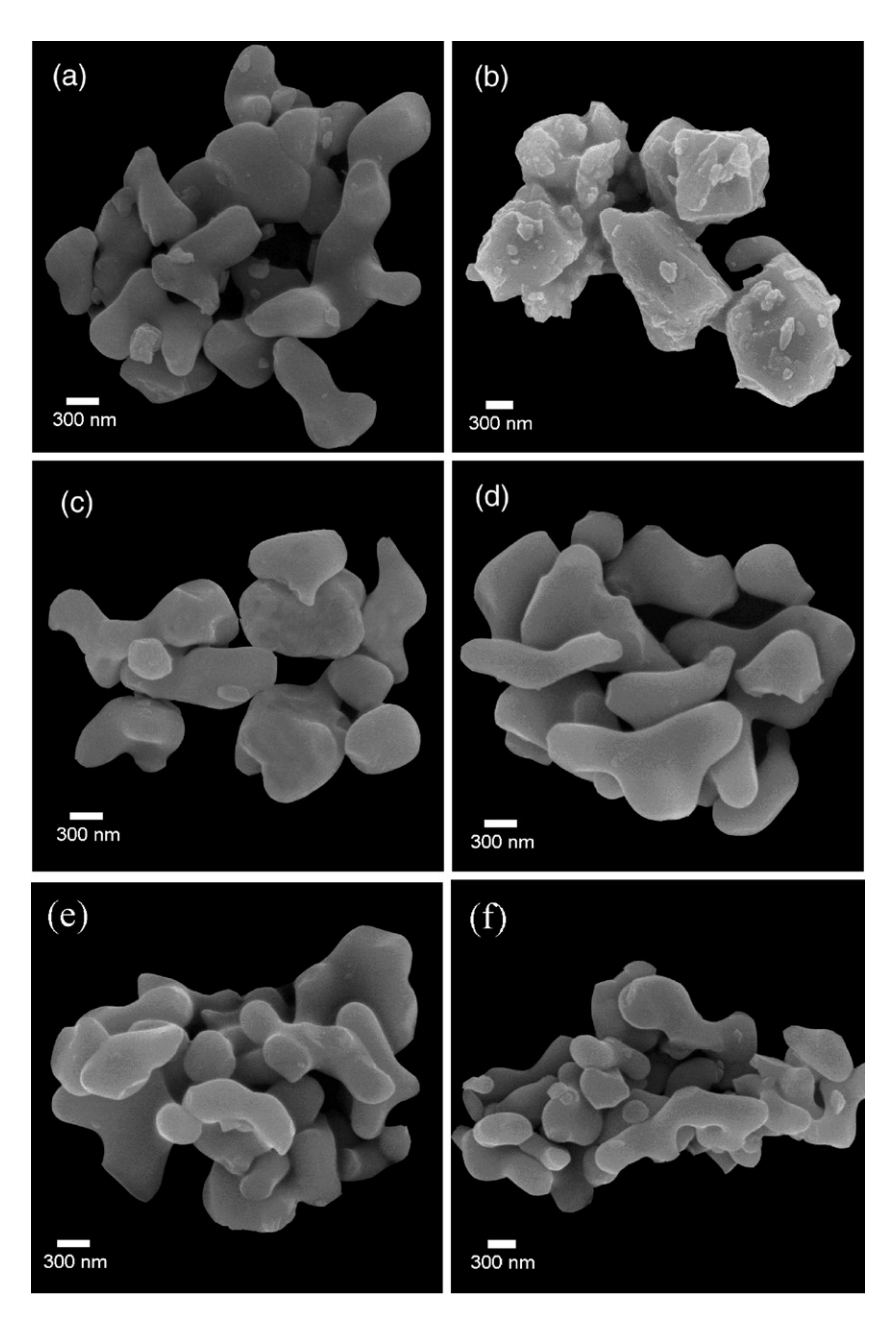


Fig. 4. SEM micrographs of ZN powders calcined for 1 h with heating/cooling rates of 10 °C/min at (a) 900 and (b) 1050 °C, and at 900 °C for (c) 3 and (d) 5 h; and at 900 °C for 1 h with heating/cooling rates of (e) 20 and (f) 30 °C/min.

Table 1
Particle size range of Zn<sub>3</sub>Nb<sub>2</sub>O<sub>8</sub> powders calcined at various conditions

| Calcination conditions |                    |                                | Particle size range |                   |
|------------------------|--------------------|--------------------------------|---------------------|-------------------|
| Temperature (°C)       | Dwell<br>times (h) | Heating/cooling rates (°C/min) | SEM<br>(±5 nm)      | XRD<br>(±0.05 nm) |
| 900                    | 1                  | 10                             | 60-1950             | 30.18             |
| 900                    | 1                  | 20                             | 80-2130             | 31.11             |
| 900                    | 1                  | 30                             | 110-2740            | 37.00             |
| 900                    | 3                  | 10                             | 283-1988            | 35.31             |
| 900                    | 5                  | 10                             | 313-2400            | 35.87             |
| 1050                   | 1                  | 10                             | 80-2110             | 40.73             |

various conditions, in closed alumina crucible, in order to investigate the formation of Zn<sub>3</sub>Nb<sub>2</sub>O<sub>8</sub>.

All powders were subsequently examined by room temperature X-ray diffraction (XRD; Siemens-D500 diffractometer), using Ni-filtered  $\text{CuK}_{\alpha}$  radiation to identify the phases formed and optimum calcination conditions for the formation of  $\text{Zn}_3\text{Nb}_2\text{O}_8$  powders. Powder morphologies and particle sizes were directly imaged, using scanning electron microscopy (SEM; JEOL JSM-840A). The chemical compositions of the phase formed were elucidated by an energy-dispersive X-ray (EDX) analyzer with an ultra-thin window. EDX spectra were quantified with the virtual standard peaks supplied with the Oxford Instruments eXL software.

#### 3. Results and discussion

The TG-DTA simultaneous analysis of a powder mixed in the stoichiometric proportions of Zn<sub>3</sub>Nb<sub>2</sub>O<sub>8</sub> is displayed in Fig. 1. In the temperature range from room temperature to  $\sim 150$  °C, the sample shows both exothermic and endothermic peaks in the DTA curve, consistent with the first weight loss. These observations can be attributed to the decomposition of the organic species such as rubber lining from the milling process similar to our earlier reports [8,13]. Corresponding to the second fall in sample weight, by increasing the temperature further to ~400 °C, a slight thermal fluctuation in the DTA curve is observed. This may be attributed to the crystallization of ZnNb<sub>2</sub>O<sub>6</sub> as reported earlier [8]. Increasing the temperature up to  $\sim$  1100 °C, the solid-state reaction occurred between ZnO and Nb<sub>2</sub>O<sub>5</sub> [8,14]. The broad exotherm with several peaks in the DTA curve represents that reaction, which has maxima at ~830 °C and 900 °C. These are supported by the third falls in sample weight over the same temperature ranges. However, it is to be noted that there is no obvious interpretation of these peaks, although it is likely to correspond to a phase transition reported earlier [1,8,14]. These data were used to define the range of calcination temperatures for XRD investigation between 350 and 1100 °C.

To further study the phase development with increasing calcination temperature in the powders, they were calcined for 5 h in air at various temperatures, up to 1100 °C, followed by phase analysis using XRD. As shown in Fig. 2, for the uncalcined powders and the powders calcined at 350 °C, only X-ray peaks of precursors ZnO (O) and Nb<sub>2</sub>O<sub>5</sub> ( $\blacksquare$ ), which could be matched with JCPDS file numbers 89-1397 [15] and 30-0873 [16], respectively, are present, indicating that no reaction had yet been triggered during the vibro-milling and low firing processes. However, it is seen that a small portion of the crystalline phase of the ZnNb<sub>2</sub>O<sub>6</sub> crystallites (+) as reported by Ngamjarurojana et

al. [8] was found as separated phases in the powders calcined at 400 °C, and became the predominant phase in the powder calcined above 450 °C. As the temperature increased to 800 °C, the intensity of the ZnNb<sub>2</sub>O<sub>6</sub> peaks was further enhanced whereas some new peaks ( $\nabla$ ) of the desired Zn<sub>3</sub>Nb<sub>2</sub>O<sub>8</sub> phase, started to appear, mixing with the ZnNb<sub>2</sub>O<sub>6</sub> and ZnO phases after calcinations above 600 °C. These observations are associated with the DTA peaks found at the same temperature range within the broad exothermic effects in Fig. 1. In a first approximation, this ZnNb<sub>2</sub>O<sub>6</sub> phase has a columbite-type structure with an orthorhombic unit cell (a=1420.8 pm, b=572.6 pm and c=504.0 pm, space group *Pbcn* (no. 60)), consistent with JCPDS file number 76-1827 [17]. This observation could be attributed mainly to the poor reactivity of zinc and niobium species [8]. Upon calcination at 900 °C, a single phase of Zn<sub>3</sub>Nb<sub>2</sub>O<sub>8</sub> is already formed. For the present work, there are no significant differences between the powders calcined at temperatures ranging from 900 to 1100 °C. This Zn<sub>3</sub>Nb<sub>2</sub>O<sub>8</sub> phase (JCPDS file number 79-1164 [18]) has a corundum structure with a monoclinic unit cell (a=1909.3 pm, b=592.7 pm and c=522.0 pm, space group C2/c (no. 15)), in agreement with the literature [11].

Apart from the calcination temperature, the effect of dwell time was also found to be quite significant. From Fig. 3, it can be seen that the single phase of Zn<sub>3</sub>Nb<sub>2</sub>O<sub>8</sub> (yield of 100% within the limitations of the XRD technique) was found to be possible in powders calcined at 900 °C with dwell time of at least 1 h (Fig. 3(a-d)) applied. This is probably due to the effectiveness of vibro-milling and a carefully optimized reaction. The observation that the dwell time may also play an important role in obtaining a single-phase corundum product is also consistent with other similar systems [8,19]. It is also very interesting to see that the on-set temperature is approximately 200-250 °C lower than that reported earlier with a conventional ball-milling method [9,14]. The difference could be attributed to nano-sized mixed powders obtained from a rapid vibro-milling. Most importantly, this study suggests that a rapid vibro-milling method can significantly lower the optimum calcination temperature for formation of single-phase Zn<sub>3</sub>Nb<sub>2</sub>O<sub>8</sub> powders.

In the present study, an attempt was also made to calcine  $Zn_3Nb_2O_8$  powders under various heating/cooling rates (Fig. 3(b, e and f)). In this connection, it is shown that faster heating/cooling rates can also lead to crystallization of the  $Zn_3Nb_2O_8$  phase. Based on the TG–DTA and XRD data, it may be concluded that, over a wide range of calcination conditions, a single phase of  $Zn_3Nb_2O_8$  cannot be straightforwardly formed via a solid-state mixed oxide synthetic route, unless a careful design of calcination is performed. The experimental work carried out here suggests that the optimal calcination conditions for single-phase  $Zn_3Nb_2O_8$  (with impurities undetected by XRD technique) are 900 °C for 1 h with heating/cooling rates as fast as 30 °C/min. Moreover, the formation temperature and dwell time for the production of  $Zn_3Nb_2O_8$  powders observed in this work are also much lower than those reported

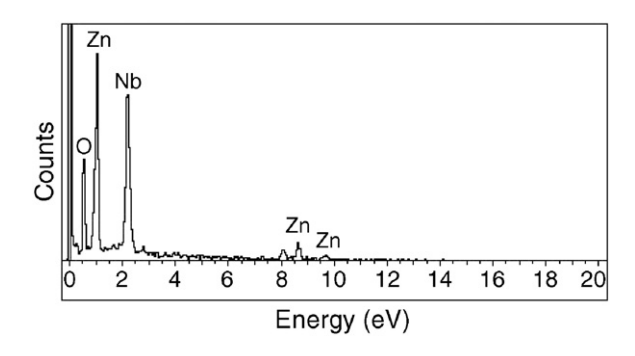


Fig. 5. EDX analysis of the Zn<sub>3</sub>Nb<sub>2</sub>O<sub>8</sub> powders.

earlier [9,14]. This clearly emphasizes the advantages of a rapid vibromilling technique.

Finally, the morphological changes in the Zn<sub>3</sub>Nb<sub>2</sub>O<sub>8</sub> powders formed by a mixed oxide are illustrated in Fig. 4(a-f) as a function of calcination temperatures, dwell times and heating/cooling rates, respectively. The influence of calcination conditions on particle size is given in Table 1. In general, the particles are agglomerated and irregular in shape, with a substantial variation in particle size, particularly in samples calcined at high temperature (Fig. 4(b)) or with fast heating/cooling rates (Fig. 4(e, f)). This finding is also similar to that in ZnNb<sub>2</sub>O<sub>6</sub> and ZrTiO<sub>4</sub> powders [8,20]. The results indicate that calculated crystalline size and degree of agglomeration tend to increase with calcination temperatures or heating/cooling rates (Table 1). All powders seem to display a significant level of necking and bonding as if they were in the initial stages of sintering. This observation could be attributed to the mechanism of surface energy reduction of the ultrafine powders, i.e. the smaller the powder the higher the specific surface area [21]. To the authors' knowledge, the present data are the first results for the morphology-calcination relationship of Zn<sub>3</sub>Nb<sub>2</sub>O<sub>8</sub> powders prepared by the solid-state reaction. It is also of interest to point out that mass production of single-phase  $Zn_3Nb_2O_8$  nanopowders with the smallest particle size of  $\sim 60$  nm (estimated from SEM micrographs) can be achieved by employing a simple solid-state reaction combined with a rapid vibro-milling technique. In addition, EDX analysis using a 20 nm probe on a large number of particles of the calcined powders confirms that the parent composition is Zn<sub>3</sub>Nb<sub>2</sub>O<sub>8</sub> (Fig. 5), in good agreement with XRD results.

#### 4. Conclusions

The potential of a rapid vibro-milling technique as a significant time saving method to obtain single-phase  $Zn_3Nb_2O_8$  nanopowders at low calcination temperatures has been demonstrated. The calcination conditions have been found to have a pronounced effect on both phase formation and particle size of the calcined  $Zn_3Nb_2O_8$  powders. The resulting  $Zn_3Nb_2O_8$  powders consist of a variety of agglomerated particle sizes, depending on the calcination conditions.

#### Acknowledgements

This work was supported by the Thailand Research Fund (TRF), the Commission on Higher Education (CHE), the Faculty of Science and the Graduate School, Chiang Mai University.

#### References

- [1] A.J. Pollard, J. Am. Ceram. Soc. 44 (1961) 630.
- [2] R.R. Dayal, J. Less-Common Met. 26 (1972) 381.
- [3] R.C. Pullar, J.D. Breeze, N.M. Alford, J. Am. Ceram. Soc. 88 (2005) 2466.
- [4] Y.C. Zhang, Z.X. Yue, Z.L. Gui, L.T. Li, Ceram. Int. 29 (2003) 555.
- [5] J. Wang, W. Dongmei, X. Junmin, N.W. Beng, J. Am. Ceram. Soc. 82 (1999) 477.
- [6] A.J. Moulson, J.M. Herbert, Electroceramics, 2nd ed.Wiley, Chichester, 2003.
- [7] C.L. Li, C.C. Chou, Int. Ferro., vol. 55, 2003, p. 955.
- [8] A. Ngamjarurojana, O. Khamman, R. Yimnirun, S. Ananta, Mater. Lett. 60 (2006) 2867.
- [9] D.W. Kim, J.H. Kim, J.R. Kim, K.S. Hong, Jpn. J. Appl. Phys. 40 (2001) 5994
- [10] H. Kasper, Z. Anorg, Allg. Chem. 355 (1967) 1.
- [11] M. Isobe, F. Marumo, S.I. Iwai, Y. Kondo, Bull. Tokyo Inst. Technol. 120 (1974) 1.
- [12] F. Laves, G. Bayer, A. Panagos, Schweiz. Mineral. Petrogr. Mitt. 43 (1963) 217
- [13] R. Wongmaneerung, R. Yimnirun, S. Ananta, Mater. Lett. 60 (2006) 1447.
- [14] Y.C. Lee, C.H. Lin, I.N. Lin, Mater. Chem. Phys. 79 (2003) 124.
- [15] Powder Diffraction File No. 89-1397, International Centre for Diffraction Data, Newton Square, PA, 2000.
- [16] Powder Diffraction File No. 30-0873, International Centre for Diffraction Data, Newton Square, PA, 2000.
- [17] Powder Diffraction File No. 76-1827, International Centre for Diffraction Data, Newton Square, PA, 2000.
- [18] Powder Diffraction File No. 79-1164, International Centre for Diffraction Data, Newton Square, PA, 2000.
- [19] S. Ananta, Mater. Lett. 58 (2004) 2530.
- [20] S. Ananta, R. Tipakontitikul, T. Tunkasiri, Mater. Lett. 57 (2003) 2637.
- [21] J.S. Reed, Principles of Ceramic Processing, 2nd ed.Wiley, New York, 1995.